The Development of Aluminium Foams for Enhanced Heat Transfer

Faye Elizabeth Senior

Submitted for the Degree of PhD

Department of Materials Science and Engineering

Supervisor: Dr Russell Goodall

March 2017

University of Sheffield

ABSTRACT

A novel replication technique for the production of open-celled aluminium foam has recently been devised and is undergoing commercial development by the company Constellium. The technique allows close control over the pore size and shape; a feature that is uncharacteristic of metal foam production methods in general and control to such an extent is unprecedented. The method provides an excellent pathway for the exploration of pore geometry/heat transfer behaviour relations, which is the objective of this study. This also aligns with the commercial goals of Constellium as heat transfer applications have been identified as a key market for their foams.

Based on the technique; the focus of this work was the development of a laboratory protocol to allow the production of aluminium foam samples with a range of different mesostructures. The heat transfer behaviour, including permeability, of foams with differing matrix metal, pore size, pore aspect ratio and pore shape were examined under forced convection conditions. Decreasing pore size was found to provide enhanced heat transfer, although for pores <3mm the benefit was outweighed by a large decrease in permeability. Small changes in pore shape as a result of preform compaction during processing may be exploited to provide improved heat transfer without reducing permeability. Elongation of pores provided no enhancement of heat transfer or permeability.

ACKNOWLEDGEMENTS

I gratefully acknowledge The Engineering and Physical Sciences Research Council (EPSRC) for funding the research described in this dissertation.

I would like to personally thank my supervisor, Dr Russell Goodall, for the outstanding level of support, advice and encouragement he has provided throughout.

Special thanks should go to Constellium and in particular Dr Yves Conde and Dr Vincent Mathier; without the expertise and materials provided by them, this work would not have been possible. For their continued support, many thanks also go to The Advanced Metallic Systems CDT, Dr Claire Hinchliffe, Prof Bradley Wynne, Prof Panos and Prof Michael Preuss.

Of course a big, big, big thank you goes to the technical support staff (now better described as my friends); Ian Watts, Kyle Arnold, Lisa Hollands and Ben Palmer. I don't know how many times I commandeered your time/equipment/office/kettle/fridge/heater/what-ever-else-was-lying-around-and-I-took-fancy-to, but it was definitely too many to show all my thanks here and I will be ever grateful.

Lastly, the appreciation I have for my Husband, son, mum, dad and mother-in-law Brenda cannot be put into words. I love you all dearly.

CONTENTS

PREFACE

Metal foams have a unique and versatile set of properties that permit their use in a number of engineering applications; however, one of the major potential application areas is thermal management. Heat exchangers are used to heat or cool systems and/or specific components within a system to aid function, prevent damage, maintain performance or recapture waste energy. There is a rapidly growing need for more and more efficient heat exchangers due to weight reduction and miniaturisation of technology alongside increased performance and decreased cost. This is especially true for applications such as electronics cooling whereby the level of heat dissipation required is approaching the limits of current thermal management solutions [1]. As candidates to provide enhanced heat transfer, open-cell metal foams have attracted considerable attention from both the scientific community and industry alike. The combination of; high thermal conductivity of the matrix metal, permeability to fluid flow and large surface to volume area, allows open-cell metal foams to be well suited as efficient heat exchangers. A number of studies have already suggested that the heat transfer capabilities of open-cell, metal foam show improvement over traditional heat exchanger designs.

Although a range of techniques are available for the manufacture of open-cell metal foam, a common limitation is the lack of control over the pore size and shape. A novel “salt-dough” replication technique for the production of open-celled aluminium foam has recently been devised to rectify this limitation and is undergoing commercial development by the company Constellium. The method provides an excellent pathway for the exploration of pore geometry/heat transfer behaviour relations, thus opening up the possibility to further enhancing the effectiveness of a metal foam heat exchanger using the pore architecture.

In this work, a laboratory scale version of the salt-dough manufacturing technique has been developed, closely based around a pilot, industrial set-up used by Constellium. Novel, aluminium foams with different pore configurations such as pore size, shape and aspect ratio have been produced. The heat transfer behaviour of foams made both in-house and by Constellium, have been characterised using a specially constructed rig developed previously by another member of the research group. In addition, the foams have also been assessed for their level of permeability to fluid flow. Foam permeability is an important factor to consider in heat exchanger design as it can be detrimental to the range of suitable heat exchange applications. For example, many applications require a pump to drive the fluid through the exchanger; a decrease in permeability would require greater pumping power to maintain fluid flow and thus increase costs.

The relationships found between pore architecture and heat transfer behaviour of novel foams made using the salt-dough technique have been reported. Recommendations based on the findings are given with respect to the most beneficial pore architectures to use for heat exchangers of similar size to the samples used here.

1. LITERATURE REVIEW

1.1 INTRODUCTION

Deliberately processed to be highly porous in the solid state, metallic foam has a structure similar to that found in bone or natural sponge. The cellular geometry, in combination with the physical and mechanical characteristics of the metal, generates a diverse and unique combination of properties. Metal foams therefore lend themselves well to a wide range of structural and functional engineering applications, heat exchange being just one of many. A large surface area to volume ratio, low specific weight, high stiffness, permeability, thermal conductivity and high energy absorption are just some of the common, broad-spectrum properties that can be boasted by metallic foams [2][3][4][5].

Aluminium foams are by far the most widely investigated and developed, however foams based on nickel, magnesium, lead, zinc, copper, bronze, titanium, iron, cobalt, gold and various metallic glasses have all been successfully produced [6]. In general, the suitability of a particular metal as a foam-matrix material depends on its compatibility with the various “foaming” methods that are available, including techniques based on casting, powder metallurgy and metallic deposition. Similarly, the cellular architecture of the foam is also often defined by the processing route and can vary drastically with a large number of parameters to be considered. Included within the term “architecture” for example is the pore interconnectivity, pore size/ shape, pore orientation and pore distribution.

As the processing route controls both the foam matrix material and the cellular architecture [5][7], it also in turn dictates the foams properties. Establishing the critical properties required of the foam for an intended application is therefore

essential in order to choose an appropriate manufacture method. The function of a heat exchanger is to act at an interface separating two or more substances such that one is able to transfer thermal energy to another. On the most fundamental level therefore, the main consideration for heat transfer applications is that the foam is both thermally conducting and permeable. Highly conductive metals such as aluminium and copper are the preferred choice, although aluminium has the extra benefits of being low cost and easy to process. In addition, the use of foam with an interconnected pore network is a necessity to allow a fluid to pass through it and heat to be exchanged between the two effectively. The manufacturing routes are therefore limited to those that can produce open-cell, aluminium or copper foam.

Due to the vast number of compositional, structural and process variables producing a single, comprehensive definition for what exactly is meant by the term “metal foam” is difficult. Following modern convention the expression has so far been used to describe all metallic structures that are highly porous in the solid state, regardless of the processing route and resultant pore geometry. The term can however be misleading and, as is true for this case, is often used in the wrong context if its original meaning is considered. Banhart [4] defines the term “foam” to classically mean a dispersion of gas bubbles in a liquid, whereby the individual bubbles are isolated from each other and do not form an interconnected network. Subsequently, “solid foam” is then described as the preservation of a foamed liquid through solidification and thus true “metal foams” having been processed from a melt, are only those that contain isolated pores. Nowadays this type of isolated-porous structure is commonly termed “closed-cell metal foam”. There are however various techniques that produce so called “open-cell metal foams” whose pore networks can be fully or partially interconnected. Contradictory to the name therefore, these open-cell foams are not strictly speaking foams at all. Amongst many others, Banhart [4], Colombo [7], Conde [8] and Goodall [9] are in agreement that “metal sponge” would be a more suitable term.

In following sections the term metal foam will be used when describing both open- and closed-cell structures, however to avoid confusion it has been defined below to clarify exactly what is meant in the context of this review:

> *Metallic foam is a metal or alloy that has been processed to give a highly porous structure (>50%) in the solid state. Typically the cellular structure is randomly orientated (as opposed to the regular array of a lattice) wherein the pores can either be sealed; closed-cell foam, or form an interconnected network; open-cell foam.*

As permeability is required for heat transfer applications, this review will focus on open-cell foams and mostly omit studies on closed-cell unless relevant from another perspective. A general overview of the uses of metal foam will be given with the focus being on heat transfer. Different production methods for open-cell foams will then be described and evaluated in terms of the level of control offered over the structural parameters. Finally methods of measuring the heat transfer capability of metal foams will be explored along with studies that have investigated relationships between a foam's thermal properties and its cellular architecture.

In summary, this review aims to evaluate the major studies relating to the use of metal foams for heat exchange applications and the attempts made so far in tailoring various structural parameters to improve the heat transfer performance.

1.2 Applications Of Metallic Foam

The properties boasted by metal foams are an amalgamation of the properties of the matrix metal and those that arise from their cellular morphology; they can therefore often be tailored to suit a large number of applications, both functional and structural, covering a diverse range of disciplines.

Although this review will mainly focus on the heat exchange behaviour of metal foams, in order to emphasise their usefulness and versatility, a brief description of other applications has also been included.

1.2.1 General Applications

One of the most exploited features of aluminium foam is its relatively high strength and stiffness in combination with low specific weight, making it an effective material for lightweight construction. In this sense, metal foams are an attractive option for the transport industry due to the ever increasing need to reduce weight and in turn reduce fuel consumption and CO_2 emissions. For example, direct weight reductions in cars can be achieved by replacing conventional stamped steel parts with aluminium foam sandwich (AFS) panels [10][4][5]. Sandwich panels are made up of a foam core metallically bonded between two solid face sheets; this creates very stiff, lightweight panels but with better tensile performance and corrosion protection compared to bare foam without face sheets [11]. The foam cores are most commonly closed-cell although open-cell ASPs have also been produced [12][13]. Examples of AFS panels are shown in figure 1.

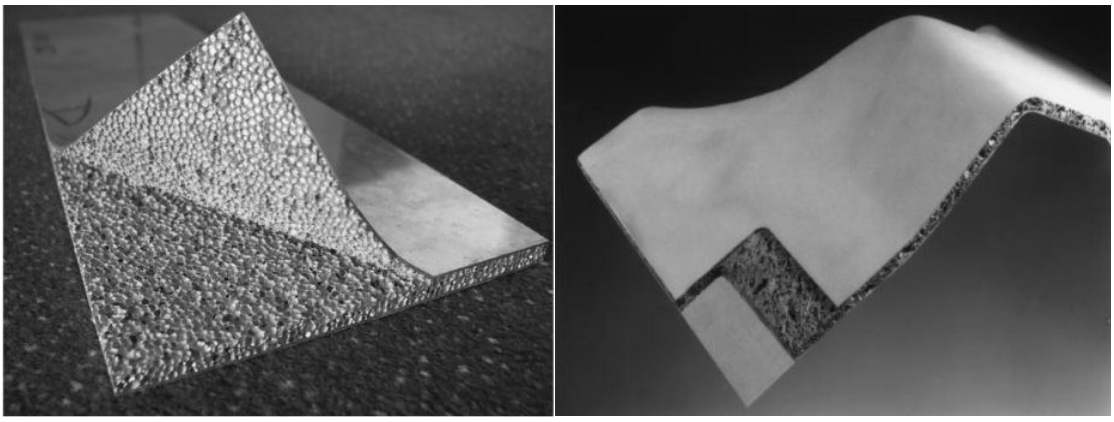

Figure 1. Left: AFS panel produced by Karmann, Germany with face sheet peeled back to expose foam core, image sourced from [10]. Right: Formed AFS panel with face section removed to expose foam core, image sourced from [15].

In one case study, AFS panels were successfully used by Teupen (Germany) as a support structure for a telescope arm that lifts a platform [14][15]. The use of AFS technology allowed the crane to have a working height of 25m but still be under the weight limit to be driven using a regular driving licence; setting it apart from competing products and providing a unique selling point.
Similar weight reductions are also of major interest to the aerospace, railway, marine and building industries.

Another well-utilised property of metal foam is its high energy absorption capacity and thus it can be used in a variety of protection-based applications from packaging to body armour. An energy absorber is used in essence as sacrificial material in order to keep the object/s it is protecting from taking the full brunt of an impact. They are designed to maximise the conversion and dissipation of kinetic energy so that the force felt by an object beyond the absorber would be below the threshold for injury/damage to occur [2]. A metal foam energy absorber does this through the progressive buckling and collapse of its cellular structure, causing non-linear deformation behaviour. As the foam structure is compacted a stress plateau is observed whereby deformation occurs at a near constant stress level over a wide range of strain [4]. Upon full densification, i.e. when the structural porosity has been removed by compaction, the plateau ends and stress rises steeply [5]. A typical stress-strain curve for metal foam is shown in figure 2.

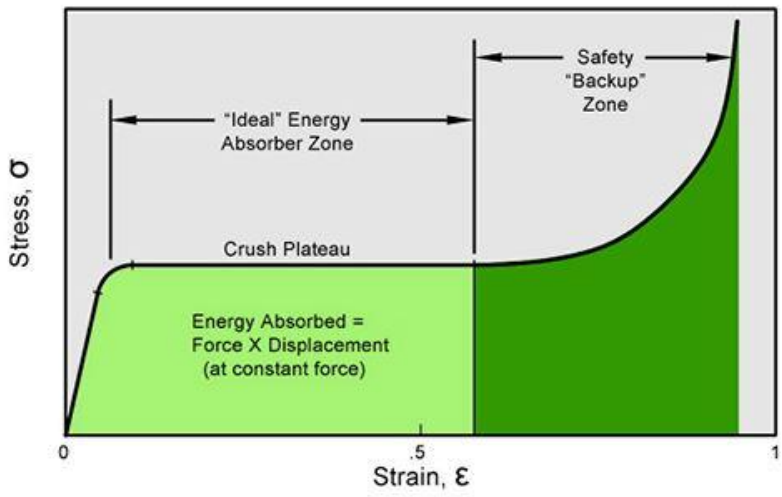

Figure 2. A typical metal foam stress-strain curve. Image sourced from [54].

Both open cell and closed cell foams can be used as energy absorbing materials. However, which one is favourable is dependent on the specific application as they exhibit slightly different deformation behaviour [5]. Similarly, both the foam density and matrix metal are also used to tailor the energy absorption capacity and efficiency of the foam to meet the needs of the application [2][16].

Aluminium foam energy absorbers can already be found in cars such as the Audi Q7, as part of the support frame of the safety net, as well as the Ferrari 360 and 430 spider, as reinforcement in the door frame [17][18]. Japanese trains contain blocks of metal foam to improve crash energy absorption [4] and a Korean bridge contains metal foam crash elements in its guardrail [18]. The energy-absorbing nature of foams is also showing promise in various bullet/blast protection applications including protective shielding for vehicles and buildings [11][19][20][21]. The manufacturer Cymat has a line of products branded SmartMetal™, which are designed specifically for blast-mitigation purposes [22]. Other potential metal foam energy absorber applications include; vehicle crash boxes [23][10], car A-pillars [24], car seats [25], car engine mounting brackets [10], crash systems in trams [10], space debris shields [26][27] and motorcycle helmets [28].

Metal foams have shown great potential in the field of noise management whereby sound-energy dissipation is achieved predominantly through viscous and thermal losses [29][30]. Open-cell foam has a much higher sound absorbing capacity than closed-cell, although closed cell could be used if the cell walls are fractured (and thus partially opened) by rolling or compaction [5][31][32] [33].

It should be noted that although metal foams have a high sound absorbing capacity improved performance can be achieved using more conventional routes such as polymer foam or glass wool [30]. Furthermore, in terms of cost, metal foams are a relatively expensive option. However in a number of circumstances, for example in high temperature and corrosive environments, metal foams can offer a much more robust sound control solution. Lightweight, high stiffness (self-supporting), fire resistance, corrosion/weather resistance and chemical stability are some of the additional properties that often make metal foam an attractive option for acoustic

absorption. Alternatively, the high sound absorption capacity itself can act as an attractive "complimentary characteristic" when sound absorption is not the primary function. As discussed previously, metal foam is of interest to the transport industry in terms of weight saving, but even more so when sound and energy absorption could be further integrated into one material. This melding of functions could in itself create additional weight reduction by minimising the number of components required.

Some real world examples of where metal foam has been used for sound management include the use of Alusion foam (Cymat, Canada) on the ceiling of an audience hall [18] and foam produced by Foamtech (South Korea) on the walls/ceiling of a shooting range [34]. Figure 3 shows Alporas foam (Shinko Wire, Japan) on the underside of an elevated motorway to absorb vehicle noise [35][5].

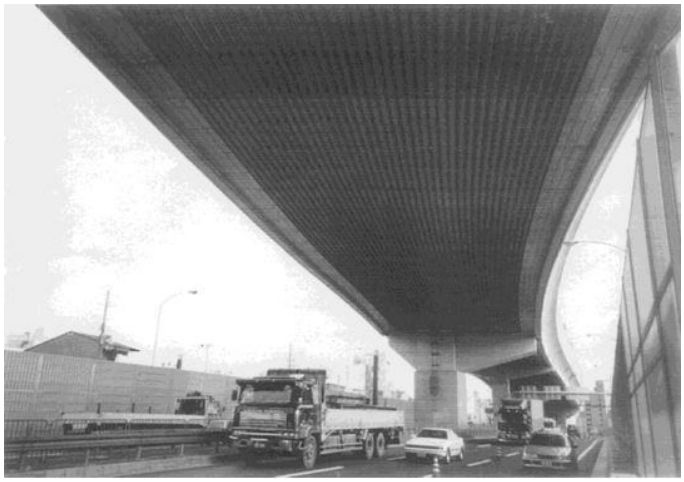

Figure 3. Alporas (Shrinko Wire, Japan) foam being used as a sound management solution on the underside of an elevated motorway. Image sourced from [35].

In relation to sound management, metal foams are also good vibrational dampeners. The resonance frequency of a metal foam structure is generally lower than of one made from the bulk metal due to a lower Young's modulus [4]. In addition, foams have a high loss factor (a measure of a materials damping capacity) meaning vibrational energy is efficiently converted to heat energy and dissipated into the environment [4]. The vibrational damping effect of foams can be further

improved by introducing imperfections into the structure (cracks, inclusions etc.) and/or reducing the thickness of the cell walls [36].

For industrial applications, vibrational damping can reduce machinery wear/fatigue issues and thus increase the operational lifespan of the piece. In turn, noise emissions generated by the vibrations are also reduced. Examples of vibrational dampening through the use of metal foams include in industrial machines/tools [18][37] and sporting equipment [38]. Again it is often metal foams multi-functionality, namely the combination of; dampening, sound absorption, lightweight and high stiffness, which in these types of application allows metal foam to compete with the more traditional, well-established materials.

In recent years metal foams have found employment as biomaterials. A number of different open-cell, tantalum and titanium foams have been produced for orthopaedic and dental implants either as coatings or standalone structures [39][40][41]. The interconnected open-cell architecture facilitates enhanced bone in-growth, creating a strong bone-implant bond and in turn reducing the likelihood of implant failure. Similarly, nickel-titanium foams [42] and titanium foam-like structures [18] for bone/dental implants are currently under development. Examples of metal foam implants can be seen in figure 4.

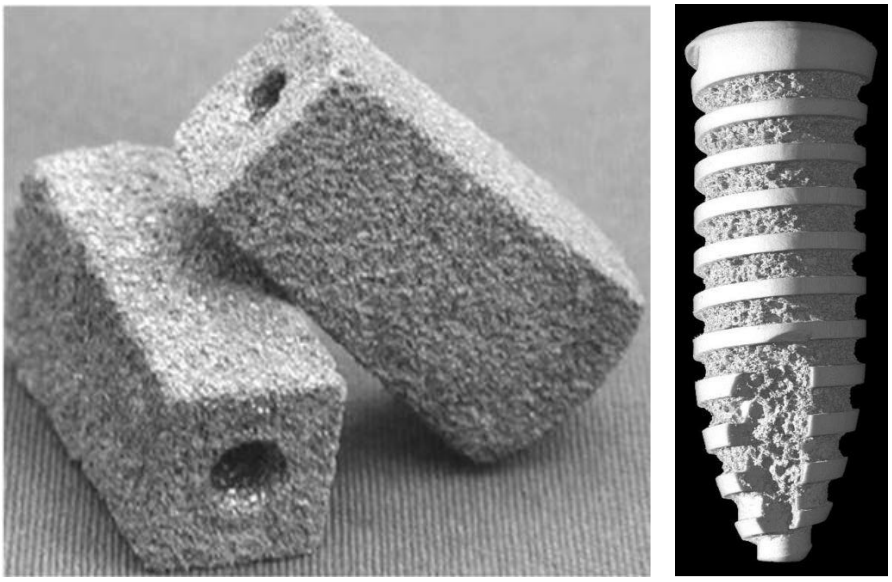

Figure 4. Left: Porous NiTi bone implant, image sourced from [42]. Right: Porous Ti-based dental implant, image sourced from [18] .

Due to their large surface area, conductivity and corrosion resistance, open-cell metal foams can be used as electrode materials, catalytic supports and reactor materials. Batteries used in household items such as power tools and video cameras often use nickel open-cell foam as their electrode material [5]. Iron-based metal foam is being considered as an anode material for microbial fuel cells (MFCs) [43] and nickel open-cell foam for electrode substrate material for alkaline fuel cells (AFCs) [44]. One method of biodiesel production has been improved by using metal foam as the reactor material and shows good potential for small-fuel biodiesel processing plants [45].

In contrast to the many highly functional applications discussed above, the unique and eye-catching appearance of metal foam has also given it aesthetic value and it has been used in various decorative, non-loadbearing, structural applications [18]. The foam manufacturer Cymat has a line of specialised architectural open and closed-cell products branded Alusion™ that have been used as wall/ceiling cladding in a number of renowned buildings such as the Prada Museum, Italy, the Vancouver Convention Centre, Canada and the 9/11 Memorial Library, USA [46]. In the same artistic approach, metal foam has also been used to create sculptures and furniture. Decorative uses of metal foam are shown in figures 5 and 6.

Figure 5. Exterior and interior cladding made from Alusion™ metal foam. Images sourced from [46].

Figure 6. Left: Chair made from Alveotec metal foam, image sourced from [55]***. Right: Signage made from Duocel foam, image sourced from*** [54]***.***

Although not discussed here, there are many more proposed applications for metal foam including; electromagnetic shielding, filtration and separation, liquid storage and transfer and water purification, amongst others. Furthermore, there is also a huge number of applications that are not well publicised either due to commercial secrecy or simply because the application is so niche. Further information can be found in various metal foam review papers and books [2][3][17][18][36].

It should be noted that, although numerous, many of the potential applications mentioned here will remain academic and/or as prototypes without ever achieving any true commercial breakthrough. There are several barriers preventing the take up of metal foam technology such as cost of the product and reliability of the manufacturing processes, including structural uniformity across the single component as well as part-to-part reproducibility. Until cost-effective manufacturing techniques can provide quality assured, reproducible parts, reservations from the major industry sectors will remain. This cautious approach is understandable given the lengthy and expensive testing regimes for new materials in sectors such as aerospace for example. As research into metal foams and their manufacture continues to eliminate these problems, the likelihood of commercial up-take can be maximised by utilising the multi-purpose approach in order to offer the most financial advantages.

1.2.2 HEAT EXCHANGE APPLICATIONS

There are numerous applications which require a fluid (gas or liquid) to be heated or cooled. In many cases heat exchangers can be used whereby the fluid flows over the surface of the exchanger causing convective heat transfer between the two. If the temperature of the heat exchanger is higher than that of the fluid then heat passes into the fluid, and vice versa. Heat exchangers can be found in a huge range of everyday applications; refrigeration, air conditioning, power generation and vehicle radiators to name just a few. For engineering applications, a common use of heat exchangers is to cool down systems and/or specific components within a system, either to prevent damage or to maintain performance. Examples of this type of application include, but are not limited to, exhaust gas coolers for diesel engines and compact heat sinks for power electronics and microelectronic devices such as computer chips.

Conduction is generally the predominant method of heat transfer, therefore heat exchangers are commonly made from metals with high thermal conductivities such as aluminium and copper, although aluminium has the added benefits of being lightweight and is the cheaper of the two [29]. In addition, an efficient heat exchanger has a high surface area to volume ratio in order to maximise heat dissipation through convective heat transfer [29]. Given these requirements, open-cell metal foams are well suited as heat exchangers. The metal phase is thermally conducting; both aluminium and copper can be used as the matrix metal. In addition, the large internal surface area allows a good level of contact between fluid and metal whilst the random structure creates turbulent flow paths that promote fluid mixing [47]. A basic foam-heat exchanger set-up is shown in figure 7. However, beyond such a basic design, the geometrical flexibility of metal foam allows for varied and complicated designs to be easily implemented. This in turn allows design constraints to be easily overcome, or performance enhancement through system design optimisation.

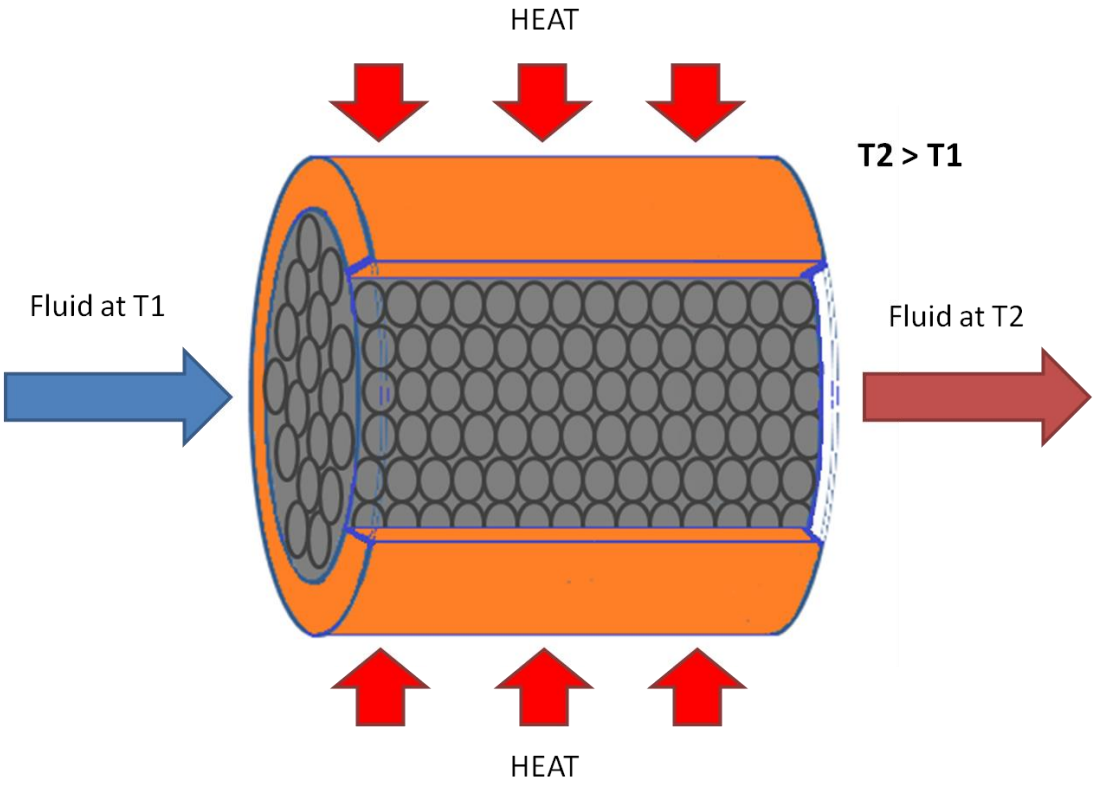

Figure 7. A basic metal foam heat exchanger set-up, where T=temperature.

A number of studies have shown great potential for metal foams as heat exchangers and have reported similar or improved heat transfer behaviour compared to traditional designs such as fin-and-tube, plate-fin and louvered-fin heat exchangers [48][49][50][51][52] (A full description of different types of heat exchanger design can be found here [53]). The company ERG aerospace, who produce aluminium and copper foams branded “Duocel”, claim that their foam heat exchangers can provide more than double the cooling performance of traditional fin heat exchangers [54]; a selection of these are shown in figure 8. Furthermore, foam heat sinks are already used in a range of engineering applications. A Duocel foam heat exchanger has been used in a scanning electron microscope to thermally stabilise the lens [18][54]. Metal foam has also been used to protect the electronics of lighting systems from the heat produced by powerful LED bulbs [18]. Similarly, a foam-like heat sink produced by Alveotec was used by Loupi Lighting systems in a 40W LED downlight to ensure proper operating temperature. The use of the metal foam allowed Loupi to halve the size of the light

system whilst maintaining performance [55]. Figure 9 shows an example of foam being used in the cooling of LED lighting.

Figure 8. A selection of Duocel foam heat exchangers. Images sourced from [54].

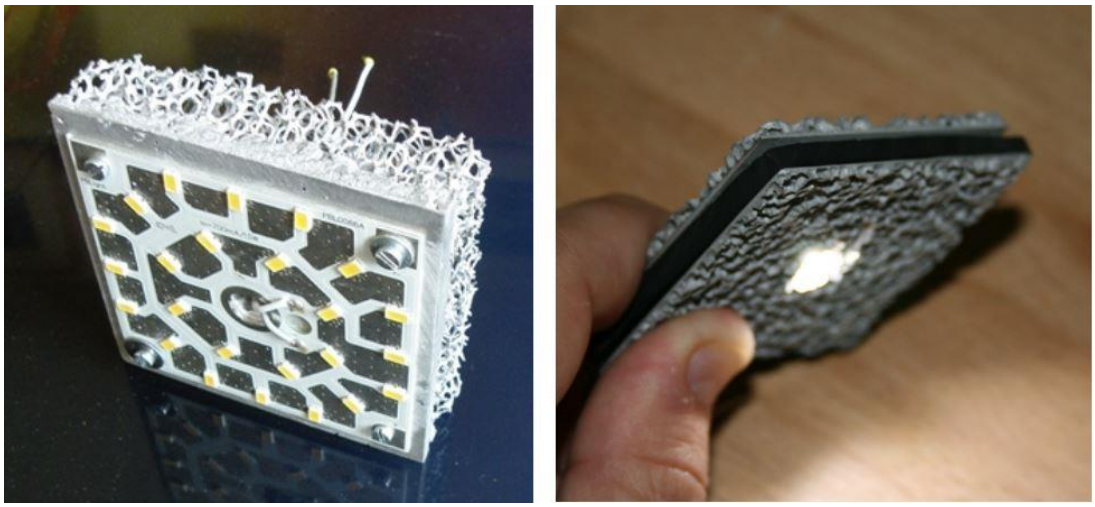

Figure 9. Metal foam being used to cool LED lamps. Images sourced from [18].

One of the application-limiting issues surrounding the use of open-cell metal foam as heat exchangers is the large pressure drops generated as the fluid flows through the foam. Fluid flow may occur by one of two mechanisms. Firstly, flow can occur via natural convection; this is caused by buoyancy forces arising from temperature variations in the fluid and so pressure drops are less of a concern. Alternatively and more commonly for high end applications, flow can be induced by an external force such as a pump; in this case heat exchange occurs via forced convection. The pump power required to drive the fluid is often a critical design parameter and so in many cases there is an application-specific, maximum pressure drop that cannot be exceeded. It has been reported several times that decreasing the foams density decreases the pressure drop, however this is also accompanied by an unwanted decrease in heat transfer performance [56][57].

It is clear that an ideal heat exchanger would both maximise heat transfer capability and minimise flow resistance however, as these characteristics are conflicting, reaching an application-specific optimum between the two is paramount. For metal foam heat exchangers, changing different structural parameters could be a way of achieving this but a better understanding is first needed. If it is possible to tailor the foams structure to attain optimum heat exchange performance, it will greatly widen the scope of applications for which metal foam would be a viable and competitive heat exchanger option.

1.2.3 CHAPTER SUMMARY

Metal foams boast many diverse, yet often complimentary, characteristics including high specific stiffness, low specific weight, high energy absorption, mechanical and acoustic dampening, resistance to burning, recyclability and good machinability. These properties afford metal foam the potential to be used in a wide range of different applications including but not limited to; lightweight

construction, energy absorption, noise control, mechanical dampening, filtration and heat exchange.

A current demand for weight saving and compaction of technology requires more and more design integration (i.e. one part does more than one function). Nowadays, multi-functionality can therefore play a major role when selecting a material for a potential application; a requirement that is opening the door for metal foams in areas where they have previously been overlooked. What is more, growing commercial interest in metal foams has meant increased research in the field leading to frequent improvements to both manufacturing methods and properties. The associated reduction in manufacturing costs is further widening the range of suitable applications and thus the uses for metal foam is continually being expanded.

Heat exchange has been identified as a particularly well suited application for open-cell aluminium foam due to its permeability, high thermal conductivity, large surface area and turbulent-flow enhancing, random structure. Furthermore, there is an increasing need for highly effective heat exchangers due to, for example, the ever increasing performance of electronic devices and computing technology. The heat transfer capability of metal foam can in some cases out-perform that achieved using traditional heat exchanger designs. However, attempts so far to further increase their heat transfer performance has often resulted in decreased permeability; an issue for some applications. There is therefore a large commercial incentive to better understand the relationship between foam structure and its overall heat transfer behaviour, including permeability, with the aim of improving performance.

1.3 PROCESSING OF OPEN-CELL METAL FOAM

There are a number of manufacturing routes available for producing aluminium open-cell foam, however the level of control over the pore topology offered by the techniques varies. Below is a description of different production methods along

with an evaluation of how/if they can be used to manipulate the foams structural architecture. It should be noted that the techniques to produce closed-cell and/or those not compatible with aluminium or copper have been omitted as foam produced through such routes would not be suitable for heat transfer applications.

1.3.1 Use Of A Non-Metallic Foam Template

Investment casting is a well-known metal forming technique and one that can be easily utilized to produce metal foam [5][58]. There are four basic steps involved; these are depicted in figure 10.

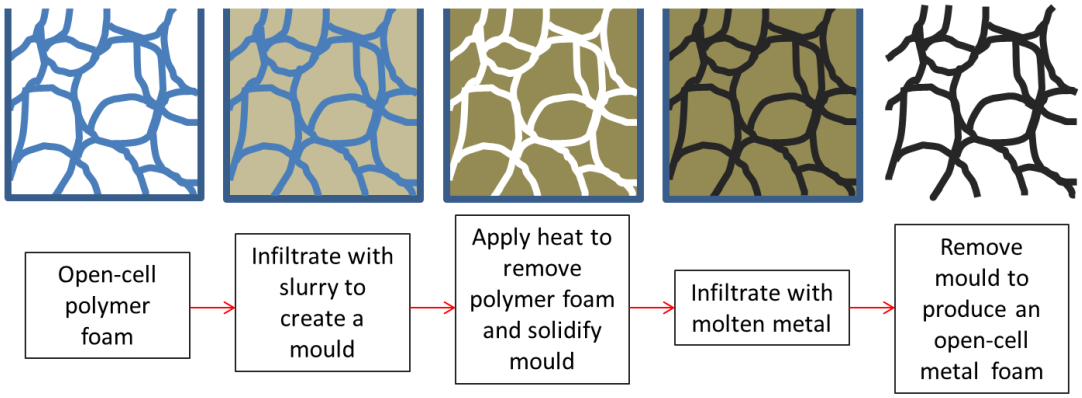

Figure 10. The basic steps of the investment casting route to produce open-cell metal foam.

Open-cell, polymer foam (commonly polyurethane) is used as a template and is permeated by a slurry of investment compound to create the basis of a mould. A heat treatment is then administered to solidify the mould and remove the foam template via liquefaction/combustion. The interconnected network left within the mould is then infiltrated with molten metal; this can be in effect any metal that can be investment cast including aluminium, copper, tin, zinc, nickel, Inconel, silicon, silver, gold and magnesium [3][5][6][8][59]. Alternatively a metal-powder-slurry can be used as substitute for the molten metal; in this case the metal is sintered rather than solidified before the mould is removed [5]. Once the metal has

solidified, the mould is removed either by mechanical agitation or high pressure water jets. The end product left behind is a fully interconnected, open-cell metal foam whose structure duplicates that of the original polymer template.

Foams made via the investment casting route typically have a homogeneous pore size that ranges between 1-10mm [6]. These type of foams are low density with the volume fraction of metal generally falling between 0.05-0.15 [6]. Commercially available metal foam thought to be produced using investment casting techniques include Duocel (ERG Materials and Aerospace Corporation, Oakland, CA, USA) and foam produced by M-Pore GmbH (Dresden, Germany) [6].

Another route to produce open-cell metal foam through the use of a polymer foam template is metallic deposition. Again the process begins with polymeric foam with a structure that corresponds to that required from the metal foam end-product. The polymer template is firstly made electrically conductive; electro-less plating or cathode sputtering for example can be used to pre-coat the foam with an electrically conductive substance such as metal or carbon [4][6]. The principal, metallic layer can then be coated onto the polymer foam using techniques such as electrolytic deposition [60], chemical vapour deposition (CVD) [61] and directed vapour deposition [62]. Metals compatible with such methods include nickel, zinc and copper [4]. Once coated, the original template can be removed through thermal decomposition or leaching. The basic process is outlined in figure 11.

In a very similar method, a metallic coating can be applied to a polymer template foam by infiltrating it with a slurry of metal powder/ binder using techniques such as roller coating or centrifugation. In this case the foam does not need to be electrically conductive and so the pre-coating step is unnecessary. Complete impregnation of the template foam without frequent structural defects can only be achieved using fine metal powders with size distributions typically less than 25µm [63]. Current availability of fine metal powders is lacking and therefore metal suitability is limited however, steel, titanium alloys and molybdenum have been used [63][64] and it is likely that the range will widen with improving powder metallurgy technology. The polymer foam is removed using a thermal treatment and lastly a sintering phase sets the debinded metal structure.

The final foam produced when using all the deposition techniques described is similar to the investment casting route in that the open-pore architecture is a copy of the original polymer foam. However, in metallic deposition methods the metal coats the polymer foam rather than directly replacing it and therefore, unlike the casting route, the metal struts are characteristically hollow once the template is removed.

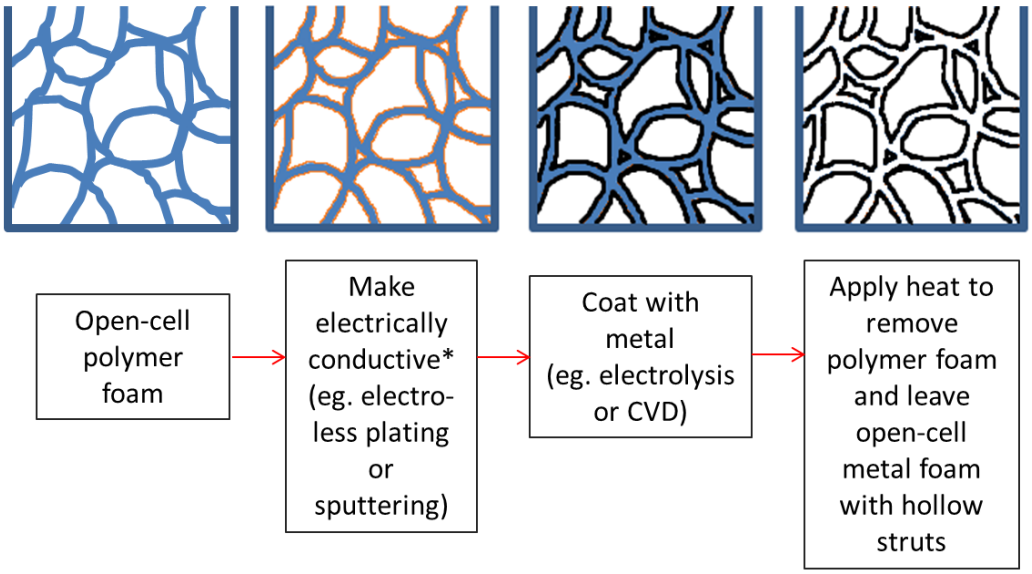

*Figure 11. The basic steps of the metallic deposition route to produce open-cell metal foam.*This step is not always required.*

The foams produced have extremely low relative densities with the typical volume fraction of metal being between 0.02-0.05 [5][6]. Suggested typical pore sizes range from 1-10mm [6] and 1-3mm [5]. Commercially available foams made through metallic deposition routes are generally those based on nickel. These include Incofoam (Vale Limited, Toronto, Canada), Retimet (Meggit Control Systems, Coventry, UK), Celmet (Sumitomo Electric, Japan) and Recemat (SEAC, The Netherlands).

In all cases where a template is used (both investment casting and metallic deposition), the pore topology of the subsequent metal foam is defined and restricted by that of the original polymer foam. Polymer foams are generally made

by introducing gas bubbles into the liquid polymer before solidification and so the resultant pore topology stems from a mixture of surface tension effects, viscous forces and competitive growth [2][65]. As a consequence, the density/pore size can be regulated but control over the pore shape is challenging and complex pore shapes are unattainable. In turn, it is therefore also difficult to control the pore shape in metal foams when using a polymer foam-template based technique.

One study has produced density graded, open-cell, aluminium foam using the investment casting technique [66]. The polymer foam used as the template was first cut into a truncated cone shape and compressed into a cylindrical mould. The diameter of the mould was smaller than that of the cones base but equal to its top therefore upon compression a density profile was created. The standard investment casting technique was then applied whereby the template was infiltrated with plaster slurry to create a mould that, after removal of the polymer template, could be infiltrated with molten metal. The resultant aluminium foam had a density that varied between that of the original polymer foam and twice that value.

1.3.2 SINTERED PARTICLES

When spherical and/or irregular shaped particles are loosely packed together, a certain amount of unfilled space is left surrounding the solid-solid contact points. This occurrence can be utilised to create porous structures simply by packing metal powder and then sintering to make the contact points permanent, as shown in the schematic in figure 12. The amount of empty space between the packed particles, and thus the overall porosity of the sintered structure, depends on the particle geometry, the randomness to which they are packed and the sintering time/conditions. If a wide range of particle sizes are packed together the porosity will usually be lower than if the particles were of uniform size [6]. Similarly, and as a general rule, the more irregular the particle shape (opposed to perfectly spherical) the higher both the porosity and number of contact points per particle

[6]. Vibrating the particles to create more ordered packing will decrease porosity as will compaction of the particles [6]. In addition, the sintering process itself will cause partial densification of the porous structure although how much depends on the sintering conditions. The method is suitable for essentially any metal powder that can be sintered. For aluminium, sintering can be hampered by the formation of a surface oxide layer around the powder particles; milling the powder with sintering aids such as Sn and Mg can help combat this [67].

Although porosity can be controlled to a certain extent as seen above, foams made through metal powder sintering are generally low porosity and the interconnectivity can sometimes be only partially open. This may present issues for applications such as heat transfer whereby the foams permeability ideally needs to be maximised. Furthermore, as the pores are a result of the gaps between packed particles, any real level of control over the size and shape of the pores is unrealistic.

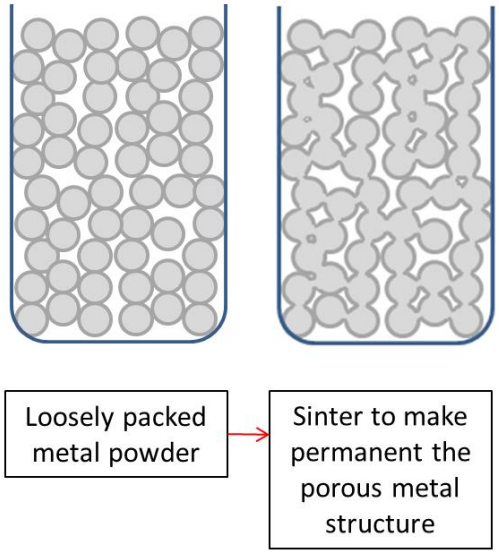

Figure 12. Schematic of the metal powder sintering route to produce open-cell metal foam.

A closely related technique is a sintered particle/space-holder hybrid and is represented schematically in figure 13. In this method, metal powder is packed along with second phase particles that can subsequently be removed in order to greatly enhance the porosity of the structure.

Open-cell copper foams have been made by co-compacting copper powder with powdered potassium carbonate (K_2CO_3) [68]. After sintering, the carbonate powder was removed either by dissolution in water or by increasing the temperature so that decomposition of the carbonate occurred. Aluminium open-cell foams have been produced in the same manner using NaCl [69][70] and carbamide (commercial fertilizer) [71] powders as the removable phase; both of which can be removed by dissolution in water. Similarly, titanium foams have been made using tapioca starch that was removed by pyrolysis during the sintering stage [72].

The use of a space-holder allows much more control over both the porosity and pore morphology; this is discussed in more detail in terms of the original space-holder technique in section 1.3.4.

Foamet® (Hollomet, Dresden, Germany) is commercially available foam made through a powder-metallurgical casting procedure, which uses an organic carrier as the removable second phase.

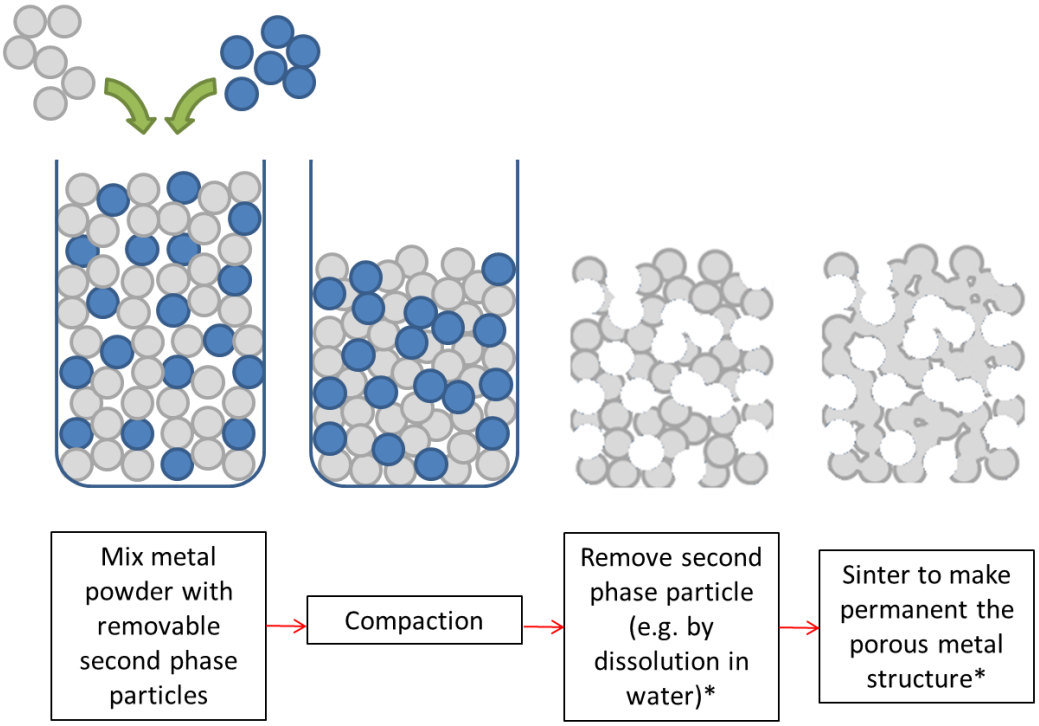

*Figure 13. Schematic of the sintered particle/space-holder technique to produce open-cell metal foam.*Note in some methods removal of the space-holder occurs after or during the sintering step.*

Another powder-sintering based method to produce open cell foam involves suspension of the powder in a foamable liquid such as a polymer. The polymer/metal-powder mix is foamed to initially produce closed-cell foam. The foam is then heat treated to remove the polymer component and open up the cell walls to create an interconnected pore network. Finally the metal powder assembly is sintered to make permanent the porous metal structure. Copper [73], iron and titanium [74] open-cell foams have all been produced using this method.

The overall porosity and pore size of the foam decreases as the volume fraction of suspended metal powder is increased [74]. Furthermore, shrinkage that occurs during the polymer removal step decreases with increasing metal powder volume fraction [74]. Despite these controllable parameters, the overall architecture of foams produced in this way is essentially defined by the initial liquid-foaming technique. As mentioned in a previous section, polymers are generally gas-foamed meaning the porosity and pore size can be influenced but there is generally no control over the pore shape. When foams are produced using gas-based methods the shape of the pores is governed by naturally occurring scientific principles relating to the formation of liquid-gas interfaces. This said, a common polymer foaming method involving a two-part polyurethane may have the potential to create foams with elongated pores. The polymer is made up of two separate components that when mixed, react to eliminate H_2O, which is released as steam and consequently foams the liquid. As the mixture rises it is held in a mould to prevent the formation of elongated cell structures [73], thus theoretically, intentional pore elongation could be achieved if left unrestrained.

1.3.3 Sintered Fibers

Permeable, foam-like structures can be made using metal wire/fibres. Intertwined wire can be sintered or brazed to make permanent the metal-metal contact points, or it can simply be left entangled but un-bonded; though this latter type is less likely to be favourable for heat transfer. Aluminium [75], titanium [76] and steel

[77] foams have been made using this technique. The architecture of porous wire structures can be very varied depending on how the wires are intertwined. Wires can be woven together or entangled using various coiling and winding processes [75][77][78] to produce porous structures that range in regularity; some of these structures can be better described as lattices as opposed to foams. Short fibres/wires can also be packed and sintered [79], producing much more random, foam-like structures.

The porosity of wire structures can be controlled by compaction before sintering. In addition, what are essentially the struts of the foam can be adjusted simply by using wires of different thickness and/or cross sectional shape. The gaps between the wires act as the pores and so, excluding the regular lattice structures, very little control is held over their shape. Suggested typical pore sizes range between 0.1-5mm, with the volume fraction of metal being between 0.05-0.3 [6][7].

1.3.4 Additive Manufacturing Technologies

Additive manufacturing (AM) technology, commonly referred to as 3D printing, can produce complex, real life objects from virtual models created using computer aided design (CAD) software. There are a number of different metallic AM techniques available but the main principles are broadly applicable to all. Firstly the virtual model is broken down into cross-sectional slices. Then, slice by slice, a highly directional energy source (electron beam, laser, plasma arc etc), driven by the CAD system, selectively melts or sinters an additive layer of metal onto the one previous to build up the complete 3D structure. The source metal can be in powder or wire form. A fresh bed of metal powder can be swept across the build surface between each successive layer or powder/wire can be fed directly to the build surface through a nozzle. A schematic of a powder bed AM system is shown in figure 14.

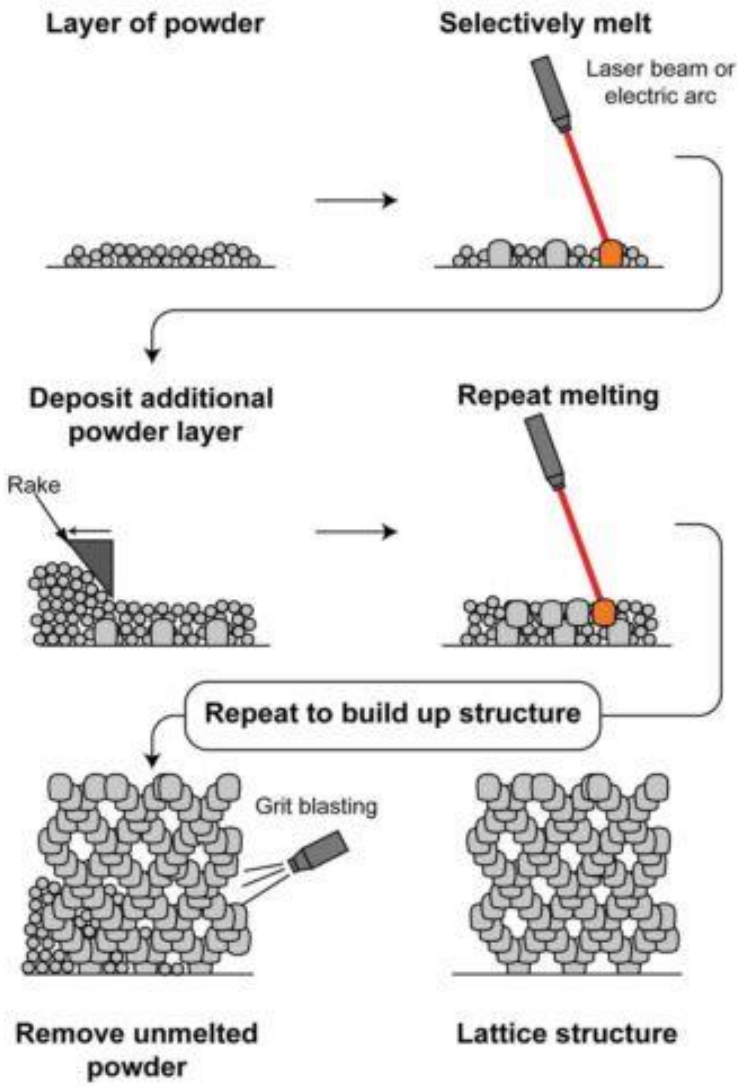

Figure 14. A schematic of the powder bed additive layer manufacturing process. Image sourced from [6].

The technique is most commonly associated with the manufacture of titanium parts and, although compatible, the commercial availability of aluminium powders is limited at present [80]. The method has however been included here due to the high degree of architectural control offered. Lattice structures are easily achievable; a single CAD element can be designed which is then repeated spatially to form the full structure. Creating original CAD models of foams with random pores may prove more difficult and would certainly require more computing time. Titanium foam has already been made using an AM technique called electron beam melting [81]; here, CT scans of an existing aluminium foam was used to create the

CAD model. As with other methods that make use of a template, the pore topology of the titanium foam in this case was defined and restricted by that of the original template foam. However, parts with extremely complex geometries are possible thus, given proficient software is available; essentially any pore size, shape or orientation could be achieved.

Cost and manufacturing time per part is often a limiting factor to this technique and for heat transfer applications it is likely that it would not be cost effective. If foams were to be produced using AM they would be better suited to high end applications or those where cost poses less of an issue such as in the medical, art/design and sports sectors.

1.3.5 REPLICATION / SPACE HOLDER

Replication methods, sometimes referred to as space-holder methods, employ a removable preform (the space-holder) material to produce a porous/ void-containing mould. As the mould is infiltrated the molten metal "replicates" the shape of the voids to create an inverted version of the preform. The space occupied by the preform material therefore becomes the pores within the foam once the metal has solidified and the preform removed.

Removal of the preform depends on the space-holding material used, which in turn depends on the metal/alloy used to create the foam matrix. Some examples of preform materials include salt (removed via dissolution in water) [82], bonded particulate material (disintegrated and removed via mechanical agitation) [83] and amorphous silica gel or sodium aluminate (both removed via dissolution in acid) [84][85]. Aluminium lattice structures made using a removable silica/resin preform are commercially available and are produced by Alveotec (Echirolles, France).

When producing aluminium open-cell foam, one of the most well suited techniques in terms of cost, simplicity and versatility is replication using a leachable preform such as sodium chloride (NaCl). The process is schematically shown in figure 15. With respect to aluminium (and various other metals), NaCl possesses all the

qualities required from a suitable preform material. Firstly, removal of the preform is straightforward as it can be very easily dissolved in water. Secondly, and perhaps most importantly, it is chemically compatible with the aluminium at all stages of the process. During infiltration, processing temperatures reach around 750°C; NaCl remains stable with a melting point of around 800°C and is chemically inert when in contact with the molten metal [8]. During the preform dissolution stage the salt solution has little corrosive effect on aluminium, especially over the short time periods taken for the leaching process to complete [8].

Aluminium foam produced using the NaCl space-holder technique is commercially available from Exxentis (Wettingen, Switzerland).

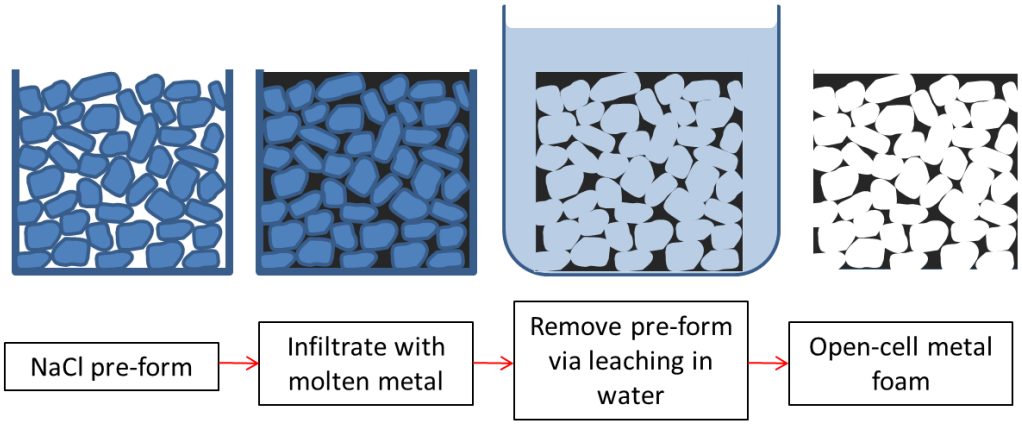

Figure 15. Schematic of the NaCl space-holder technique to produce open-cell metal foam.

Using the standard NaCl replication technique some of the basic architectural parameters can be controlled. The percentage porosity can be manipulated by densifying the NaCl preform and/or varying the infiltration pressure [86][87]. The average pore size can also be varied in a controlled manner simply by sieving the salt to produce mono-sized particles prior to preform manufacture [86]. The size of the pore openings or windows can be varied by adjusting the infiltration pressure, preform particle size, surface tension of the molten metal (for example through alloying) or wetting angle between the molten metal and particle [31]. Although efforts have been made to counteract the issue, one of the main drawbacks of the technique is still the lack of control over the pore topology; specifically the shape of

the pores. Goodall et al (2007) [82], Despois et al (2006) [86] and Gailard et al (2004) [88] all produced foams with different pore geometries by altering the initial shape of the salt particles used to make the preform. A variety of differently shaped cubic salt particles were produced via antisolvent precipitation [88] and spherical particles were produced by melting and re-solidifying the salt [82][86]. Scanning electron microscopy images show that the pores of the resultant foams duplicate well the inversed-form of the different salt shapes. Goodall et al (2006) [87] found that the pore shape could also be altered by using different preform densification methods. Preforms densified by cold pressing produced metal foams with irregular/jagged ligaments whereas preforms densified by sintering at high temperatures resulted in metal foams with more rounded ligaments.

When using the NaCl replication technique, as previously explained, the space occupied by the preform material goes on to become pores within the foam once the mould has been infiltrated and the preform removed. It is obvious therefore that the pore shape is predominantly (although not entirely) controlled by the initial shape of the material/particles used to produce the preform; an observation supported by the studies discussed above. With this concept in mind, a novel technique based on the standard NaCl replication method has recently been devised to overcome the pore-topology control obstacle [9]. The technique, named the “salt-dough technique”, contains additional preform processing steps so that although still using NaCl as the preform material, it is not used directly in its standard particulate form. A brief explanation of the process is given below, however a more detailed description is given by Goodall et al (2007) [9]. Figure 16 shows a schematic of the salt dough replication process in its entirety. The first step is to combine the major preform component; salt, with flour and water to produce a salt-dough, hence the naming of the technique. The consistency of the dough enables it to be formed into many different shapes, defined either by the fabricator (if shaped by hand) or by the geometry of the equipment (if using conventional shaping techniques such as extrusion). In order to make permanent the shape and to pyrolize the flour component, the dough is then heat treated at temperatures of around 500°C. The resultant salt “shapes” can then be used to make up the preform, and in turn the aluminium foam, in the same manner as in the standard

replication technique previously described. The formability of the salt-dough allows almost any shape to be created and thus almost any shape to be mimicked in the pores of the foam [9]. This technique is under development by Constellium (Schiphol-Rijk, The Netherlands) and their foams have been given the brand name "Corevo".

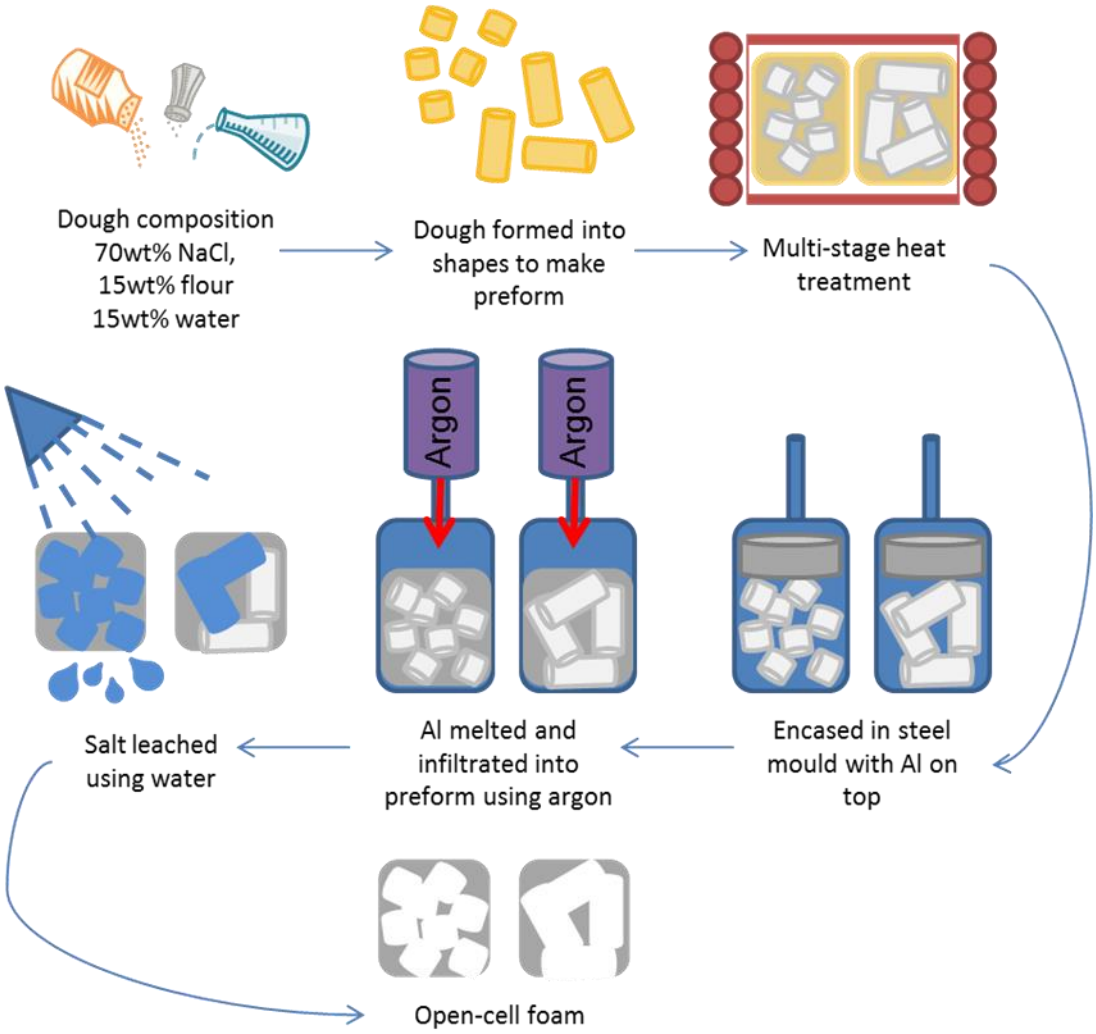

Figure 16. Schematic of the "salt dough" technique to produce open cell foam, currently under development by Constellium.

1.3.6 CHAPTER SUMMARY

There are various methods currently available to produce aluminium or copper open cell foam including those based on casting, powder metallurgy and gas

deposition. Most of the methods allow some control of the porous architecture, namely the overall porosity and the pore size. Controlling the shape of the pores however appears more difficult and out of the methods discussed only two fully had the ability to do so.

Additive layer manufacturing can produce porous metal structures with architectures entirely user defined. However, the high cost and lengthy manufacturing time means this method is currently suited for high end products and is commercially unrealistic as an option to produce foams for heat transfer applications.

The “salt dough” replication/space-holder technique allows close control over the pore size and shape whilst maintaining relatively low manufacturing costs. This method is therefore suitable for exploring the relationship between pore architecture and heat transfer behaviour. Furthermore, any beneficial changes to the foam mesostructure could be implemented industrially within the existing pilot scheme currently under development by Constellium, to be ultimately exploited in heat exchanger design.

1.4 STRUCTURAL CHARACTERISATION

Solid material can be described in terms of the microstructure (small scale features <100µm such as phases, grains, defects etc.) and the macrostructure (the overall dimensions of the component >1mm). Porous materials such as metal foam can also be described on the structural level in-between these, often referred to as the mesostructure. This scale generally describes the architecture of the pores and/or struts and incorporates parameters such as pore size, pore shape, pore orientation, wall thickness etc. Many properties of metal foam are a direct consequence of pore architecture or are at least strongly affected by it, quantification of these parameters is therefore particularly important. To do this, a number of characterisation techniques can be applied to metal foams using the same

principles as for solid, non-porous material. Some commonly used techniques are discussed below.

1.4.1 DENSITY

The density of metal foam is defined by the volume fractions of both metal and gas. As with solid metal, density can be calculated simply by dividing mass by volume however, this is assuming the shape of the foam is regular and its volume can be calculated using measurable dimensions.

When determination of volume cannot be easily calculated, Archimedes principle (the volume of fluid displaced by an object is equal to the volume of said object) can be applied and volume can be measured using a density meter. In this case, as open-cell foams are permeable, the foam must first be coated with a barrier material (e.g. a polymer film, wax, grease) to prevent liquid penetration and in turn the mass of the barrier material must then also be taken into account.

So that it can be more easily compared, an effective way to convert density into a dimensionless property is to relate it to that of the solid i.e. the relative density. Relative density is calculated by dividing the mass of foam for a specific volume, by the mass of the solid material if occupying the same volume. Typical metal foams have relative densities ranging between 0.03 to 0.3 [89]. Terms relating to relative density include metal volume fraction, mass density and porosity (the inverse of relative density) amongst others.

1.4.2 OPTICAL AND SCANNING ELECTRON MICROSCOPY

Optical microscopy can be a useful characterisation tool and allows 2D imaging of a number of different parameters on the mesostructural scale. To provide reliable

sections ready for imaging with optical microscopy, the foam must first be carefully sectioned, fully impregnated with resin and then polished using conventional techniques. This provides contrast between the walls of the pores and their interior. Due to the preparation steps, optical imaging can be best described as a destructive testing technique. An example of an optical micrograph after different stages of sample preparation and image analysis is given in figure 17.

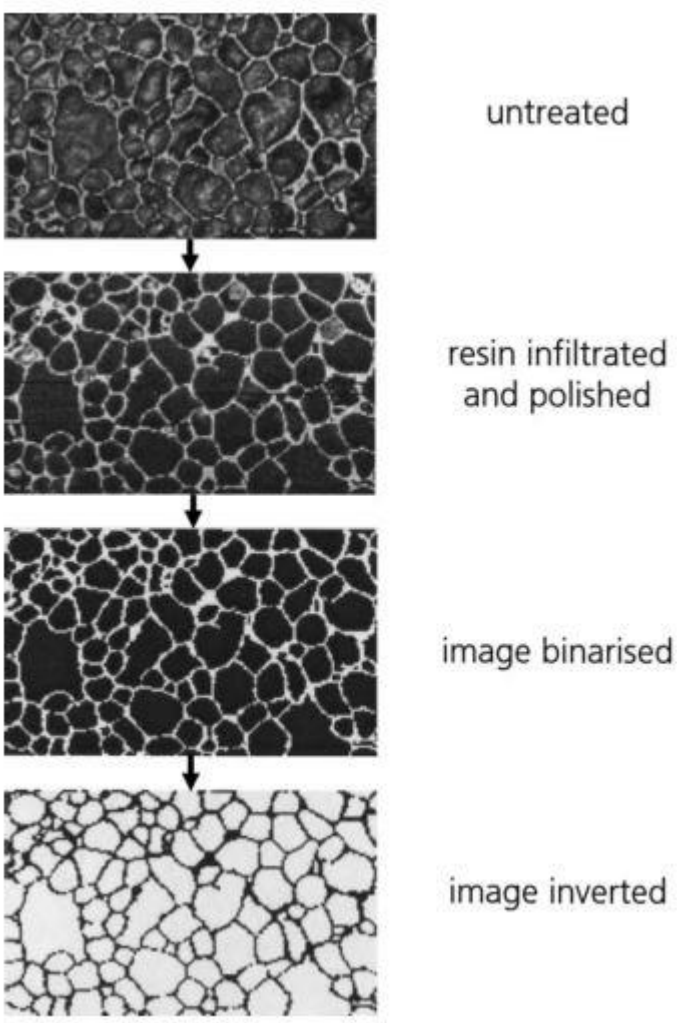

Figure 17. An optical micrograph of metal foam after different stages of preparation and analysis. Image sourced from [4]***.***

Scanning electron microscopy (SEM) is another imaging technique that can be used in the structural characterisation of porous metal. Unlike optical microscopy, SEM does not require multiple stages of sample preparation, especially as metal foams

are naturally conductive. SEM is particularly useful in displaying depth of structure for open-cell foams.

Characterisation of the pore structure, including geometrical features like pore shape/size/distribution as well as metal/pore volume fractions, can be derived from the analysis of cross sections. Such quantitative image analysis can be carried out using commercial image analysis software or manual methods such as point or lineal counting. When using automated software programmes in the analysis of open-cell structures, often an amount of manual image processing and/or watershed/thresholding transformations are required to distinguish individual pores prior to any representative measurements being taken [90]. In order to produce meaningful results, a large number of features should be evaluated in order to compensate for the random nature of foams. Due to the complexity of the foam structure, not enough information can be gained from 2D images to reliably and fully characterise all aspects of the structure.

1.4.3 TOMOGRAPHY OF POROUS MATERIAL

X-ray CT is particularly useful as it provides a powerful but completely non-destructive method of structural analysis. In simple terms, the technique works by rotating the foam sample around a single axis whilst an extensive series of radiographs are taken. The 2D images can then be mathematically reconstructed to produce a 3D image. Metal foams are well suited to the technique as the metal and air components exhibit vastly different x-ray absorption behaviour, thus allowing good contrast between the two phases.

The reconstructed 3D image can be used qualitatively to compare different structures or to inspect for internal defects. It can also be used for quantitative measurement of complex architectural features such as pore window size, strut size, wall defects, wall thickness distribution, density fluctuation and surface area. For open cell foams again methods for pore separation are often required.

X-ray CT for 3D image analysis of foam structures has been widely utilised and featured in numerous studies in the literature [91][92][93][94][95]. Additionally, cross sectional slices (much resembling those attained using optical microscopy) can be taken from the reconstructed volume and processed in the same manner as for other 2D image analysis. Figure 18 shows a 2D and 3D image of a metal foam produced using X-Ray CT.

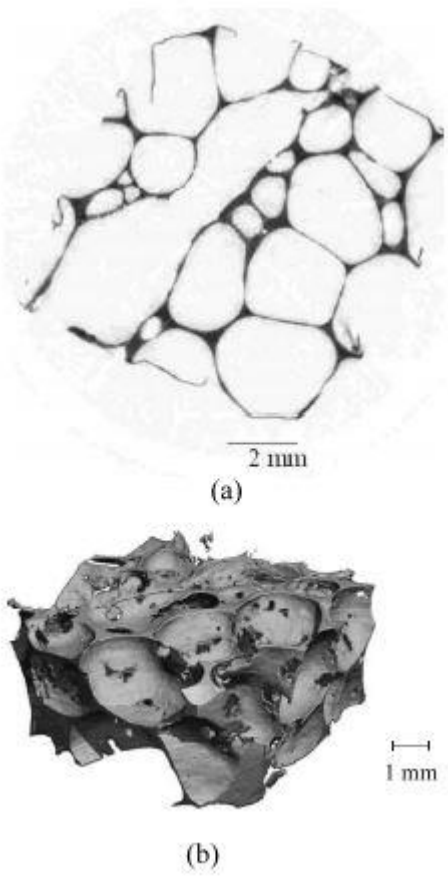

Figure 18. a) A 2D cross sectional image and b) a 3D reconstructed image of a metal foam. Image sourced from [95].

1.4.4 Chapter Summary

Various techniques for qualitative and quantitative structural characterisation of open cell foams are available. Often conventional techniques that are used to

examine dense structures can also be applied to porous material although, due to the inherent randomness of foams, more extensive assessment is required. Both 2D and 3D examination of the different structural parameters is common and although no standard techniques yet exist for foams, methods are well developed. Which technique is most appropriate depends on the specific parameter being measured and whether it can be translated from 2D to reliably describe the 3D structure.

1.5 Heat Transfer Capability Of Foam

As discussed in section 1.2.2, heat transfer applications have been identified as a key application sector for open cell metal foams. Open-cell metal foams are particularly suited to heat transfer due to their permeability and high conductivity of metal in combination with their ability to withstand high gas pressure, irradiation and high temperatures.

The material, from which the foam is made, coupled with the structural architecture defines the overall heat transfer capability of a particular foam. In turn, different service conditions can cause changes to the fluid flow and active heat transfer mechanisms. The interactions are complex but heat transfer behaviour can be separated into two distinct categories, thermal transport and fluid flow, these are discussed below.

1.5.1 Thermal And Fluid Flow Properties

1.5.1.1 General Mechanisms Of Heat Transfer

Relating fundamentally to the laws of thermodynamics, the transfer of thermal energy between systems occurs due to temperature differences/gradients across

those systems. There are three fundamental modes by which this transfer of energy can occur; conduction, convection and radiation.

Conduction relates to the transfer of heat when a temperature difference occurs within one or more bodies that are in direct thermal contact with each other. Heat transfer through conduction occurs due to particle interactions in a stationary medium and is not concerned with flow or mixing; it is therefore mostly, but not entirely, associated with heat transfer through solids. Equation 1 gives energy transfer as described by Fourier's law of heat conduction;

$$q_x = - k A (\partial T/\partial x) \qquad \text{(Equation 1)}$$

where; q_x is heat transfer in the x direction (W), k is the thermal conductivity of the medium (W/mK), A is the area normal to the direction of heat flow (m^2) and $(\partial T/\partial x)$ is the temperature gradient (K/m).

Convection is heat transfer relating to the motion of fluid and occurs at surfaces, over which flow is occurring. The transfer of heat energy is a result of molecular diffusion and bulk flow in combination. The rate of transfer is defined by the fluid properties and is independent of material properties relating to the surface. However, any interactions with the flow (by for example the surface shape/roughness) will influence heat transfer.

If flow is induced by an external force such as a pump, heat exchange is said to occur via forced convection. Alternatively fluid motion can occur as a result of buoyancy forces arising from temperature variations in the fluid; in this case heat is transferred via natural convection. Forced convection conditions tend to create more rapid fluid flow and in turn typically achieve increased rates of heat transfer.

Using the example of uniform flow over a heated plate, the heat transferred through convection is given by equation 2.

$$q_c = h_c A (T_p - T_f) \qquad \text{(Equation 2)}$$

where; q_c is heat transfer by convection (W), h_c is the average convective heat transfer coefficient (W/m^2K), A is the surface area of the plate in contact with the fluid (m^2), T_p is the uniform, maintained temperature of the plate (K) and T_f is the free stream temperature i.e. the temperature of the fluid far from the plate (K).

Radiation is the transfer of heat energy by way of electromagnetic waves. Unlike conduction and convection, radiation does not require a material medium for energy to be transported and so radiative heat transfer can even occur in a perfect vacuum.

Regardless of temperature, all surfaces absorb and emit thermal radiation. The rate at which heat energy is transferred, given in equation 3, is related to the Stefan-Boltzmann law; this states that heat radiation is proportional to the fourth power of the absolute temperature of the surface.

$$q = F \sigma A (T_1^4 - T_2^4) \qquad \text{(Equation 3)}$$

where; q is rate of radiative heat transfer, F is a factor relating to geometry and surface properties, σ is the Stefan-Boltzmann constant ($5.67x10^{-8} W/m^2K^4$), A is area of the emitting surface, T_1 is absolute temperature of emitting surface, T_2 is temperature of absorbing surface and $T_1 > T_2$.

1.5.1.2 Thermal Conductivity Of Foam

The thermal conductivity of metal foam is always lower than the bulk metal from which it is made [36]. Unlike the solid material, to determine the apparent thermal conductivity of metal foam a number of different influences should be considered; the thermal conductivity of solid metal that makes up the cell walls, the thermal

conductivity of the gas/fluid within the pores, convection occurring within the pores and radiation along the surface of the pores. In addition, thermal conductivity is further complicated by the presence of surface oxides and cracks [36].

This said, conduction through the solid is by far the most dominant heat transfer mechanism for metal foams. In contrast, heat conduction through the gas/fluid contributes so little to the thermal conductivity that it can essentially be dismissed [6][36]. Whilst the contribution from fluid convection is less important to consider in closed-cell foams, for open-cell foams, fluid convection through the interconnected pore network can occur. However, as pores get small it too becomes insignificant.

Due to the opacity of metal, radiation through the solid is not possible nevertheless, the porous network does allow for electromagnetic radiation to be reflected, emitted and absorbed at the pore surface. At moderate temperatures, the influence from radiative heat transfer on the effective thermal conductivity of metal foam is practically negligible [6]. This is especially true when the conductivity of the cell wall material is greater than $20 Wm^{-1}K^{-1}$ [36], as it would be for aluminium. However, as discussed previously many applications involve the use of metal foams at elevated temperatures; when this is the case radiative heat transport may make a significant contribution to the foams overall thermal conductivity [96].

A huge number of models can be found in the literature relating to the estimation of effective thermal conductivity of porous media. The models fall into three main categories; asymptotic solutions (upper and lower bounds), empirical correlations (fitting of experimental data) and unit cell approaches (theoretical models based on geometries). A review paper has been recently published and provides evaluation of those models with specific applicability to estimating the effective thermal conductivities of aluminium foams [97]. For relatively high density aluminium foams like those produced using replication/space-holder techniques, it has been suggested that the differential effective medium (DEM) models to estimate thermal conductivity as a function of volume fraction porosity, provide good agreement

with experimental data [98]. The DEM models for non-conducting spherical and ellipsoidal phases are given in equations 4 and 5 respectively.

$$K_f/K_0 = (1 - V_p)^{1.5} \qquad \text{(Equation 4)}$$

$$K_f/K_0 = (1 - V_p)^{n} \quad n>1.5 \qquad \text{(Equation 5)}$$

Where; K_f is the thermal conductivity of the foam, K_0 is the thermal conductivity of the solid, non-porous metal and V_p is the volume fraction porosity.

1.5.1.3 FOAM PERMEABILITY

When evaluating the complete heat transfer behaviour of foam it is important to consider its permeability as well as its heat transfer capability. Both properties are important as enhanced heat transfer performance is generally accompanied by an increased pressure drop in fluid flow through the foam [4]; this can be a large drawback for some applications as greater power would be required to drive circulation of the fluid.

Unless extreme flow velocities and/or pore sizes are used, the fundamental law describing unidirectional fluid flow through porous metal structures is the Dupuit-Forcheimer modification of Darcy's law as given in equation 6.

$$-\partial P / \partial x = (\mu_f / K) v_D + \rho_f F v_D^2 \qquad \text{(Equation 6)}$$

Where; P is the pressure in the fluid, x is distance along the direction of macroscopic flow, μ_f is the dynamic viscosity of the fluid, K is the Darcian permeability (m^2), v_D is the superficial fluid velocity, ρ_f is the density of the fluid and F is the form coefficient.

In theory, the quantification of a foams resistance to fluid-through-flow, as a measure of its permeability, is straightforward and the experimental set-up relatively simple. As described in ref [6]; a fluid, which could be a gas (air) or liquid (water), is forced to flow through a straight section of metallic foam. If a constant volume/mass of fluid per second is imposed across the sample, the pressure differential across the test specimen (ΔP) can be measured and used as an indication of the foams permeability or vice versa. Various test set-ups have been used [99][100][101][102][103][104] however, although there are various standards for measuring the permeability of rigid porous materials, these standards do not specify the required geometry of the sample or sample holder [105] (see section 1.5.1.6 for more information on sample size).

1.5.1.4 KEY MEASUREMENTS

Throughout the literature, a number of common measurements are used to describe heat transfer and fluid flow behaviour of metal foams.

The effective heat transfer coefficient (H_c) is used as a measure of thermal performance. It is related to heat flux as given in equation 7 [5]. An increase in H_c shows an increase in heat transfer performance.

$$q = H_c \Delta T \qquad \text{(Equation 7)}$$

where; q is the heat flux per unit area, H_c is the effective heat transfer coefficient and ΔT is the temperature difference between the hot surface and the fluid.

The Nusselt number is the dimensionless heat transfer coefficient. It denotes the enhancement of heat transfer across a fluid as a result of convection relative to conduction. Heat transfer by conduction alone would have a Nusselt number of 1 [106]. For cellular metal it can be calculated using equation 8 [107].

$$N_u = h\,L / k \qquad \text{(Equation 8)}$$

where; h is the convective heat transfer coefficient, L is characteristic length and k is the effective thermal conductivity of the metal foam.

The Reynolds number describes the degree of turbulence in the fluid flow; the higher the Reynolds number the more turbulent the flow, the lower the Reynolds number the more laminar the flow [106]. For flow through porous media, the Reynolds number can be calculated using equation 9 [17].

$$Re = (\rho\, V\, l) / \mu \qquad \text{(Equation 9)}$$

where; ρ is the fluid density, V is fluid velocity (m/s), l is a length scale for the Reynolds number and μ is dynamic viscosity (Pa.s). Various length scales have been suggested including $\sqrt{K}$ where K is the permeability or average pore diameter, Dp [99].

The Prandtl number is used to express the relative thickness of both the velocity and the thermal boundary layers [106]. The Prandtl number can be calculated using equation 10 [52].

$$Pr = \mu\, C_p / k \qquad \text{(Equation 10)}$$

where; μ is dynamic viscosity (Pa.s), Cp is specific heat capacity and k is thermal conductivity (W/mK).

1.5.1.5 TEST CONDITIONS

There are numerous measurements, and thus test configurations, which allow data collection to characterise heat transfer and fluid flow for metal foams. As described previously, fluid flow may occur by one of two mechanisms. The flow may be

induced by an external force such as a pump; in this case heat exchange occurs via forced convection. Alternatively heat exchange can occur via natural convection; this is caused by buoyancy forces arising from temperature variations in the fluid. Techniques have been employed to characterise heat transfer under both flow conditions; forced [1][108][109] and natural [110][111][112]. Furthermore, gas (air)[52][103][113][114] or liquid (commonly water)[47] can be used as the circulating fluid. Depending on fluid and flow type, testing systems can be closed-, open- or mixed circuit type.

1.5.1.6 Sample Size

It has been observed that dimensional differences between samples of similar foam types can cause variation in experimentally obtained permeability values. The same is true for geometric differences in the sample holder. For pressure drop measurements (as an indication of permeability), such differences have most commonly been attributed to entrance/exit effects [6][115][116] and sample/sample-holder boundary effects [6][105][117][118]. In addition, the type and velocity profile of the flow will also affect how strongly the pressure drop is influenced [17]. Due to lack of information in the literature, it is still unclear what sample thickness is sufficient to avoid these effects although various critical values have been suggested. Examples include; a sample to pore size ratio greater than twenty [6], fifty times the pore size for foams with pore diameters between 0.4-0.9mm [115] and 100 times the pore size for foams with pore diameters between 1.06-4.23mm [116]. It can be concluded that when measuring the permeability of foam, it is important to consider the thickness of the test specimen with respect to the aim of the investigation. If determining foam permeability as a bulk material property it is paramount to avoid exit/entrance and wall effects as much as possible. This requires the length and diameter of the test sample to be significantly larger than the foam pore size. The specimen holder must also be tightly fitting (as to not let fluid flow around the sample) but should not constrict

the flow (i.e. the flow is exposed to the entire sample diameter) [6]. Alternatively, studies may use a sample thickness that better represents the intended application, however in this case it should be acknowledged that the measurements will be specific to the individual test set-up, may not represent the bulk material and may not be directly comparable to associated data presented by similar studies in the literature.

1.5.2 Thermal Property-Foam Structure Relationships

Enhanced heat transfer behaviour is achieved by maximising thermal conductivity whilst minimising flow resistance [4], and these must therefore be the desirable features of a metal foam for a heat exchanger. This is however hard to realize as the characteristics are conflicting. For example; it is generally accepted that increasing the foam internal surface area and/or density increases heat dissipation but also increases the pressure drop in fluid flow through the foam [56][57]. By tailoring the structure of the foam an optimum balance between the two may be reached; where the optimum lies depends on the specific application. Exploitable structural parameters include (but are not restricted to); density, porosity, cell connectivity, pore size and pore geometry [57][119]. Due to the difficulty in implementing and measuring controlled structural changes, the thermal property-structure relationship is not as yet very well characterised. This is especially true for the pore shape-heat transfer behaviour.

A number of studies have measured the effect of foam morphology on the heat transfer performance using various experimental set-ups. Mancin et al [114] explored the heat transfer behaviour of aluminium open-cell foams that varied in porosity and the number of pores per inch (PPI); this latter quantity is a measure of the pore size. The foams were electrically heated and then cooled with air under forced convection conditions in an open circuit type, wind tunnel, test rig. Various

temperature and flow measurements were made at a number of different fluid flow rates; these were used to calculate heat transfer coefficients. It was found that at constant PPI, the lowest porosity/ highest relative density samples generated the highest heat transfer. This was attributed to an increase in surface area and improved surface area efficiency. For all samples the global heat transfer coefficient increased when the air mass flow rate increased.

Reutter et al [120] also used a forced convection set-up to heat transfer test nickel foams with differing porosities. During each test, an air flow with sinusoidal alternating temperature was driven through the foam. The presence of the sample caused a phase shift and an attenuation of the temperature wave which was measured and used to calculate the volumetric heat transfer coefficient. Separate tests were performed on the samples in order to measure the fluid flow pressure drop across the foam. In addition, test measurements were generalised by using the properties of air to calculate the Nusselt, Reynolds and Prandtl numbers. The study found again that the higher density samples showed higher heat transfer but also caused a higher pressure drop.

Although the above studies identified a trend between porosity and heat transfer behaviour the range of porosities explored was limited; in particular, the foams used were generally very low density. To try to overcome this Boomsma et al [47] investigated the heat exchange performance of open-cell aluminium foams that had been compacted by differing amounts and compared them to a number of commercially available heat exchangers. A forced convection flow arrangement was used whereby the coolant flow (water) was directed through a foam sample whilst it was heated. The test data was used to calculate various parameters used to describe fluid flow and heat transfer characteristics including the pressure drop across the foam, the Reynolds number and Nusselt number. The most compacted foams (lowest porosity) were found to generate the largest Nusselt values and the largest pressure drops, again reinforcing the conflicting relationship between flow resistance and heat transfer. The foams overall were found to make a significant improvement in heat exchange efficiency over several commercially available heat exchangers. This should also be seen in the light of the fact that a foam that has been compacted to achieve a particular density is likely to have more tortuous

conducting pathways (and therefore be less efficient at conducting heat) than one that has been produced with the required fraction solid.

1.5.3 Chapter Summary

Heat transfer and fluid flow through porous media has been widely studied and methodologies are well developed. With respect to relationships between heat transfer and the structure of metal foam, a number of studies have identified that increasing the internal surface area and/or density increases heat dissipation but also increases the pressure drop in fluid flow through the foam. However, implementing and measuring controlled structural changes to metal foams is difficult thus the thermal property-structure relationship is not as yet very well characterised. Information relating to pore shape-heat transfer behaviour is especially limited.

1.6 Overview

Due to a distinct lack of information in the literature, one of the primary aims of this work is to provide key data to demonstrate how the mesostructure (the arrangement and shape of the pores) of aluminium foam influences its heat transfer behaviour.

The foam manufacture route is via an innovative replication process that is currently being investigated for commercial production by the company Constellium, who is also highly involved in the project. The process is unique with respect to the degree of control over the pore shape, size and aspect ratio, whilst remaining realistic for heat transfer applications in terms of cost.

Once novel-structure foams have been produced, heat transfer testing in a bespoke rig can provide heat transfer coefficient and pressure drop data. In

addition, 3D imaging using x-ray tomography has been identified as a well-developed technique for quantification of the pore structure.

The results of the work will greatly enhance the fundamental understanding of metal foam processing-property links, which will be of great interest to the metal foam community; including both the scientific and industrial divisions.

2. STANDARD EXPERIMENTAL METHODS

2.1 SCANNING ELECTRON MICROSCOPY

Samples of the preform material (see section 3.3 for details) used for foam manufacture were mounted in resin, under vacuum, using a cold mount (Citovac, Struers) and a pressure of 4bar. These were then left to cure for approximately 12 hours. Once hardened, the bottom surfaces of the mounted samples were ground away to expose cross sections of the preform; this was done using a grinder/polisher with P400/P250/P120/P80 papers and without water (to prevent leaching of the salt, which is the primary constituent of the preform). To avoid surface charging, the exposed faces were sputter coated with carbon and conducting links to the sample holder were painted on the sample edges using liquid silver paint (silver dag). Samples were imaged at various magnifications using SEM, operated at 15kV in secondary electron mode (JEOL JSM 6400 SEM).

2.2 FOAM MANUFACTURE

An infiltration rig for the manufacture of aluminium foam via a NaCl replication technique had been previously developed in work at Sheffield [121][122] and is described below.

The NaCl being used as a space-holding preform is placed inside a cylindrical steel mould that has been pre-coated with boron nitride spray (Kennametal Sintec) for the purpose of avoiding adhesion between the mould and the material being cast.

A block of aluminium (99.85%, William Rowland LTD.) is then placed on top of the preform before bolting the mould between two steel plates with graphite paper gasket seals, see figure 19a. An opening in the top plate allows a gas pipe to be connected to the mould, which is then placed into the centre of a furnace (TLCF10/27, Elite Thermal Systems LTD). A vacuum system (Edwards LTD) and pressurised argon cylinder (BOC) with flowmeter (BOC) and pressure regulator (8500 Series, BOC) are secured onto either side of the gas pipe and a vacuum is established. The furnace is heated to 740°C at a rate of 20°C/min and the sample is left to dwell for 1 hour 45 minutes in order to heat the interior of the chamber and melt the aluminium. The complete infiltration rig set-up is shown in figure 19b.

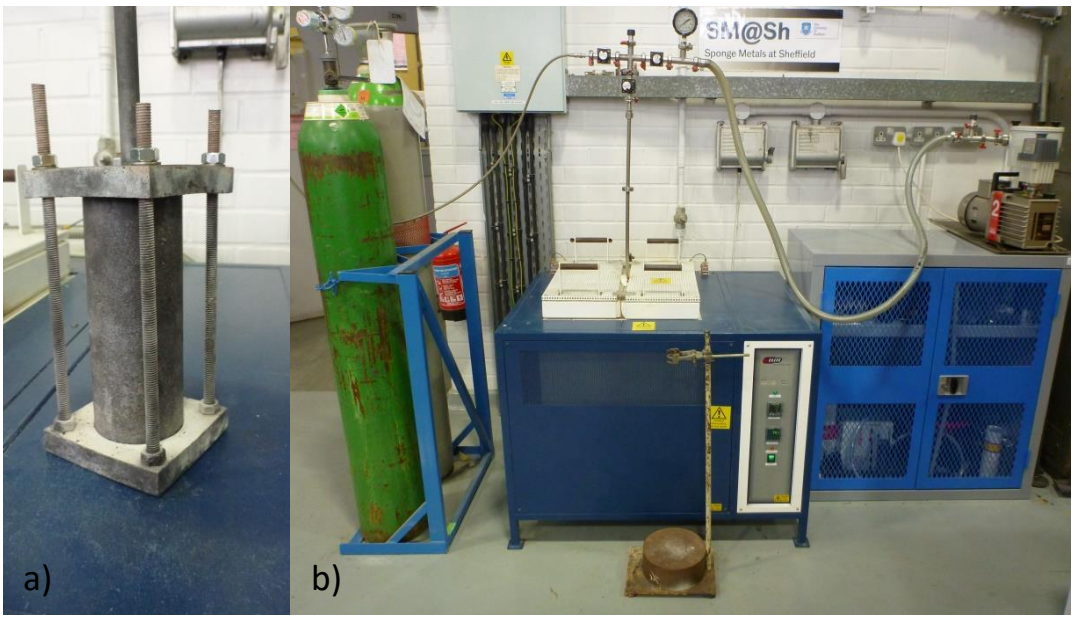

Figure 19. The in-house infiltration rig at University of Sheffield a) mould and b) overview.

Once melted, the infiltration of the aluminium into the preform is achieved by releasing the vacuum and quickly forcing argon on top of the melt at a pressure set by the user. After 30 seconds the argon is shut off and the mould removed from the furnace. The mould is placed on a copper block to promote unidirectional cooling, such that final solidification shrinkage took place outside the main sample and could be machined away. After 45 minutes the sample can be removed from

the mould and the top and bottom edges (including excess aluminium) removed using a mechanical hacksaw. The NaCl is leached by immersing the sample in water overnight.

The rig/method described formed the basis of the in-house foam manufacture method used in this work. Various modifications allowing the use of a salt-dough based preform have been explained in the relevant sections below.

2.3 SAMPLE MANUFACTURE

Throughout the work, foam has been produced both by the company Constellium and in-house at Sheffield. In both cases, individual samples were machined from the original foam blocks using a combination of mechanical band-saw cutting and wire-cut electrical discharge machining (W-EDM). EDM is generally used for the machining of electrically conductive material that is either especially hard or needs to be cut to complicated and/or precise geometries. In this case precision was essential in order to minimise thermal contact resistance between the foam and the copper cylinder used when measuring the heat transfer behaviour of the foam (see section 2.4). In addition, the process is non-loading and so the intricate structure of the foam is not damaged during cutting.

Described in detail in [123] and schematically in figure 20, the process of W-EDM removes material from a workpiece (the foam block) using high frequency electrical discharges, or sparks, in order to “cut-out” a pre-defined profile. To create two electrodes both the workpiece and tool, which in the case of W-EDM is a thin wire, are connected to a DC power supply that delivers high frequency electrical pulses. As the wire approaches the workpiece, a small space between the two is filled with deionised water (a dielectric fluid). When voltage is applied, the fluid in the gap becomes ionised allowing current to momentarily flow between the two electrodes in the form of a spark discharge; this erodes the material directly ahead of the wire. A constant flush of dielectric fluid creates an insulator-conductor cycle and material continues to be eroded as the wire moves forward. The fluid filled gap is

maintained throughout and the wire itself never actually makes contact with the workpiece. Machining of the samples in this work was carried out externally by Electrotech EDM Services LTD, Sheffield, UK. The device used was a Mitsubishi 110 SA with 0.25mm diameter brass wire (electrode) and de-ionised water (dielectric fluid).

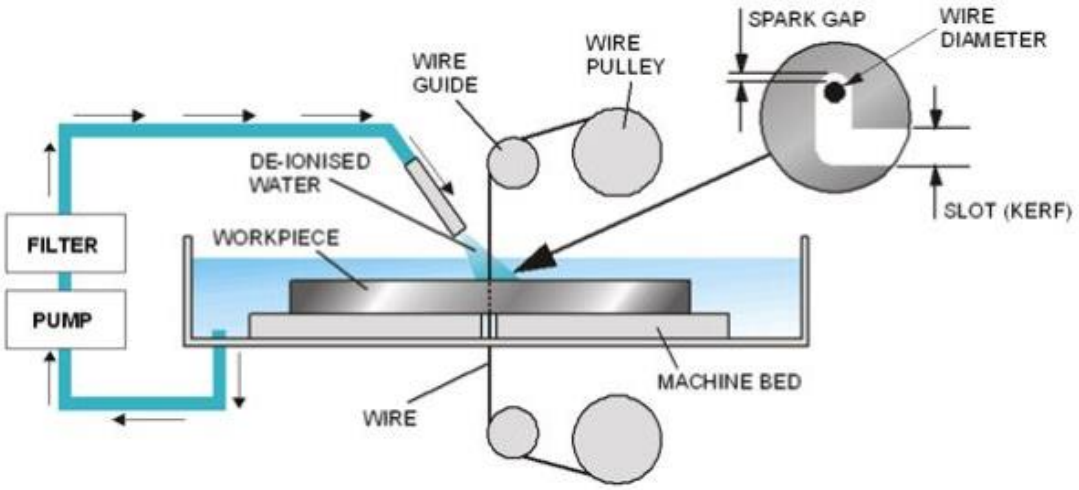

Figure 20. Schematic of the wire-cut EDM process [130].

Once machined, the exact dimensions and weight of each sample were measured using digital callipers with resolution of 0.01mm (Senator) and scientific scales accurate to 2dp. Density and percentage porosity values were calculated using equations 11 and 12 respectively.

$$\rho_{foam} = m_{foam} / V_{foam} \qquad \text{(Equation 11)}$$

where; ρ_{foam} is the density of the foam sample [g/cm^3], m_{foam} is the mass of the sample [g] and V_{foam} is the volume of the sample [cm^3] and is calculated as (π x radius^2 x length).

$$PP_{foam} = 100\ (1 - (\rho_{foam} / \rho_{metal})) \qquad \text{(Equation 12)}$$

where; PP_{foam} is percentage porosity of the foam sample, ρ_{foam} is the density of the foam sample [g/cm^3] and ρ_{metal} is the density of the metal used as the foam matrix material [g/cm^3]. For each type of metal used a set of three solid discs were machined from the stock material and their densities measured using a density meter; ρ_{metal} was then taken as the mean of the three disc density values.

2.4 HEAT TRANSFER MEASUREMENTS

To determine the heat transfer performance of a sample a specially constructed rig was used; this had been developed previously by another member of the research group [121][124]. The rig works by forcing a coolant through the foam whilst it is being heated; the set-up is shown in figure 21.

A foam sample is mounted inside a copper cylinder (see figure 21 for dimensions), which is pre-lubricated with a silicone-based heat transfer compound (Electrolube electro-chemical division). A 240V, 150W band heater (Watlow) is fixed around the outside of the copper cylinder and secured between two thermally insulating Macor ceramic discs (Corning Incorporated) that holds each end in contact with a steel chamber. Five 0.5mm diameter thermocouples surrounded by insulating wool are positioned along the copper tube at depths of 7mm (i.e. 1.5mm less than the thickness of the wall). The first (centrally positioned) is used to relay the temperature to the heater whilst the second (positioned closest to the air out chamber) records the copper temperature in contact with the foam. The remaining thermocouples are used to monitor the temperature profile across the cylinder length. Two additional 1mm diameter thermocouples are used to measure the temperature of the compressed air (the coolant) before and after it passes through the foam; these are inserted into the centre of each of the steel chambers. The temperature readings from all of the thermocouples are collected at a rate of three

data points per second and stored throughout the test by a data acquisition system. The hardware consists of a chassis (model cDAQ-9172, National Instruments) and two modules (model NI-9211, National Instruments). The associated computer programme was specially developed using a software package (LabView).

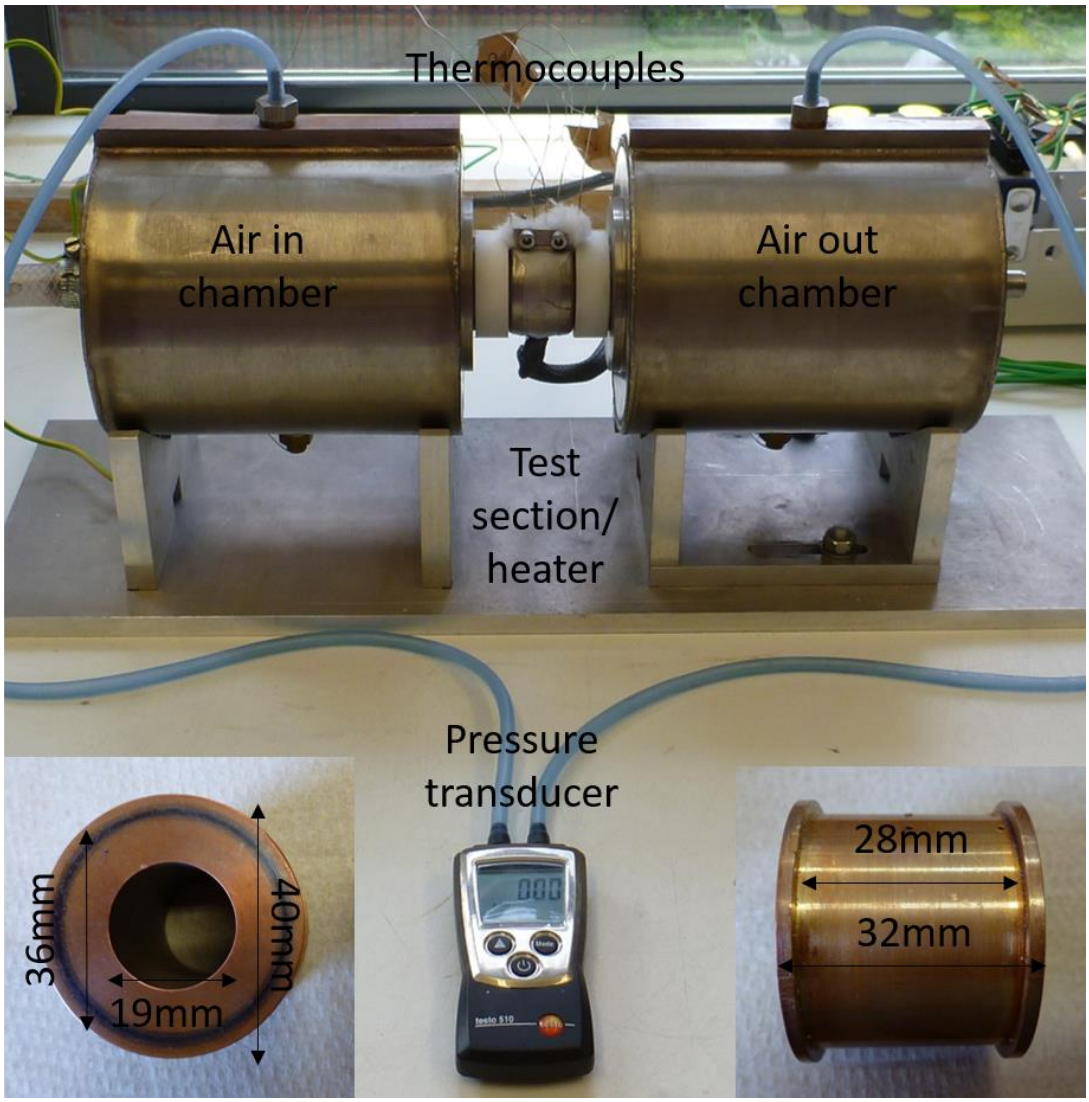

Figure 21. Rig for testing heat transfer and permeability of metal foams.

To achieve a starting temperature of approximately 150°C the band heater temperature is set to 152°C using a proportional-integral-derivative controller (PID controller) (EZ-Zone PM, Watlow) and a furnace power supply (Version 5.0, E.M Electronics Workshop, Dept. of Engineering Materials, University of Sheffield).

Once the temperature has been reached the system is left to stabilise for a further 3 minutes before the test commences; this is to ensure a uniform temperature throughout the entire sample.

Fixed flow rate conditions are used whereby compressed air from an industrial cylinder (Size N, 8.85m3, BOC) is forced through the first chamber, through the foam sample and out through the second chamber. The flow of the coolant is controlled by a flowmeter (BOC) and the pressure by a pressure regulator (Series 8500, BOC), which are set by the user before the test is started.

The test runs until steady state heat transfer behaviour is established; in previous work this was taken as being after 15 minutes [121][124]. During this time the pressure difference between the two chambers is also recorded using a pressure transducer with an operating range of 0-100mbar (Testo 510, Testo Ltd) or 0-500mbar (Model 2027P, Digitron) depending on the sample requirements. The pressure difference developed across the sample can be used as an indication of sample permeability.

For each test the following data is used for analysis:

- The gas flow rate, v [m^3/s]
- The mean temperature of the incoming air before passing through the foam, T_{in} [K]
- The mean temperature of the outgoing air after passing through the foam, T_{out} [K]
- The mean temperature of the copper cylinder, T_{Cu} [K]

Unless stated otherwise, mean values are calculated for the final minute of the test and are in turn used to calculate heat transfer coefficients using equation 13; a rearrangement of the heat flux equation.

$$H_c = q / \Delta T \qquad \text{(Equation 13)}$$

where; H_c is the heat transfer coefficient [W/m^2K], q is the heat flux transferred across an interface [W/m^2] and ΔT is the temperature difference across the interface [K].

The foam is treated as a system and so the interface is taken as the contact area between foam and heated copper cylinder, not the internal surface area of the foam. The temperature difference across the interface is calculated as T_{Cu}-T_{in}. The thermocouple used to monitor the copper cylinder temperature is intentionally positioned towards the far end of the copper cylinder close to the air out chamber. This gives the highest temperature reading and so provides a more conservative estimate of the heat transfer coefficient, and is that resulting from effects through the larger part of the sample.

The heat flux is the rate of heat energy transferred across an interface per unit time per unit area. The energy transfer per second is determined by multiplying together; the gas flow rate, v [m^3/s], the change in coolant temperature, T_{out}-T_{in} [K] and the volumetric heat capacity of air, Cv (Cv is calculated to be 1169.1J/mK using the specific heat capacity, 1.007J/gK and density, 1.161g/L of air at atmospheric pressure and 300K [125]). The energy transfer per second is then divided by the interfacial area [m^2] i.e. the surface area of the sample shaft, in order to give the heat flux [W/m^2].

The accumulative errors (+/-) for the heat transfer coefficients were estimated by performing recalculations that took into account the maximum potential error (+/-) associated with each of the individual measurements. This includes the flow rate, each temperature measurement and the interfacial area of the sample. The difference between these calculations and the original measured calculations gave the “worst case scenario” errors. For the pressure drops, the error was estimated using the standard deviation of the repeat measurements.

2.5 THERMAL PROPERTY ANALYSIS

Throughout the work foams have been made from commercially pure aluminium (Al_{pure}) (99.85%, William Rowland LTD), an aluminium-silicon-magnesium casting alloy provided by Constellium (Al_{Con}) and tin (99.75-99.9%, William Rowland LTD). To assist in comparing the foams heat transfer behaviour, thermal conductivities for the solid materials were measured using the laser flash technique [126][127]. The technique works by subjecting one surface of a sample of known thickness to a short energy pulse causing heat absorption. The temperature rise on the opposite face of the sample is recorded as a function of time and is in turn used to calculate the thermal diffusivity of the material using equation 14.

$$\alpha = 0.1388\ L^2/t_{1/2} \qquad \text{(Equation 14)}$$

where; α is thermal diffusivity, L is sample thickness and $t_{1/2}$ is the time taken to reach half of the maximal temperature increase.

Specific heat values can also be measured by comparing the time-temperature profile of the test sample to that of a reference sample (whose specific heat is already known) when tested under the same conditions. Thermal conductivity is then calculated using equation 15.

$$K = \alpha\ \rho\ Cp \qquad \text{(Equation 15)}$$

where; k is thermal conductivity, α is thermal diffusivity, ρ is density and Cp is specific heat.

The instrument used was the Flashline 3000 (Anter USA), which has a high speed Xenon discharge (HSXD) pulse source and infrared furnace. One reference disc of Al_{pure} and three sample discs each of Al_{con} and tin were machined from the stock material. An additional Al_{pure} disc was also machined to be used as a control. All discs were ground and polished using P400/P800/P1200 papers and 6/3/1µm

colloidal silica, which was watered down with Metadi fluid for polishing the tin. Exact sample dimensions were measured using digital callipers with resolution of 0.01mm (Senator). Samples were also weighed using scientific scales accurate to 2dp and density measurements were taken using a density meter. For all tests the Al_{pure} disc with sourced specific heat values (shown in table 1 [128]) was used as the reference sample allowing thermal conductivities to be calculated for the remaining samples.

Table 1. Thermal property data for Al_{pure} reference sample sourced from [128]

Temp. in °C	Temp. in K	Cp in J/mol.K	Cp in J/kg.K
26.85	300	24.25	898.81
76.85	350	25.11	930.69
126.85	400	25.78	955.52
226.85	500	26.84	994.81

Immediately prior to testing, each disc was cleaned using IPA and coated with graphite spray to aid the pulse absorption. All tests were run under a nitrogen atmosphere. The temperature programme was set to perform flashes, and thus calculate thermal conductivities, at 50, 100 and 150°C (Al_{pure}, Al_{con} and tin) and at 200°C (Al_{pure} and Al_{con} only), with a ramp of 5°C/min. Three repeat flashes were performed at each temperature with a constant power level of 500 for all flashes. The thermal conductivities for each metal type were taken as the average of the repeat measurements.

The accuracy for specific heat capacity measurement as stated by the manufacturer is +-5% (worst case). In addition, room temperature density values for the samples were used throughout regardless of the test temperature therefore thermal expansion of the samples was not taken into account.

2.6 X-RAY COMPUTED TOMOGRAPHY

A number of the foam samples used throughout this work were imaged using X-ray computed tomography (X-ray CT), allowing non-destructive inspection of the structures internally. The technology works by placing the sample between an x-ray source and detector. It is then rotated around a single axis in small steps whilst a series of 2D images, or radiographs are taken; these can then be mathematically reconstructed to produce the 3D image.

The system used was the Nikon Metris XTH225 housed in a customised bay at the Henry Molesley X-ray Imaging Facility, University of Manchester; this is shown in figure 22.

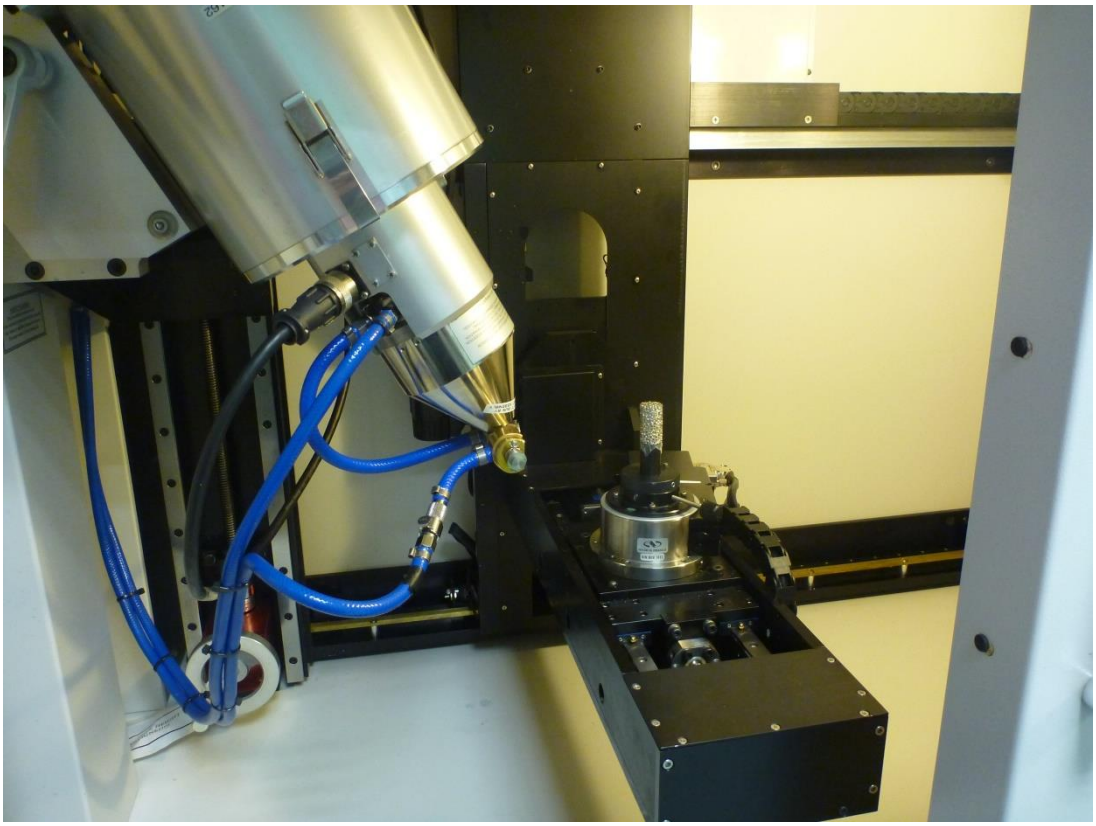

Figure 22. Foam sample being imaged using X-ray tomography at The Henry Molesley Imaging Facility, University of Manchester.

Images of the Al_{pure} and Al_{con} samples were taken over two sessions, in-between which the system was fitted with a new detector and therefore two different settings were used. For scan session one the exposure was set at 708ms and the

accelerating current and voltage of the x-rays at 250µA and 85kV respectively; this gave an effective voxel size of 20.7µm. A 0.1mm copper filter was also used to help reduce beam hardening. Beam hardening is a type of artefact or error in the image whereby the edges of a homogeneous sample can appear brighter than the bulk material. As a rudimentary explanation, this can occur because of complications in data acquisition resulting from the incident x-ray beam being polychromatic (i.e. made up of a spectrum of energies). The copper filter reduces the range of energies that make up the beam so the x-ray attenuation is more uniform throughout the sample.

For scan session two no filter was used, the exposure was set at 708ms, current at 148µA and voltage at 80kV; this gave an effective voxel size of 15.96 µm. To image the tin samples a 0.5mm copper filter was used and the current and voltage were increased to 150µA and 221kV respectively. The voxel size remained at 15.96 µm.

2000 x-ray radiographs were acquired for each sample and reconstructed into 3D volumes using Nikon Metris CT-Pro reconstruction software.

3. Development Of Foam Manufacture Method

The salt-dough replication technique (discussed in section 1.3.5 of the literature review), as practiced on a pilot industrial scale, was observed first hand at the Constellium factory; Sociétés de Fonderies d'Ussel (Ussel, Central France). Due to confidentiality restrictions some details of the industrial process have been omitted although a basic outline is given below and depicted in figure 23.

The dough composition was in the range of 50-80wt% NaCl, 5-20% flour and 15-25% water. Dough pellets were formed via an extrusion process and allowed to dry at room temperature before being compressed into a preform block; the compression pressure subsequently determined the percentage porosity of the preform and hence the foam. Each block then underwent a multi-stage heat treatment to fully dry and remove the flour prior to being encased in a sand mould. The mould was fed with an aluminium-silicon-magnesium (Al-Si-Mg) alloy to infiltrate the preform. Once solidified, the resultant block was composed of a foam core with dense outer shell, and therefore required machining before the salt leaching process could be carried out. After machining and leaching an optional age-hardening heat treatment could be administered so that the foam was either in the T6 or as-cast condition depending on customer requirements.

From the visit, key information was gained allowing the development of a laboratory protocol to commence; the objective being to produce foam samples as comparable as possible to those made at the factory. Various modifications to the protocol could then be made in order to produce foams with different

sized/shaped pores, thus allowing the effect of pore shape on heat transfer behaviour to be investigated. Where possible, any dough forming methods employed to modify the shape of the foam pores were developed with respect to the industrial process in order to maximise the potential for future industrial implementation.

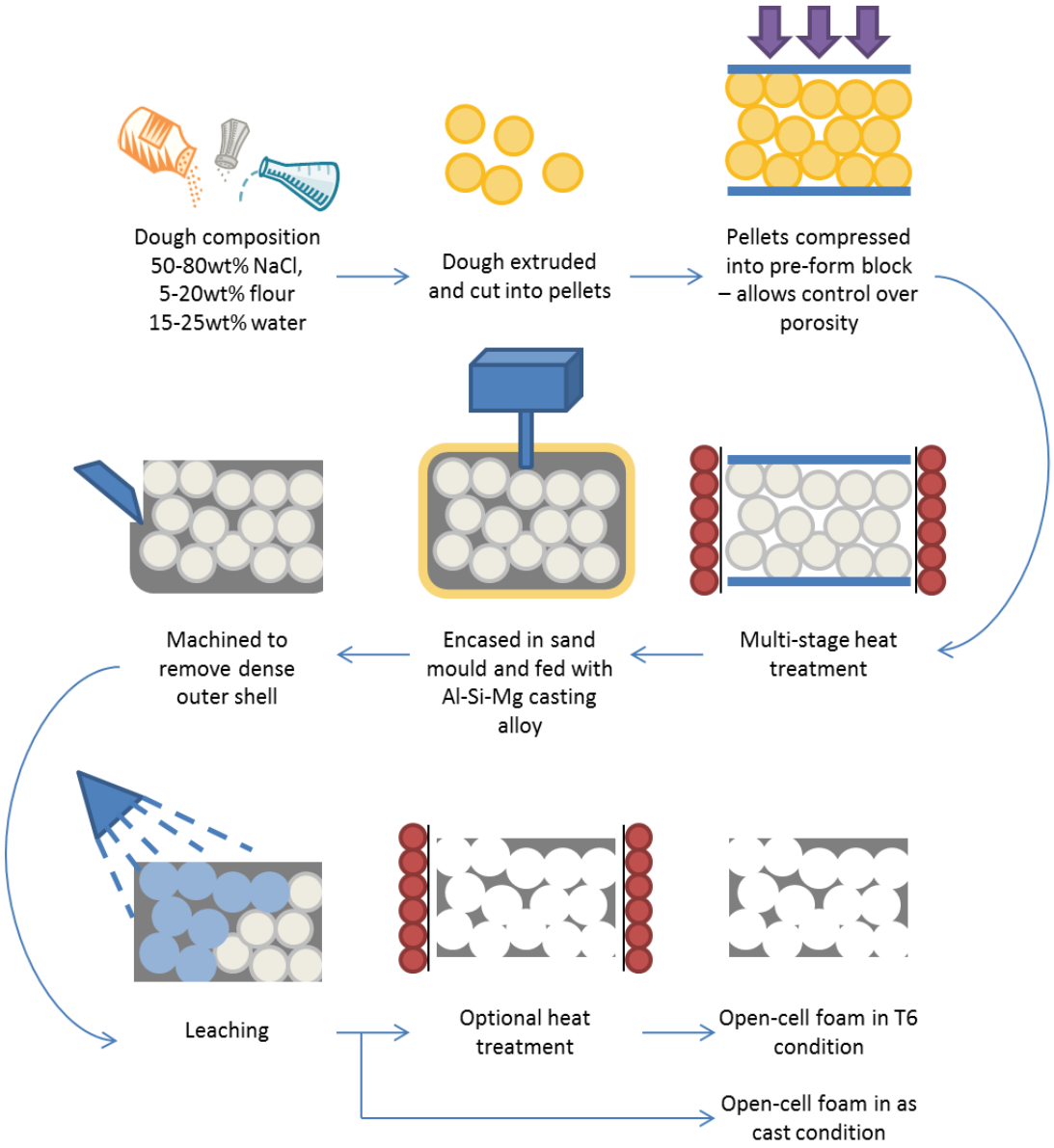

Figure 23. Schematic of the replication process used by Constellium.

3.1 DOUGH COMPOSITION

The compositional range of salt-dough suitable for laboratory scale preform production was investigated. The main considerations were that the dough; had the required workability to form shapes prior to heat treatment, had sufficient strength to be handled post-heat treatment, retained its shape throughout and the final preform was easily dissolvable.

Twenty-six different combinations of salt, flour and water were examined; these are shown in table 2.

Table 2. The various weight combinations of salt, flour and water used to determine the compositional range of dough suitable for laboratory scale preform production.

Sample Number	Nominal Preform Composition		
	Flour (g)	Water (g)	NaCl (g)
1	1	4	5
2	2	4	4
3	3	4	3
4	4	4	2
5	5	4	1
6	1	3	6
7	2	3	5
8	3	3	4
9	4	3	3
10	5	3	2
11	6	3	1
12	1	2	7
13	2	2	6

Sample Number	Nominal Preform Composition		
	Flour (g)	Water (g)	NaCl (g)
14	3	2	5
15	4	2	4
16	5	2	3
17	6	2	2
18	7	2	1
19	1	1	8
20	2	1	7
21	3	1	6
22	4	1	5
23	5	1	4
24	6	1	3
25	7	1	2
26	8	1	1

Prior to use the salt (General purpose grade, Fisher Scientific) was ground to a powder using an electric hand blender (Model HBS07, Tesco). For each dough composition the required quantities of constituents were measured using scientific

scales accurate to 2dp (XT6200C-FR, Precisa balances LTD). The dry ingredients; flour (Shipton Mill) and ground salt were added to a beaker and mixed well. The required amount of water was then gradually added whilst mixing. If possible, the resultant dough was split into four roughly equal parts and formed by hand into spheres, thus providing four repeat samples per composition. At this stage the viability of the different compositions with respect to their workability (i.e. their ability to be formed into shapes and to hold shape over time) was assessed and recorded. Samples that lacked the required level of workability were discarded. The remaining compositions were left to dry for approximately 18 hours before being transferred to a crucible containing non-reactive calcined alumina powder (to prevent sample movement) and heat treated to a maximum temperature of 700°C over a 6 hour period in a chamber furnace (Lenton Thermal Designs LTD). Post heat treatment the viability of the different compositions was again assessed in terms of their ability to be handled without fracture and their final shape. Samples that could not be easily handled and/or whose shape had been distorted were discarded. Finally the remaining samples were each placed in a beaker containing 500ml of distilled water at room temperature. Using a stopwatch, the time taken from immersion to full structural collapse (without mixing) was recorded. The dissolution time for each composition was taken as the average of the four repeats.

3.2 DOUGH SHAPING

Dough pellets of various sizes/shapes can be formed completely by hand, as shown in figure 24. However, to make the process less time consuming and to reproduce as close as possible the industrial process, a semi-automatic dough forming method was developed. Throughout the process dough was made by combining NaCl (General purpose grade, Fisher Scientific), which had been pre-powdered using a hand held blender, with flour (Shipton Mill) and distilled water using a respective ratio of 70:15:15. Dough lengths were extruded using an electric meat grinder (model MG510, PRO1600 Series, Kenwood) and three different extrusion dies

shown in figure 25. For each die a fresh batch of dough was used and the number of repeat extrusions required to achieve a good level of mixing, and thus well-formed dough lengths, was recorded.

In order to form pellets, extruded dough was cut into segments using a carbon steel surgical scalpel (Swann Morton), a 0.61mm Stanley knife blade (Stanley Europe) and steel wire with a diameter of 0.1mm. The effectiveness of the different cutting methods regarding the amount of distortion caused to the cylindrical shape was examined. The remaining dough was left uncovered to harden for 48 hours after which the cutting process and assessment was repeated.

Figure 24. Various dough shapes formed by hand.

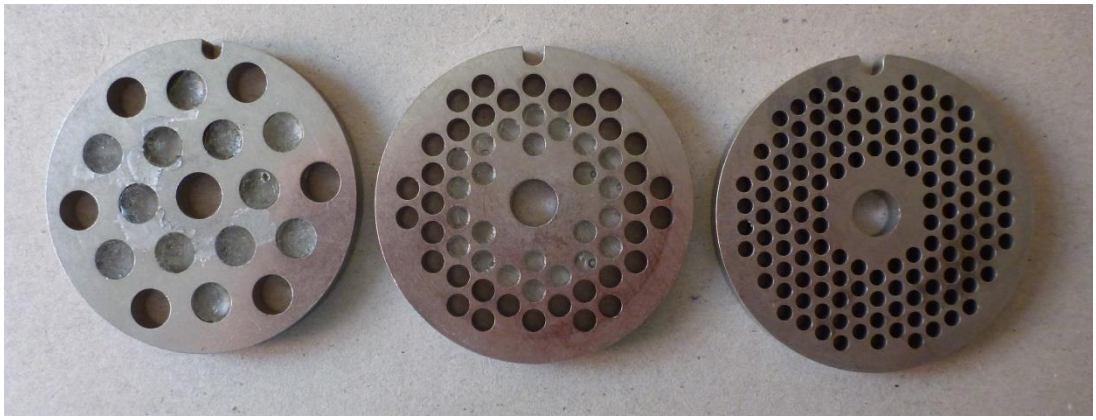

Figure 25. Extrusion dies with hole diameters (l-r) of 8mm (large), 4.5mm (medium) and 3mm (small).

3.3 PREFORM FABRICATION

Three different approaches of preform manufacture were attempted. For each method cylindrical dough lengths were produced in the same manner as that described in section 3.2 whereby six extrusions were executed using the 4.5mm die.

For the first approach (method 1), extruded lengths of dough were left uncovered to harden/dry for 48 hours. These were then cut into 0.5cm (approx.) segments using a carbon-steel surgical scalpel and transferred to a cylindrical, perforated steel mould.

For the second approach (method 2), lengths of extruded dough were immediately cut into segments of 0.5cm (approx.) in length using a 0.61mm Stanley knife blade. Whilst still soft these pellets were used to fill another cylindrical, perforated steel mould. This was then left to dry/harden in air for three weeks, to ensure completion of the drying step.

Finally, for the third approach (method 3), extruded dough lengths were again immediately cut into 0.5mm (approx.) pellets using a 0.61mm Stanley knife blade and transferred to a perforated steel mould. This mould however was not left to dry/harden before being heat treated.

The three moulds, shown in figure 26 were placed together in a chamber furnace (Lenton Thermal Designs LTD) and heat treated using a staggered heating profile with maximum temperature of 700°C over a six hour period. After cooling to room temperature the moulds were removed and the structural stability of the resulting preforms (i.e. whether the preform collapsed) was assessed.

Differences between the industrial and laboratory foam-making processes must be considered so that the two remain comparable and modifications are transferable. With this in mind, both laboratory and factory made preforms were imaged post heat treatment using scanning electron microscopy (See section 2.1). The in-house material was taken from the “method 1” preform and a sample of the Constellium preform was sent directly from their factory in Ussel, Central France.

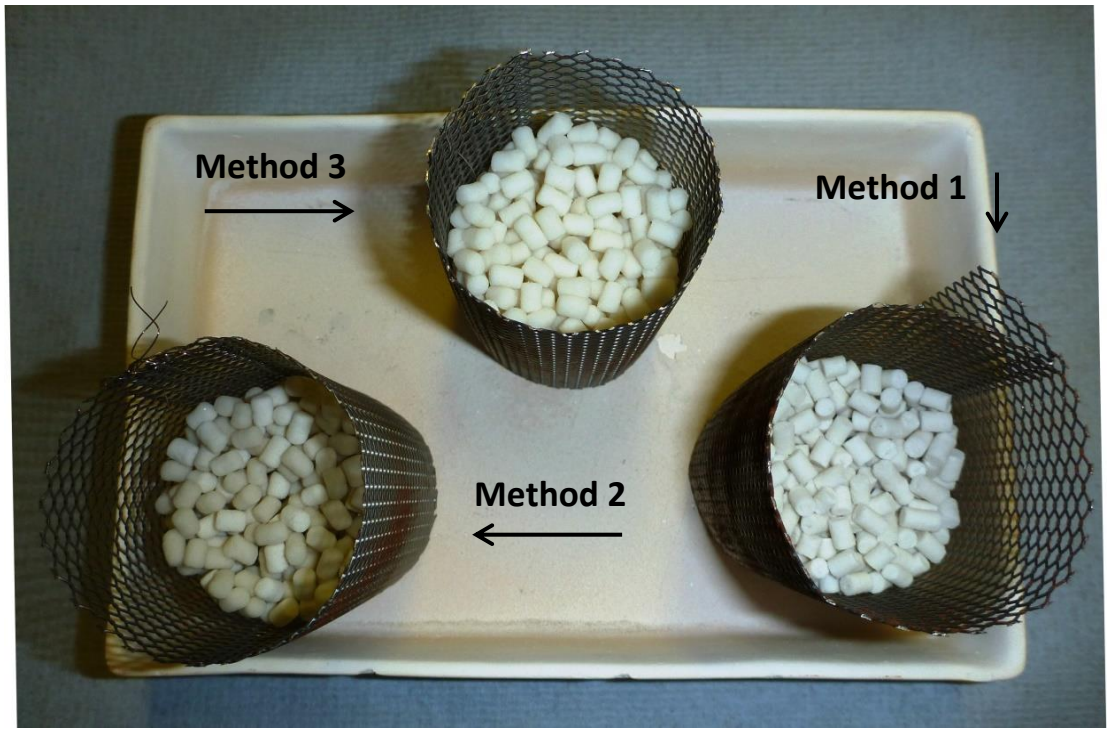

Figure 26. Three preforms made using slightly different methods before being heat treated.

3.4 PREFORM INFILTRATION

Preform infiltration was achieved using an infiltration rig described in detail in section 2.2. A preform (72.71g post heat-treatment) was made using method 3 as described in section 3.3 and then transferred to the mould along with a 151.61g block of aluminium (99.85%, William Rowland Ltd). The furnace was heated to 740°C at a rate of 20°C/min and the sample was left to dwell for 1 hour 45 minutes under vacuum, after which the vacuum was released and an infiltration pressure of 1 bar was applied for 30 seconds. The mould was then removed from the furnace and placed on a copper block to allow for unidirectional cooling.

After 45 minutes the sample was removed from the mould and the top and bottom edges removed using a mechanical hacksaw. The salt was leached by immersing the sample in water overnight and a solid shell around the sample, formed because

of a gap between the preform and the mould, was removed using a grinder/polisher with P80/P120 grade papers.

Density values were calculated using the samples dimensions and weight, measured using digital callipers and scientific scales accurate to 2dp.

The process was repeated a number of times using adjustments stated below-

- infiltration pressure reduced to 0.5 bar, preform (74.72g), aluminium (255.36g)
- infiltration pressure reduced to 0, preform (68.51g), aluminium (221.13g)
- no vacuum applied, infiltration pressure 1 bar, preform (71.22g), aluminium (248.61g)
- no vacuum applied, infiltration pressure 1.5 bar, preform (68.59g), aluminium (218.11g)

3.5 RESULTS AND DISCUSSION

Table 3 shows the various dough compositions investigated with the corresponding preform feasibility assessments; the ternary-style diagram in figure 27 also provides a visual representation of the same data. The assessment results were grouped into four distinct categories; alongside the diagram are representative images for each category.

It can be seen that using the correct dough composition is essential for the success of the salt dough replication technique. The compositional range that remains suitable throughout the laboratory based preform manufacture process has been outlined and is roughly in the region of 80-30% salt, 40-10% flour and 30-10% water.

Table 3. Preform feasibility assessment results for different dough compositions.

Composition			Workable before HT?	Stable after HT?	Dissolution time [s]				
Flour [g]	Water [g]	Salt [g]			1	2	3	4	mean
1	4	5	NO(WET)	NA					
2	4	4	NO(WET)						
3	4	3	NO(WET)						
4	4	2	NO(WET)						
5	4	1	NO(WET)						
1	3	6	NO(WET)						
2	3	5	NO(WET)						
3	3	4	NO(WET)						
4	3	3	YES	NO	NA				
5	3	2	YES	NO					
6	3	1	YES	NO					
1	2	7	NO - WET	NA					
2	2	6	YES	YES	92.89	122.31	130.31	116.47	115.5
3	2	5	YES	YES	87.81	55.45	93.85	70.32	76.9
4	2	4	YES	YES	17.65	61.15	57.65	52.87	47.3
5	2	3	YES(DRY)	NO	NA				
6	2	2	YES(DRY)	NO					
7	2	1	YES(DRY)	NO					
1	1	8	YES(DRY)	YES	156.34	143.57	128.38	132.17	140.1
2	1	7	YES(DRY)	YES	129.57	123.74	143.36	90.91	121.9
3	1	6	YES(DRY)	YES	85.96	141.52	157.04	139.35	131.0
4	1	5	NO(DRY)	NA					
5	1	4	NO(DRY)						
6	1	3	NO(DRY)						
7	1	2	NO(DRY)						
8	1	1	NO(DRY)						

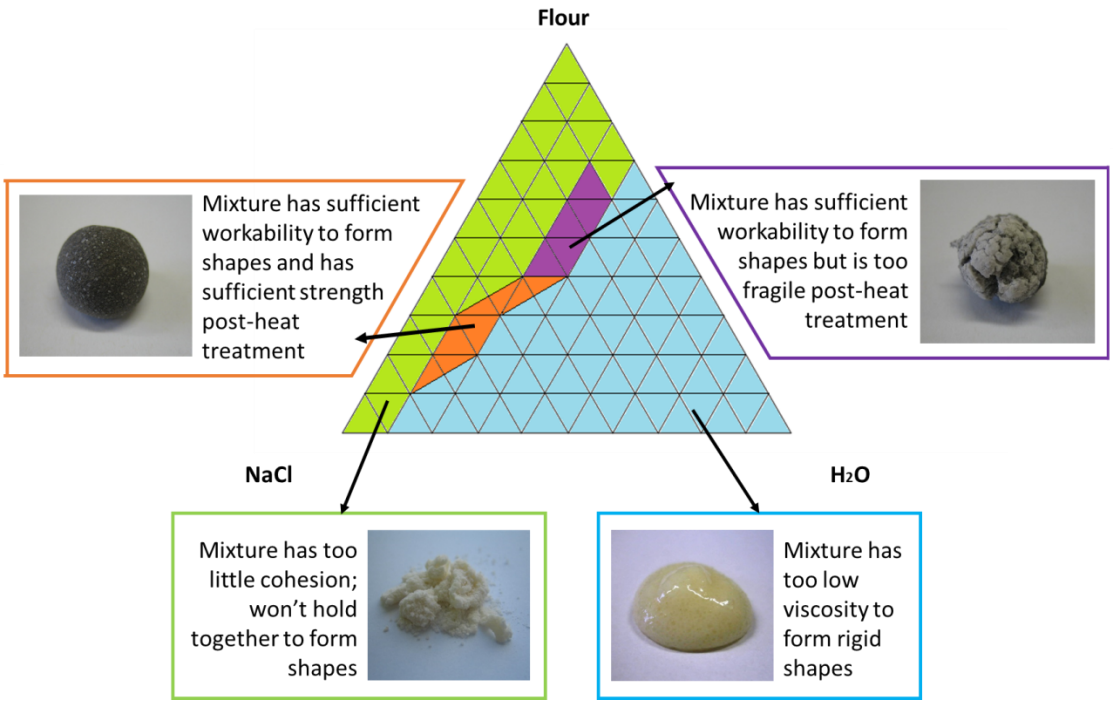

Figure 27. Ternary style diagram of dough composition and corresponding preform feasibility assessment.

It should be noted that a number of variables may affect the result and the presented range may be subject to change. Factors that could cause a shift in the compositional limits include; the heat treatment temperatures and dwell times, the type of flour used (especially the gluten content), the coarseness of the salt and the volume of the individual dough particle formed. Taking into consideration the number of parameters involved, the suggested range should only be used as a rough guide with semi-flexible boundaries.

In general it was observed that the greater the flour/water content relative to that of the salt, the more workable the dough became pre-heat treatment and the quicker the time for dissolution (and thus also for the leaching stage in the foam manufacture process). In contrast, as the percentage of salt increased the more strength the shapes had post-heat treatment. This was attributed to the fact that the flour/water content of the dough is burned away during the heat-treatment phase therefore by increasing the percentage of flour/water the porosity of the preform is also increased. The choice of dough composition could therefore be

based on the main requirement of the preform; speed of foam production or consistency of the pore shape.

The dough composition that was used for all successive investigations in this work was 70% salt, 15% flour and 15% water. This was the closest composition to that used by Constelllium and which also came within the limits deemed suitable for the proposed laboratory preform manufacture method bearing in mind the need for reliability in the pore shape.

A large variety of shapes could be produced through manual forming of the dough although this method was very time consuming and achieving consistent sized samples time and time again was difficult. A semi-automatic shaping method based on that used at the Constellium factory was therefore developed whereby the dough was extruded using an electric meat grinder and dies.

The small and medium sized circular dies produced cylindrical shapes that could be cut into any desired length. To achieve fully cylindrical shapes with the larger sized die, the number of holes had to first be reduced using resin as a filler material; enough dough could then be forced through the remaining holes and fully formed dough cylinders were possible.

For all die sizes the consistency of the dough changed following extrusion and became much more pliable/elastic. For the small, medium and large die, well-formed shapes occurred at 6, 7 and 9 extrusions respectively. Additional extrusions resulted in the dough becoming sticky with no benefit to the shape. Figure 28 shows development of the dough shape through multiple extrusions using the medium die but is representative of the extrusion behaviour observed for all the dies.

After extrusion the dough lengths were cut using; steel wire, a Stanley knife blade and a scalpel. It can be observed in figure 29 that cutting of the cylindrical dough lengths slightly distorted the shape, the resultant pellet being more of a “pillowcase” rather than a true cylinder. The steel wire caused least distortion although the process was time consuming. The Stanley knife blade provided the best balance between shape and time consumption. For the blade and scalpel, the

amount of distortion increased as more dough was cut and fouling occurred thus regular cleaning with isopropanol was required.

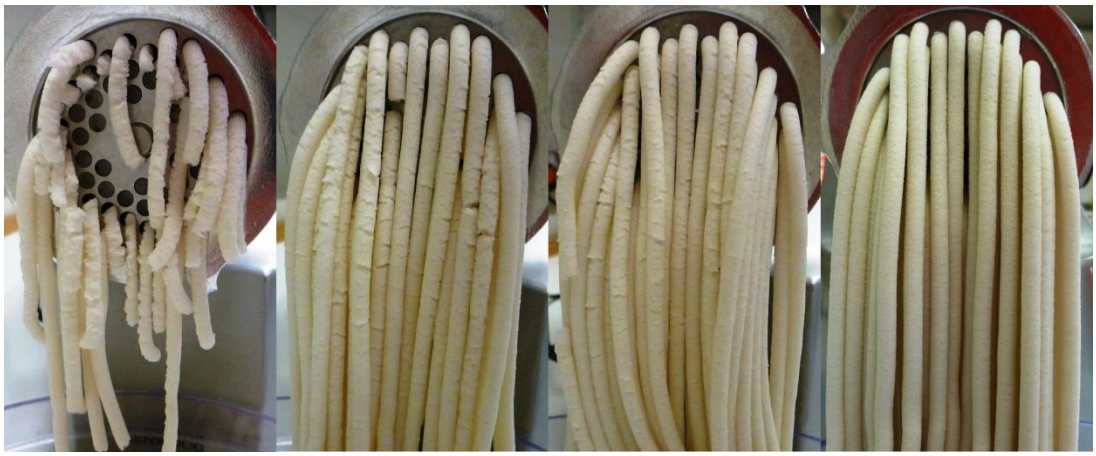

Figure 28. Dough extruded through the medium (4.5mm) die. From l-r; 1, 2, 4 and 7 extrusions.

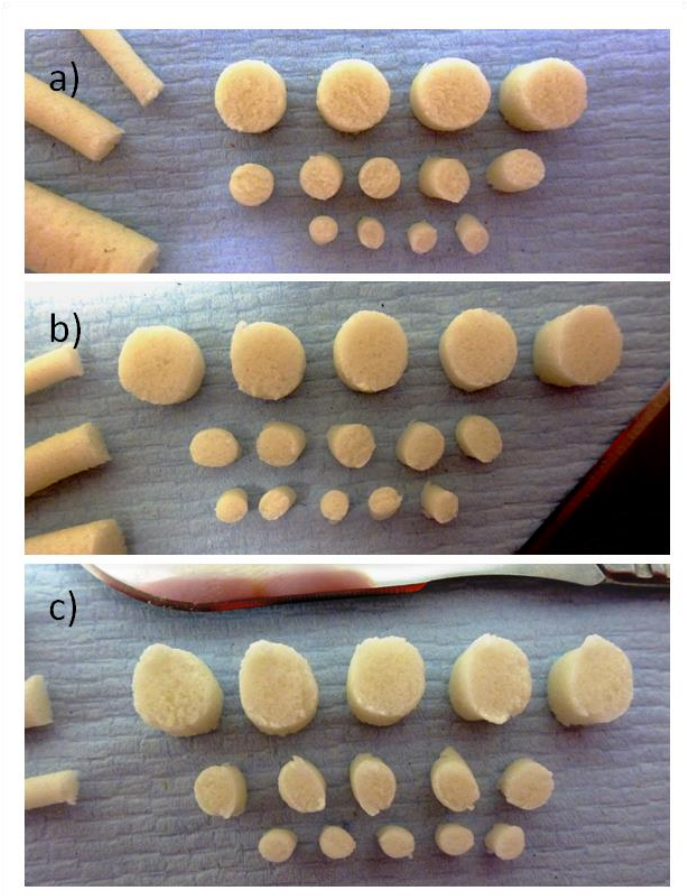

Figure 29. Dough lengths cut using a) steel wire, b) a Stanley knife blade and c) a scalpel.

The dough was left to harden and the cutting process was repeated. The hard dough could not be cut using the wire but when using both the blade and the scalpel very little distortion was caused to the shape; see figure 30.

Figure 30.Pre-heat treatment dough lengths with 4.5mm diameters, extruded using the medium die and cut using a scalpel.

The semi-automated method provided a higher level of reproducibility and achieving uniform pellet sizes was much more straightforward compared with shaping by hand. The extrusion process has the capacity to produce a number of different foam structures and is especially well suited to investigations involving pore aspect ratio. The shapes that can be produced via extrusion are however limited to those that can be created using a die; spherical pellets for example would not be possible. In this investigation only circular dies were used although various other shapes are feasible.

The amount of distortion caused to the soft dough by the cutting is minimal however problems may arise if very precise or complex shapes, for example large surface area “stars”, are required. If this is the case it may be an option to leave the dough to harden before cutting, which would allow the exact shape formed by the

extrusion die to be retained. This would however mean that the density of the resultant foam could not be controlled using preform compaction.

Using the semi-automatic shaping technique, preforms were subsequently made via three slightly different processes, which are described fully in section 3.3. Post heat treatment, only method 3 produced a preform that held together once the mould had been removed; this method did not allow the dough to harden at any stage up to heat treatment. The preform made via method 2, whereby the dough was cut into particles whilst soft then left to dry/harden inside the mould before heat treating, was partly intact. Method 1's preform completely collapsed; for this method the dough was left to harden before cutting into particles and transferring to the mould. All three preforms, post-heat treatment, can be seen in figure 31.

Achieving a fully interconnected foam structure will be assisted if the individual pellets that make up the preform are bonded together as seen when using Method 3. This method would also allow for density control using compaction as used in the Constellium process. Although, due to the pellets still being soft when filling the mould, shape distortion could occur especially if being compacted. This may cause complications if a specific pore shape is being investigated.

Infiltration of individual particles, such as the hardened dough pellets used in method 1, is possible and does have some benefits. Using hardened pellets would allow for the exact shape of the particles to be retained and mirrored in the pores of the resultant foam. The foam would also require less machining as individual pellets can move to more fully fill the space of the infiltration mould, reducing the thickness of the foams solid shell post-infiltration.

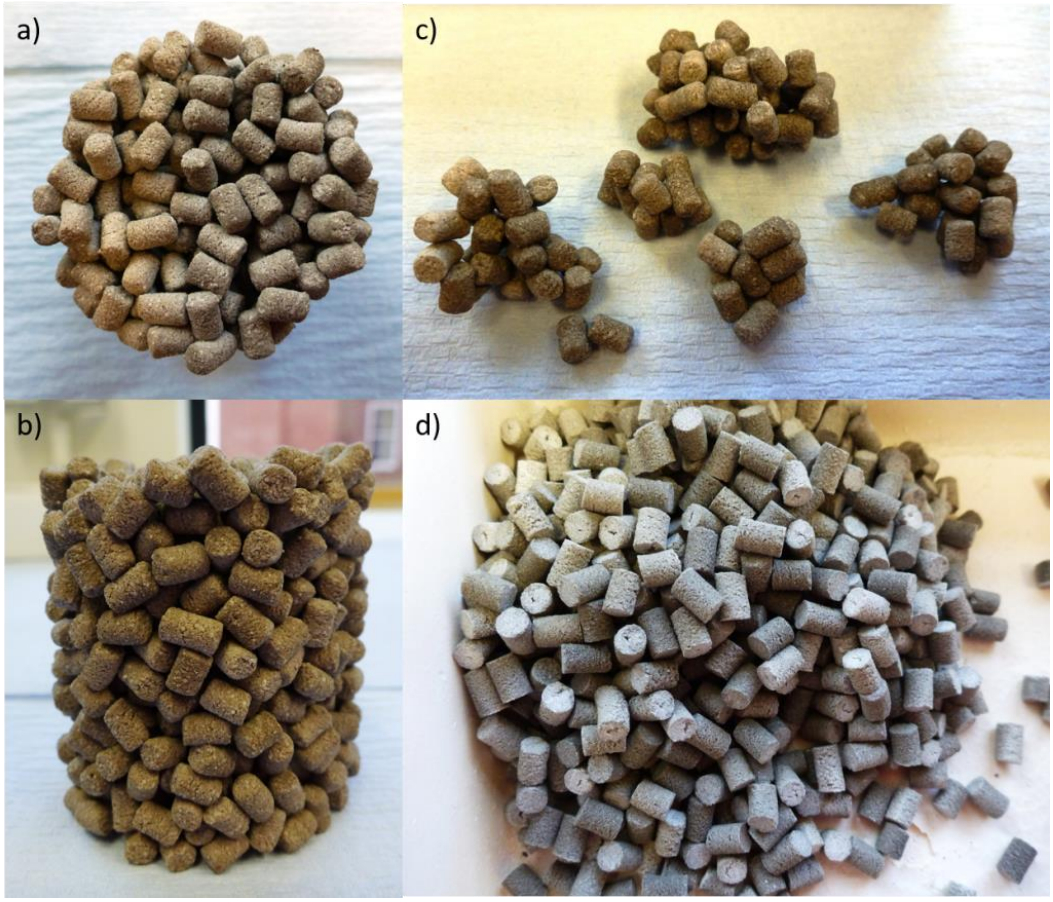

Figure 31. a) top view and b) side view of fully intact preform made via method 3, c) partial preform made via method 2 and d) collapsed preform made via method 1.

Post heat-treatment, the preform materials made via the industrial and laboratory processes, were imaged using scanning electron microscopy (SEM), see figures 32 and 33 respectively.

A relatively large number of scratches are visible on the samples surfaces, which could not be avoided as it was not possible to use water-based lubrication during grinding since this would wash away the salt. The bright spots on the images are assumed to be small air pockets in the resin (or where salt particles have been pulled out) that have been filled with dust from the grinding process.

Nevertheless, it can be clearly seen that there are major differences between the two preforms. The Constellium preform appears to be much denser with tightly packed, smaller salt grains. In contrast, the in-house produced preform contains a relatively high level of porosity due to the much larger, irregular salt grains that prevent close packing.

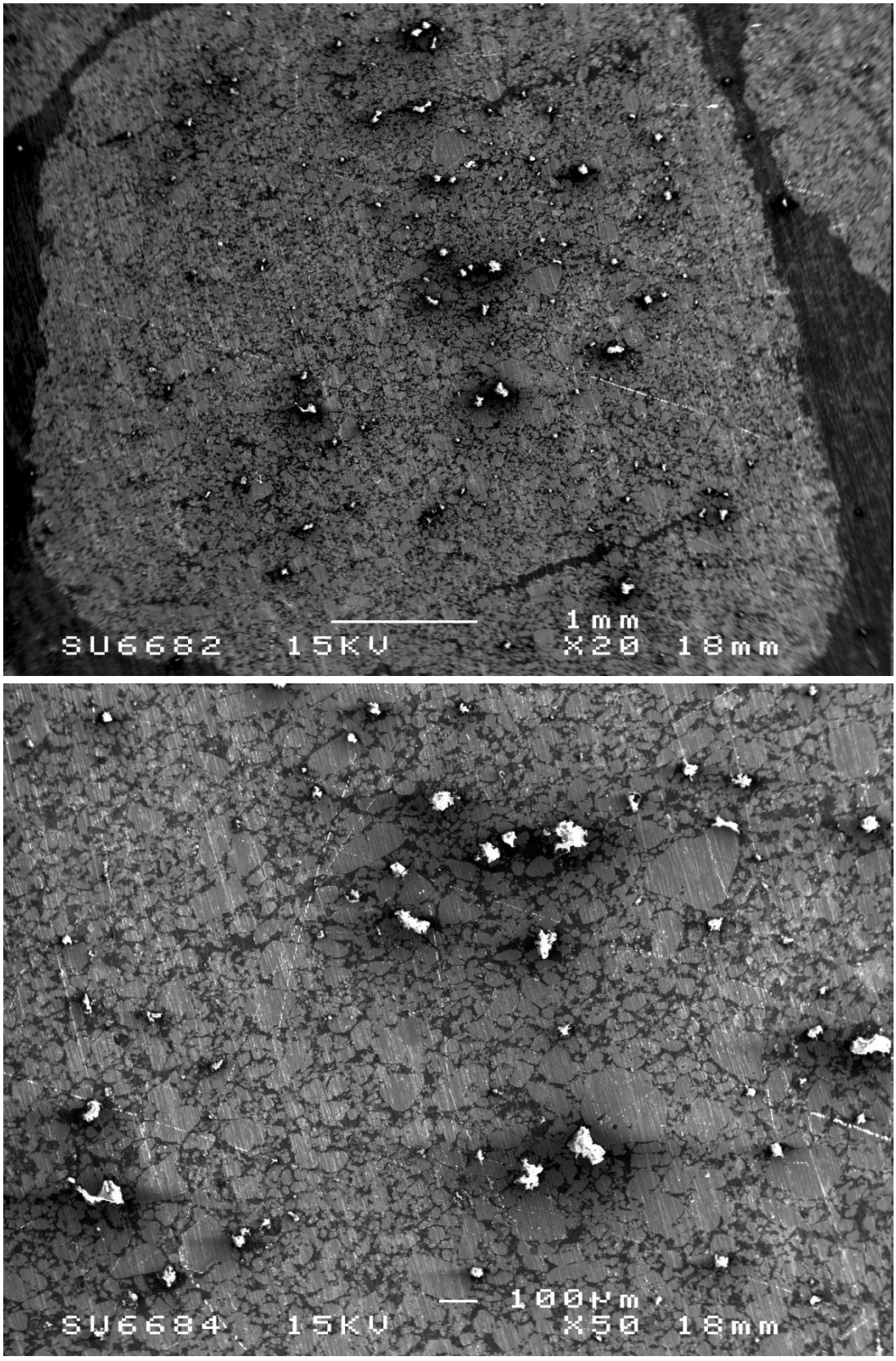

Figure 32. Heat-treated Constellium preform material imaged using SEM, top: x20 magnification and bottom: x50 magnification

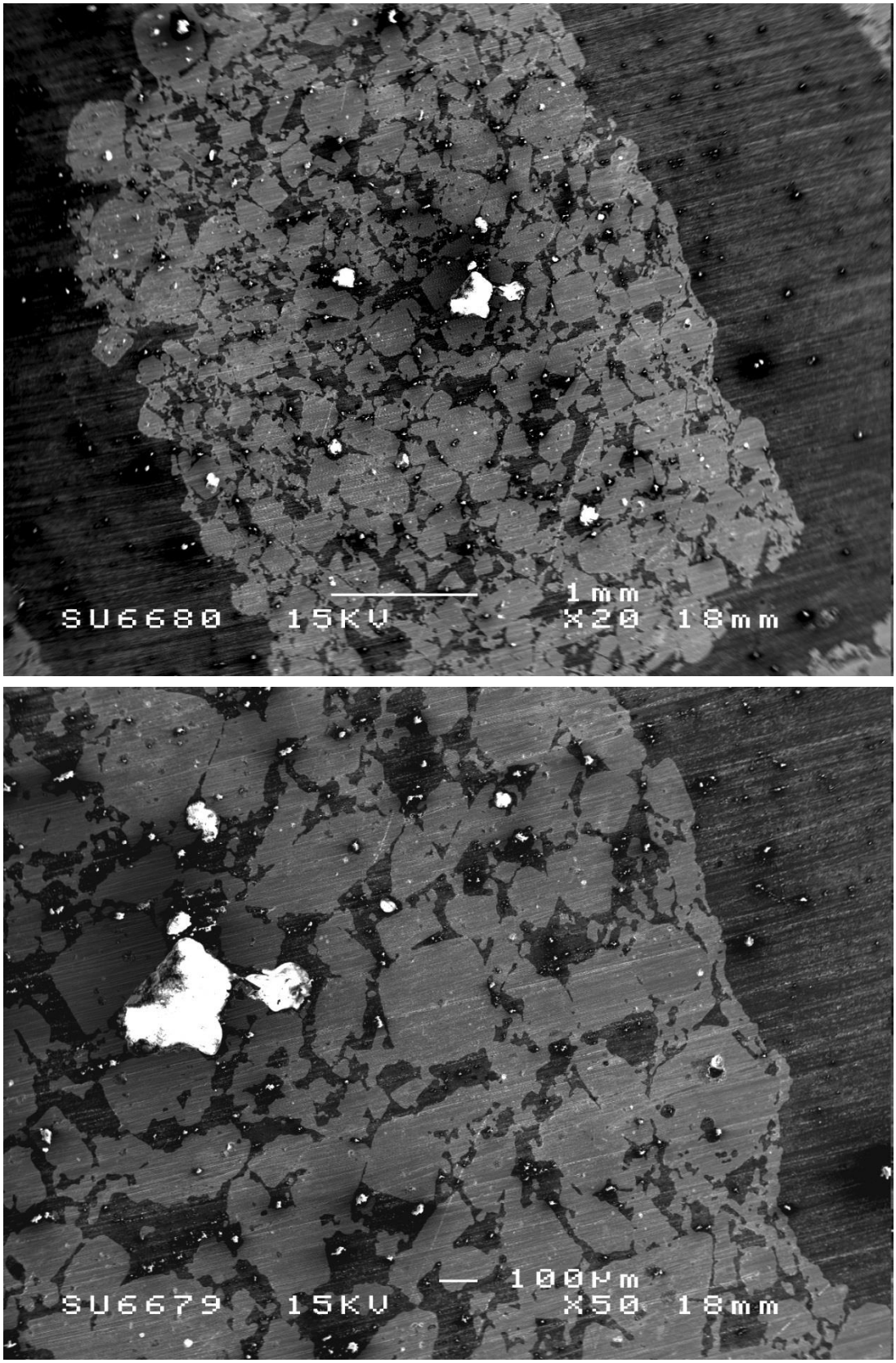

Figure 33. Heat-treated in-house preform material imaged using SEM, top: 20x magnification and bottom: 50x magnification

It was known previous to the investigation that Constellium use a finer initial salt grade than that used in the laboratory technique. They also have a more extensive dough-mixing process, using higher powered equipment, during which the salt may be broken down further. In order to closer replicate the industrial preform, the in-house salt was ground before use using a hand blender; nonetheless it seems that this approach is inadequate to reproduce exactly the industrial preform structure. The higher level of porosity within the laboratory-made preform could reduce the time taken to complete the salt leaching process, however, it may also have aggravated initial problems experienced with the infiltration process (described in detail below). These issues were solved by changes in processing and foams produced in-house are structurally comparable to those made by Constellium therefore, despite the differences, no alterations to the laboratory preform were made.

A preform (made using method three) was infiltrated using a pressure of 1bar; this produced a sample with a partial foam structure shown in figure 34a. A visual inspection found that the pores replicated well the shape of the preform and some were interconnected however, a high proportion of pores appeared to be closed and some of the preform had itself been infiltrated. This was even more apparent once the foam was cut in half to reveal the internal structure. There was no evidence that any of the aluminium remained in the solid state during the infiltration process suggesting the melting parameters were sufficient. Some solidification shrinkage was visible and so a greater initial quantity of aluminium was required.

The second preform was infiltrated at a lower pressure of 0.5bar and with an increased volume of aluminium. Solidification shrinkage only affected an area of surplus aluminium and did not reach the foam beneath. However, when the sample was cut in half it could be seen again that the preform itself was infiltrated as shown in figure 34b. This was unexpected as such a low gas pressure should have corresponded to less infiltration and a more interconnected structure. The increased weight of the aluminium will have caused a slight increase in infiltration

pressure however it is unlikely that this alone would have caused the preform to be infiltrated to such a degree.

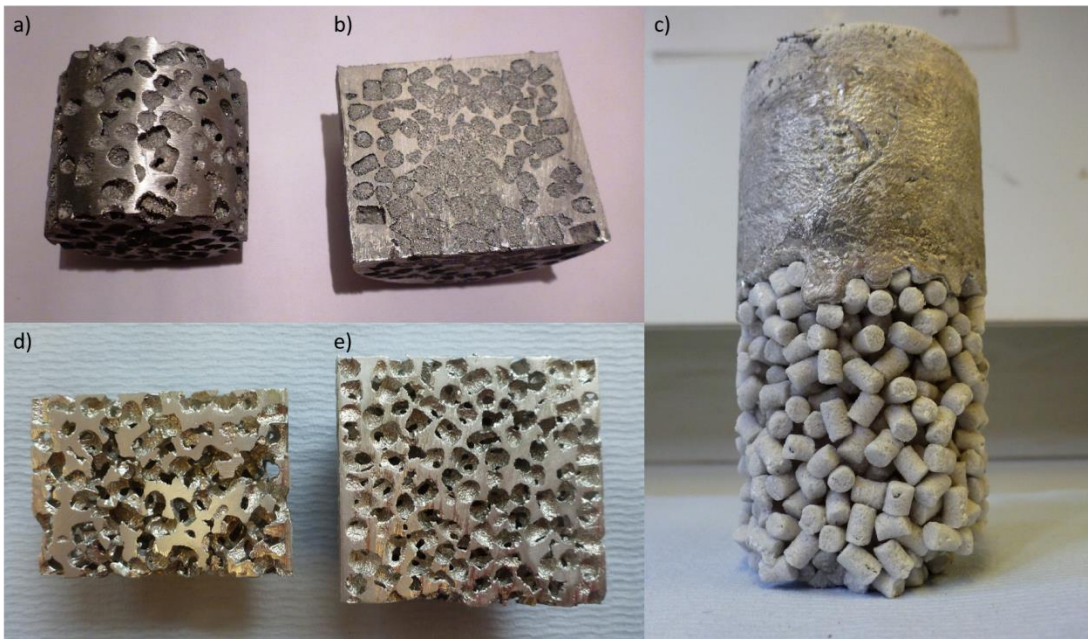

Figure 34. a) unsuccessful infiltration with pressure of 1 bar (with vacuum), b) unsuccessful infiltration with pressure of 0.5 bar (with vacuum), c) unsuccessful infiltration with pressure of 0 bar (with vacuum), d) successful infiltration with pressure of 1 bar (without vacuum) and e) successful infiltration with pressure of 1.5 bar (without vacuum)

No external pressure was applied to the third preform to see if the weight of the molten aluminium alone was sufficient to infiltrate. Once cooled and removed from the mould it was clear that no infiltration had occurred and thus some gas pressure was needed, see figure 34c.

The fourth preform shown in figure 34d, was infiltrated using a pressure of 1 bar however, unlike previous attempts, the vacuum was not applied. The infiltration was successful in producing a fully interconnected foam structure whose pores replicated well the shape of the preform.

Finally, a further preform was infiltrated in the same manner but using a pressure of 1.5 bar. The resultant foam, shown in figure 34e, again had a fully interconnected network of pores that replicated the shape of the preform. The pore windows appeared smaller than those of the previous foam advocating that the gas pressure can be used to control the level of infiltration and thus the density of the resultant foam. This was further confirmed once samples were machined

and density measurements taken; the average percentage porosity of the foams successfully infiltrated with 1 and 1.5 bar pressures being 76% and 72.5% respectively.

Having the melt under vacuum alone does not cause any infiltration of the molten aluminium. However, once the gas pressure is applied infiltration takes place, indeed in some cases to a larger extent than desired, penetrating into the pore regions. Attempts to avoid this with reduction in infiltration pressure proved unsuccessful, down to pressure levels that would challenge the precision and repeatability of the equipment available. Instead, avoiding the use of vacuum before melting seemed to give the required performance. In this case the air present in the mould will find a refuge in the porous space holder particles, and, as it becomes compressed, will counteract the pressure driving the metal in, thus helping to resist these structures being infiltrated.

Where infiltration of the pore region does happen, it creates a dense aluminium/salt sample from which the salt cannot be leached. Even when the gas pressure was set very low (0.5 bar), the additional force produced by the vacuum caused the preform to be fully infiltrated. To allow for a more impenetrable preform, the pellets could have been densified through the use of a finer salt grain and/or decreasing the flour/water fraction as far as possible within the limits set from the investigation described in section 3.1. However, the indeterminate additional pressure caused by the vacuum still may not have allowed for a well interconnected pore network and could also have caused repeatability issues as controlling the foams density would only have been possible through preform compaction alone, if at all.

Without a vacuum, infiltration was controllable and suitable foam structures were achieved using practical gas pressures between 1-2 bar. Melting aluminium in air opposed to under vacuum accelerates the formation of an oxide film on the melt surface; this in turn increases the risk of the film being entrained into the bulk liquid metal and thus into the sample. However, turbulence to the melt caused by the infiltration process is thought to be low and so the risk of oxide film defects is minimal. It was therefore decided that the vacuum would be sacrificed in favour of a more reliable infiltration process.

For all subsequent investigations wherein foam samples were manufactured in-house, the method described in section 2.2 was followed with the omission of the vacuum. The gas pressure used for infiltration was varied for each experiment and used to alter the density of the foam. Specific pressure values for each set of samples produced are given in the corresponding chapters. The preform composition was not altered.

4. STRUCTURAL CHARACTERISATION

4.1 X-RAY TOMOGRAPHY IMAGE ANALYSIS

A number of samples to be used in the heat-transfer investigations described in section 5 (along with specific details regarding sample manufacture) were first imaged using X-ray tomography. Information regarding the tomography equipment, scan settings and 3D image reconstruction can be found in section 2.6. Analysis of the tomography data was carried out in order to ascertain basic structural information that would otherwise be difficult to measure or would require destruction of the sample. All image analysis was carried out using the Avizo 9.2 software package.

The contrast between the foam matrix (metal) and the pores (air) is high due to the large difference in their x-ray attenuation. Segmentation of the porosity could therefore be achieved via image intensity thresholding whereby an inbuilt algorithm was used to automatically calculate the threshold values. This allowed qualitative inspections of the 3D structures as well as measurement of the metal and pore volume fractions (Vf). It should be noted that a relatively small amount of internal, closed porosity was identified within the Constellium-made samples. The size difference between the closed and open porosity was such that there was no overlap and each type could be easily separated from the other. Volume fraction measurements therefore include that of the metal, the open-porosity and where necessary, the closed porosity. Figure 35a shows a cross section through a Constellium foam sample with 5mm, open pores but which also contains closed porosity within the struts. Figure 35b shows the same cross section but where the

closed porosity has been removed during image processing to allow calculation of the volume fraction of open porosity only.

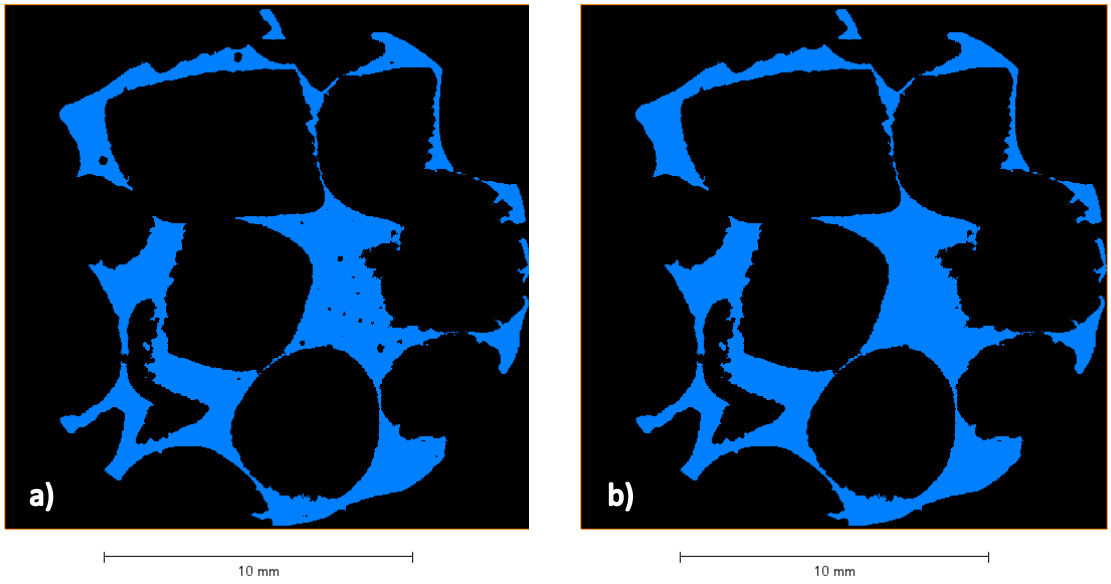

Figure 35. Cross section of a Constellium foam with 5mm pores, a) closed porosity present and b) closed porosity removed during image processing.

For samples that required quantitative measurement of features relating to the open porosity, the thresholded metal-matrix volume was inverted. As the foams have an interconnected pore network, discrete boundaries then needed to be introduced to isolate pores. This was achieved using an inbuilt watershed algorithm to separate objects. Due to cutting of the samples from a larger foam block, the pores surrounding the sample edge will be reduced from their original size/shape. A border kill function was therefore used to remove edge-connected pores so not to skew the pore analysis. Analysis of the segmented pores allowed estimation of their size and distribution. For the Constellium samples, analysis was performed separately on both types of porosity, open and closed.

4.2 Results And Discussion

One of each foam-sample type was chosen to be imaged using x-ray tomography. Image analysis was then performed on specific samples to allow estimation of various structural parameters. Figures 36 to 42 show various segmented volumes for each sample type.

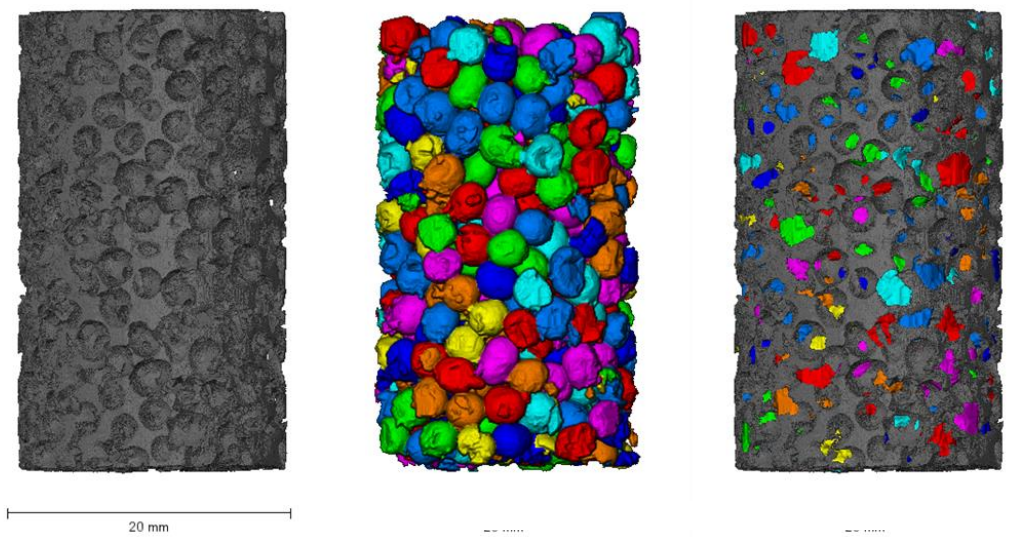

Figure 36. Foam produced in-house using spherical, 2.36-2.8mm diameter, salt preform. From l-r, segmented volumes of metal matrix, open porosity and matrix with open porosity combined. Sample type used to investigate the effect of metal conductivity (section 5.2.1).

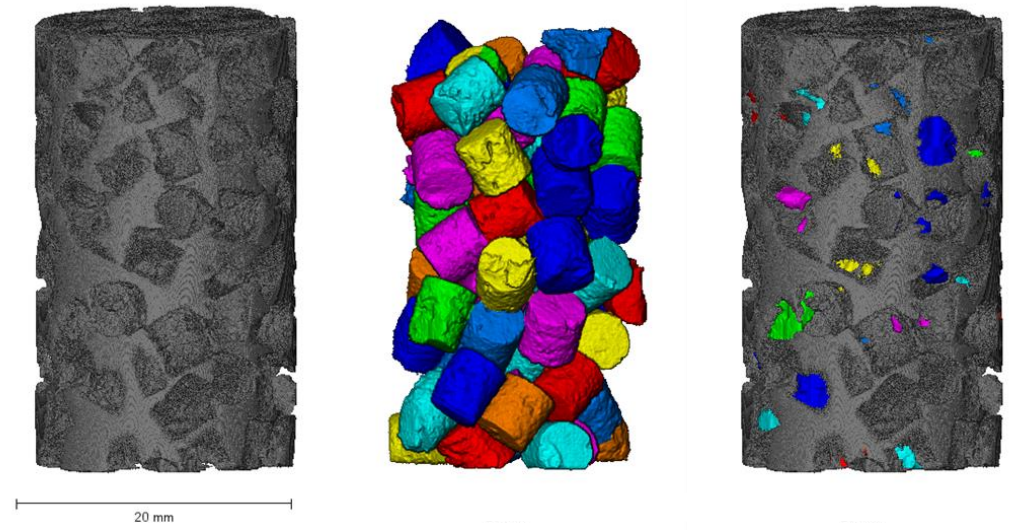

Figure 37. Foam produced in-house using cylindrical, 4.5mm diameter, equiaxed, salt-dough preform. From l-r, segmented volumes of metal matrix, open porosity and matrix with open porosity combined. Sample type used to investigate the effect of metal conductivity (section 5.2.1) and pore aspect ratio (section 5.2.4).

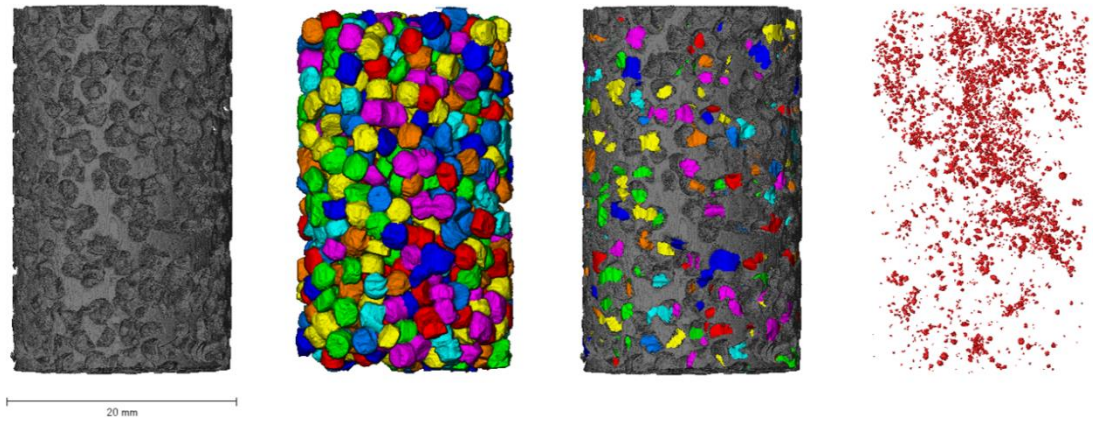

Figure 38. Constellium made foam with pore size of 2mm. From l-r, segmented volumes of foam matrix, open porosity, matrix and open porosity combined and closed porosity. Sample type used to investigate the effect of pore size (section 5.2.2).

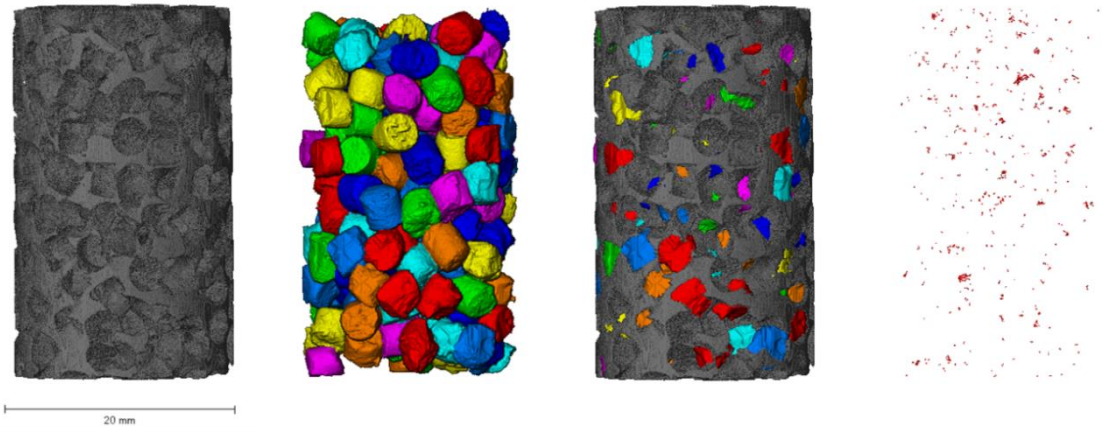

Figure 39. Constellium made foam with pore size of 3mm. From l-r, segmented volumes of foam matrix, open porosity, matrix and open porosity combined and closed porosity. Sample type used to investigate the effect of pore size (section 5.2.2) and machining direction (section 5.2.3).

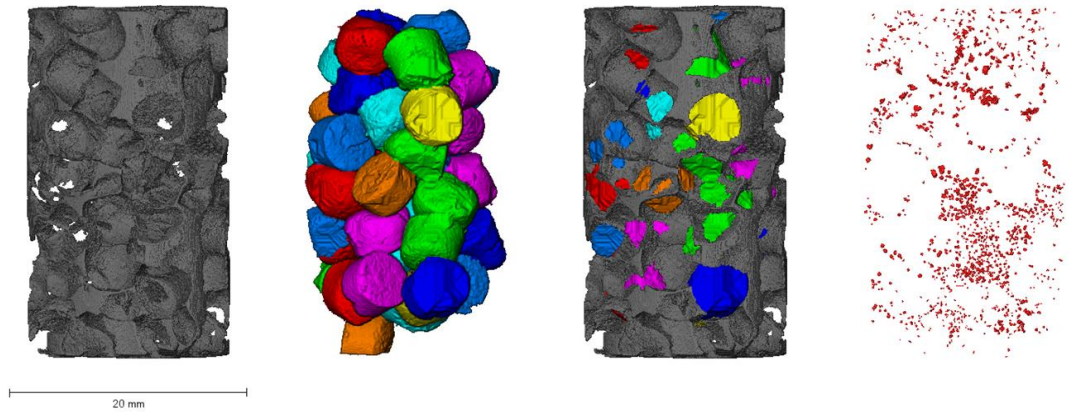

Figure 40. Constellium made foam with pore size of 5mm. From l-r, segmented volumes of; foam matrix, open porosity, matrix and open porosity combined and closed porosity. Sample type used to investigate the effect of pore size (section 5.2.2) and machining direction (section 5.2.3).

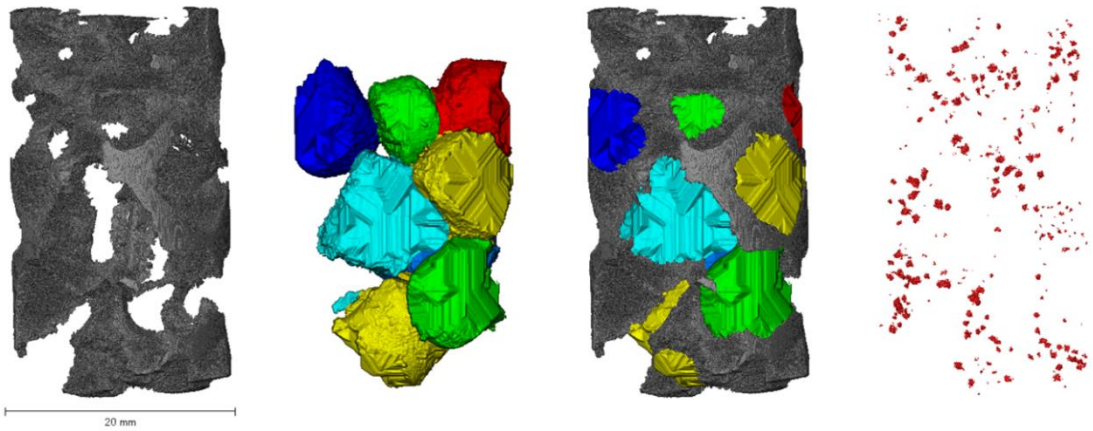

Figure 41. Constellium made foam with pore size of 8mm. From l-r, segmented volumes of; foam matrix, open porosity, matrix and open porosity combined and closed porosity. Sample type used to investigate the effect of pore size (section 5.2.2) and machining direction (section 5.2.3).

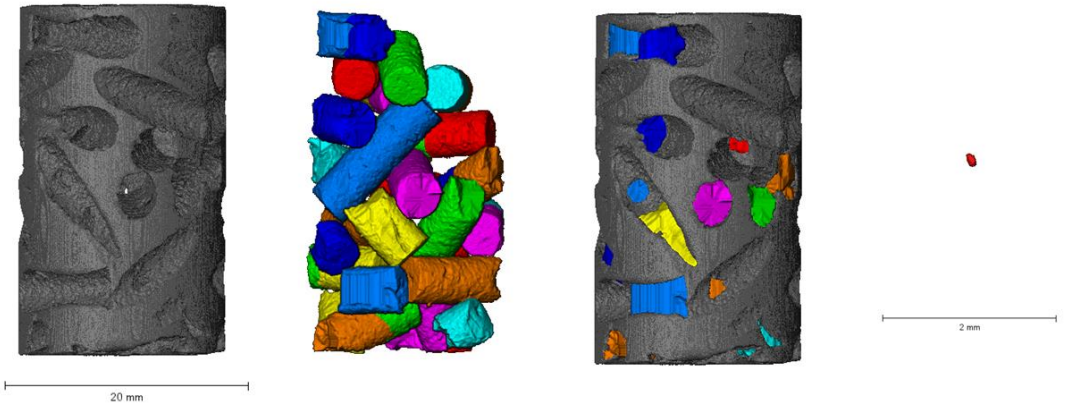

Figure 42. Foam produced in-house using cylindrical, 4.5mm diameter x 13.5mm length, elongated, salt-dough preform. From l-r, segmented volumes of metal matrix, open porosity, matrix with open porosity combined and closed porosity (magnified). Sample type used to investigate the effect of pore aspect ratio (section 5.2.4).

Visual inspection of the 3D volumes and 2D cross-sectional slices found that; all of the intentional porosity (i.e. that as a result of preform removal) was completely interconnected; all preform material had been removed effectively and the shape and size of the pores closely resemble that of the original preform. The scans also revealed that the Constellium-produced foams contain unintentional, closed porosity within the metal matrix whereas the foam samples produced in-house

contained very little, if any. Image-based measurement of metal, open and closed porosity volume fractions are given in table 4.

Table 4. Volume fraction of metal, open and closed porosity for different foam samples.

Manufacturer	Matrix Metal	Preform Shape	Machining Direction	Preform Size in mm		CT Based Open Pore Vf %	CT Based Closed Pore Vf %	CT Based Metal Vf %
				Diameter	Length			
Metal Conductivity (Section 5.2.1)								
In-house	Pure Al	spherical	NA	2.36 -2.8	NA	70.48	0	29.52
In-house	Al Alloy	spherical	NA	2.36 -2.8	NA	70.2	0	29.8
In-house	Pure Al	cylindrical	NA	4.5	4.5	65.35	0	34.65
In-house	Al Alloy	cylindrical	NA	4.5	4.5	65.60	0	34.40
Pore size and Machining Direction (Sections 5.2.2 and 5.2.3)								
Constellium	Al alloy	cylindrical	unknown	2	2	67.35	0.21	32.43
Constellium	Al alloy	cylindrical	horizontal	3	3	68.12	0.004	31.88
Constellium	Al alloy	cylindrical	vertical	3	3	67.50	0.01	32.49
Constellium	Al alloy	cylindrical	horizontal	5	5	84.75	0.06	15.19
Constellium	Al alloy	cylindrical	vertical	5	5	85.37	0.07	14.56
Constellium	Al alloy	cylindrical	horizontal	8	8	82.55	0.06	17.39
Constellium	Al alloy	cylindrical	vertical	8	8	82.79	0.06	17.15
Pore Aspect Ratio (Section 5.2.4)								
In-house	Al pure	cylindrical	NA	4.5	4.5	61.88	0	38.12
In-house	Al pure	cylindrical	NA	4.5	13.5	59.92	8.32E-06	40.08

The differing amounts of in-matrix porosity are most likely a result of the different infiltration methods used; the Constellium preform being gravity fed whilst the in-house system uses a pressure assisted approach. For heat transfer applications, any closed porosity within the foam is undesirable as it is detrimental to heat transfer whilst providing no benefit to the fluid flow characteristics. The 2mm pore size sample contained the most amount of closed porosity whilst the 3mm samples contained the least. It is therefore likely that the amount of closed porosity within the matrix is a result of the processing conditions rather than being linked to the preform size (i.e. the open porosity pore size).

Due to the processing technique, the structure of foam produced by Constellium is thought to differ slightly in the x- and y-axes (this is discussed more thoroughly in section 5.2.3). For the 3mm, 5mm and 8mm pore sizes, samples were cut both horizontally and vertically from the same parent block. One of each type was then imaged and analysed with the aim of characterising any structural differences arising from the difference in machining direction.

Unsurprisingly, it can be seen from table 4 that the overall volume fractions of open and closed porosity are very similar for samples with the same pore size regardless of machining direction. The largest variance between vertically and horizontally cut samples is 0.63% metal volume fraction for the 5mm pore samples. In addition, figures 43 to 45 show how the volume fractions of open and closed porosity differ across the sample lengths for both horizontally and vertically cut samples. The open porosity is uniformly distributed across both the 3mm and 8mm samples regardless of machining direction and the same is true for the 5mm sample that had been vertically cut from the block. For the horizontally cut, 5mm pore size, the open porosity is less uniform and one end of the sample appears to be denser than the other. Figure 44 includes 2D cross sections that represent the most and least dense areas. The closed porosity is also uniformly spread across the sample lengths for all but one of the samples. In the 3mm pore sample, vertically cut from the block, there is a concentration of closed porosity towards one end.

Although there are some differences between horizontally and vertically cut samples, there is no obvious trend between pore distribution (both open and closed) and machining direction that holds true over all pore sizes.

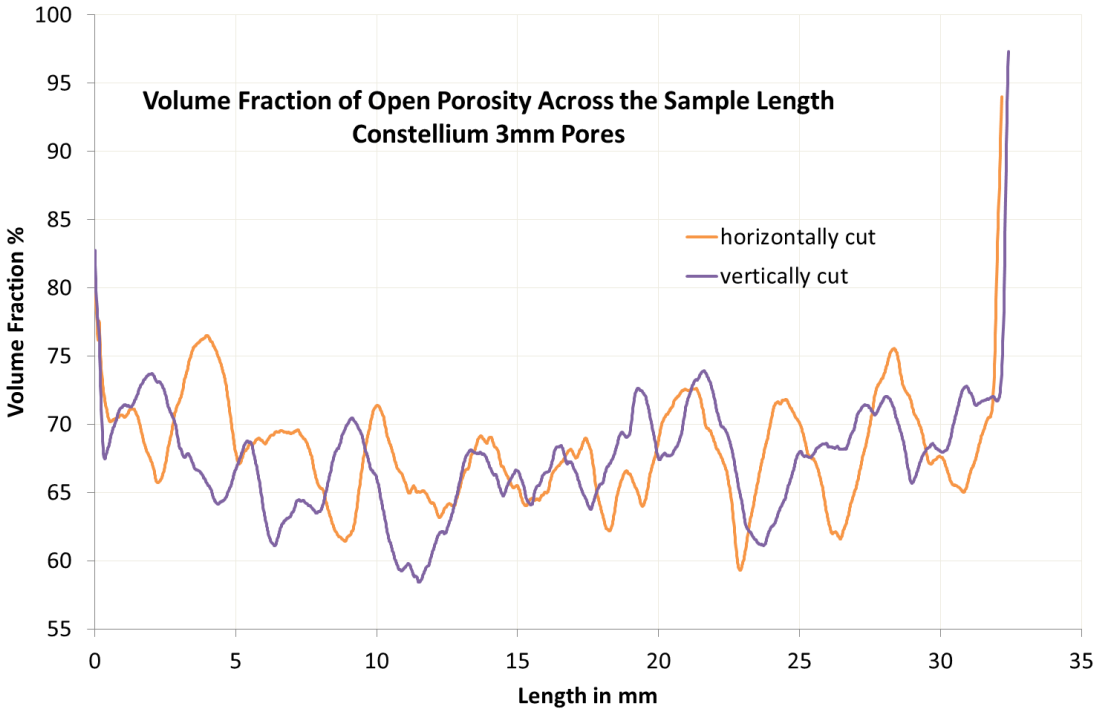

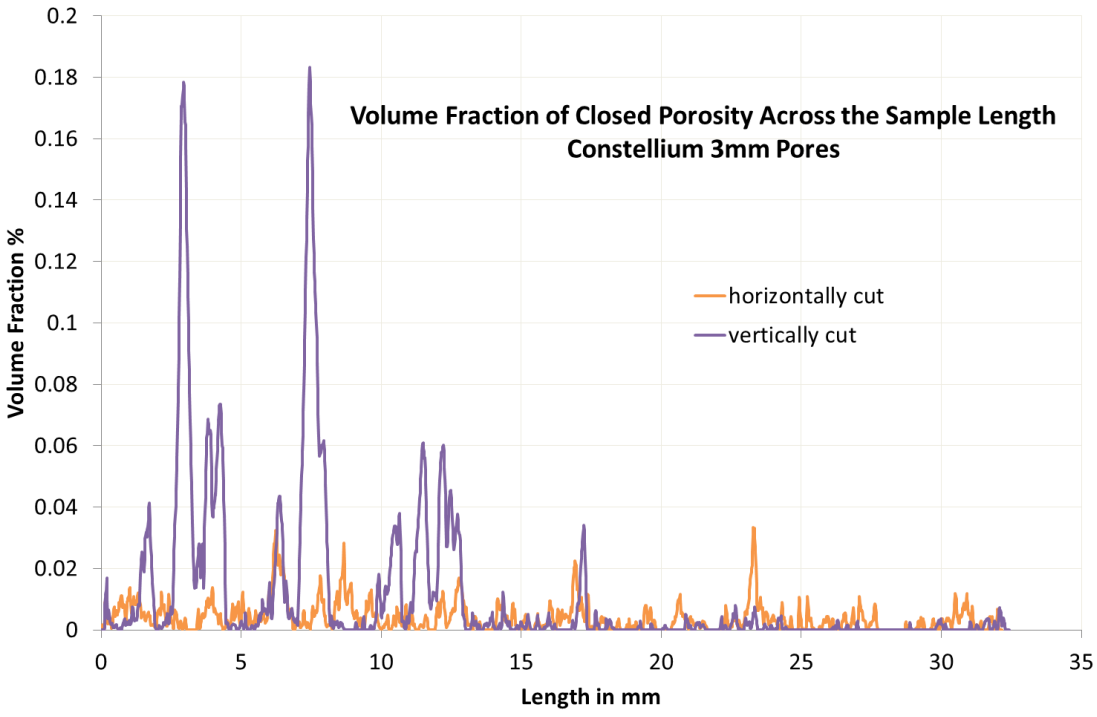

Figure 43. Constellium-produced, 3mm pore samples cut horizontally and vertically from a parent block, top: Volume fraction of open porosity across the sample lengths and bottom: volume fraction of closed porosity across the sample lengths.

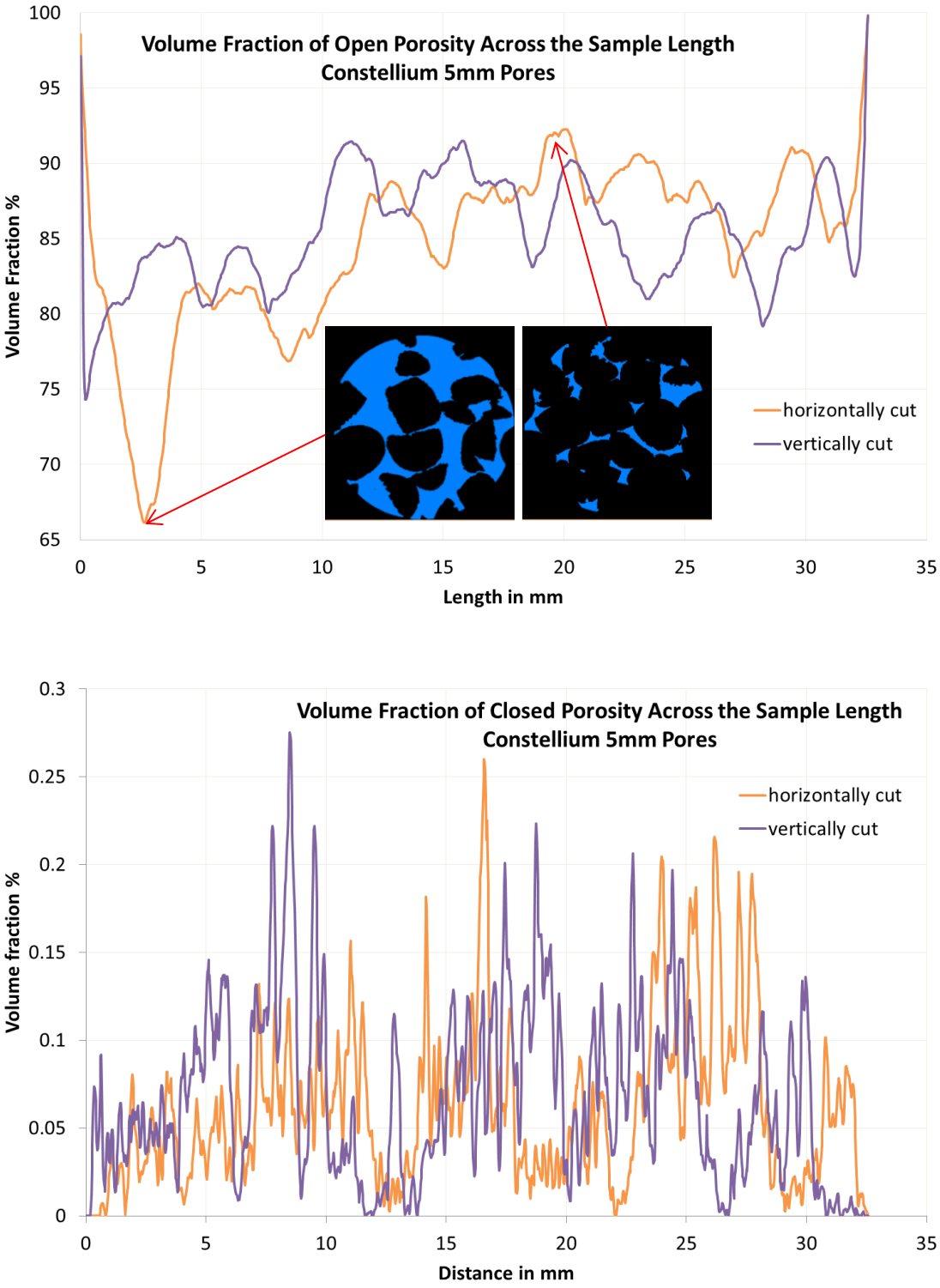

Figure 44. Constellium-produced, 5mm pore samples cut horizontally and vertically from a parent block, top: Volume fraction of open porosity across the sample lengths and bottom: volume fraction of closed porosity across the sample lengths.

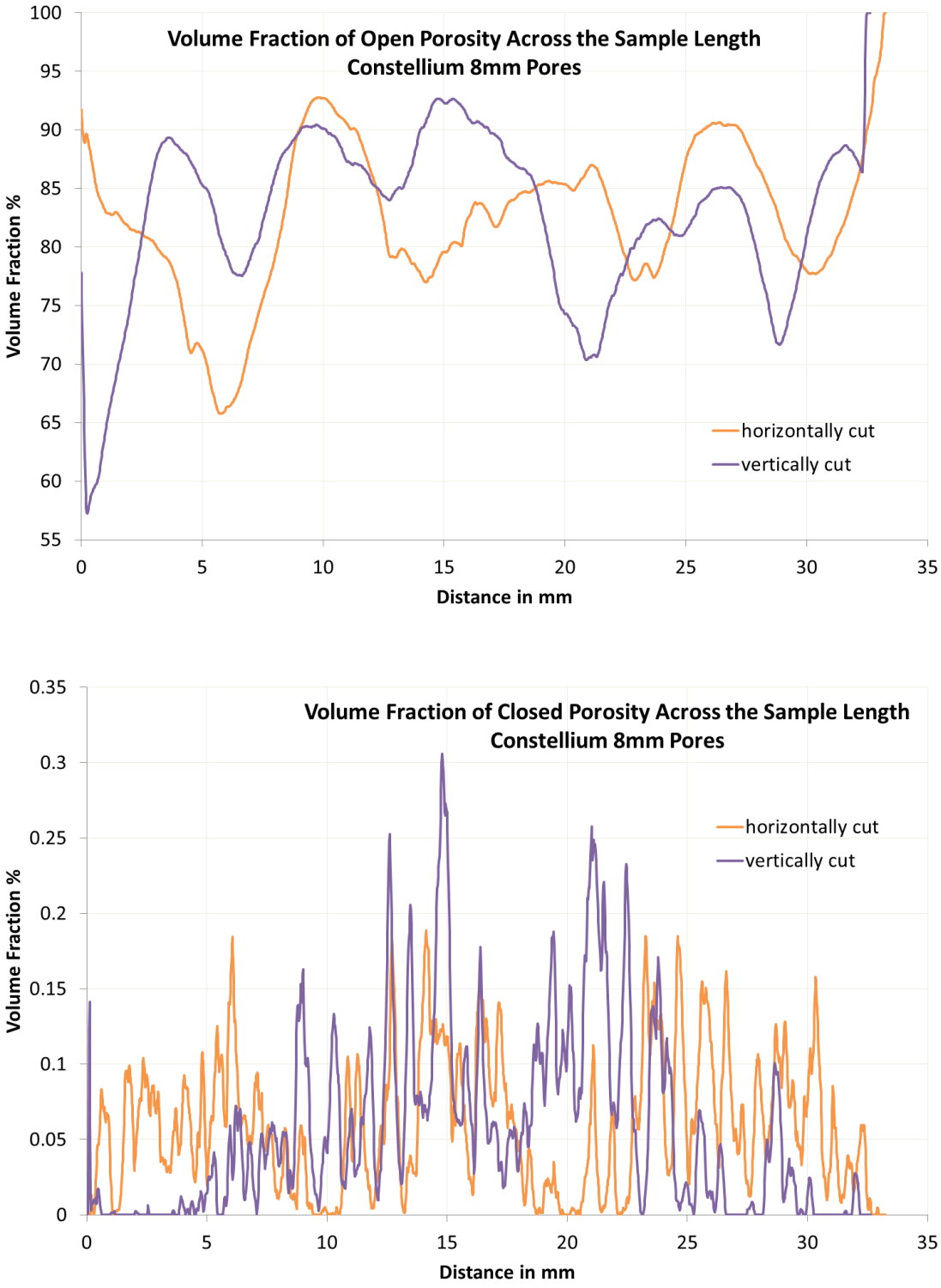

Figure 45. Constellium-produced, 8mm pore samples cut horizontally and vertically from a parent block, top: Volume fraction of open porosity across the sample lengths and bottom: volume fraction of closed porosity across the sample lengths.

Samples were also produced in-house with cylindrical pores but different pore aspect ratios, equiaxed and elongated. Due to the difference in packing behaviour of the different preform types, it was difficult to produce samples with consistent porosity. One of each sample type, elongated and equiaxed pores, with the most similar level of open porosity were imaged and analysed. The image-based volume fraction measurements are given in table 4 whilst figure 46 shows the distribution of open porosity. For both sample types the open porosity is fairly uniform across the sample lengths.

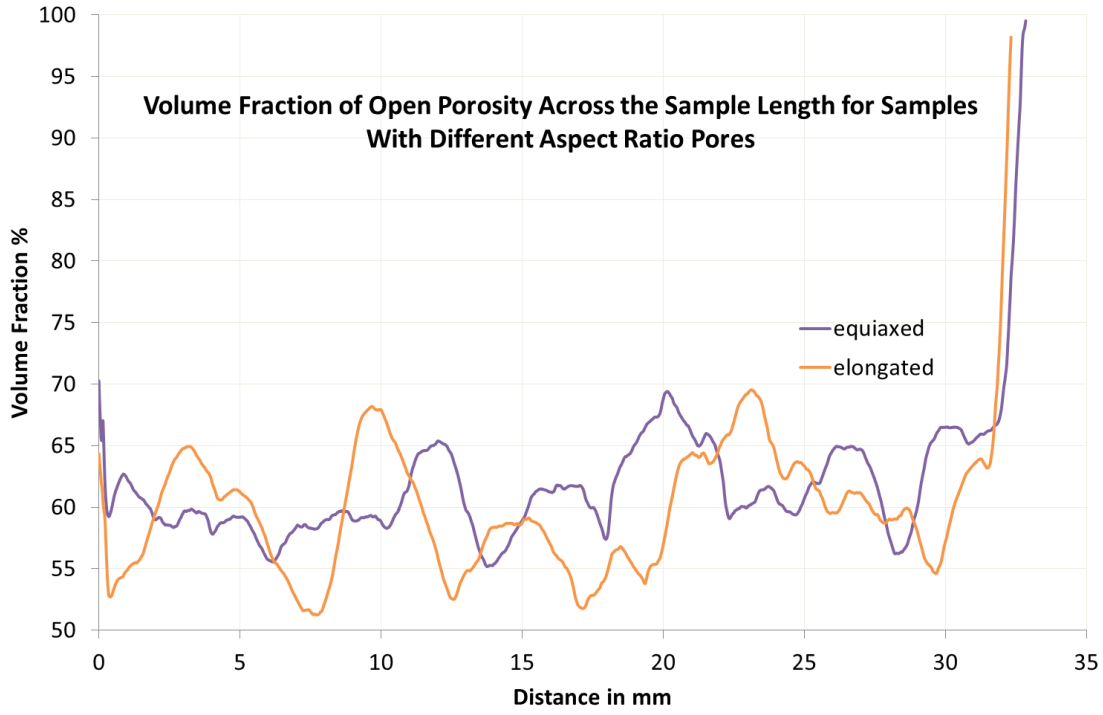

Figure 46. Volume fraction of open porosity across the sample lengths for samples made in-house with differing pore aspect ratio.

Further analysis was performed on those samples to be used to investigate the effect of structural changes (pore size, machining direction and aspect ratio) on their heat transfer behaviour. Image-based characterisation of the open and closed porosity is given in tables 5 and 6 respectively. In addition, figures 47 to 51 show the pore size distribution of the open porosity. It should be noted that for the pore size/machining direction samples (figures 47 to 50) the graphs show distribution of

pore size in terms of the volume equivalent spherical diameter whereas for the aspect ratio samples (figure 51) the graph presents the distribution of pore size in terms of the maximum pore length.

*Table 5. Pore size of open porosity for different foam samples. *Constellium.*

Manufacturer	Matrix Metal	Preform Shape	Machining Direction	Preform Size in mm		CT Measured Pore Size (Open Porosity Only)				
				Diameter	Length	Total Number of Pores	Mean Max Length mm	Mean Min Length mm	Mean Pore Volume mm^3	Mean Volume Equivalent Spherical Diameter mm
Pore size and Machining Direction (Sections 5.2.2 and 5.2.3)										
Const*	Al alloy	cylindrical	NA	2	2	942	2.75	1.93	4.99	2.09
Const*	Al alloy	cylindrical	horizontal	3	3	201	4.55	3.30	21.99	3.42
Const*	Al alloy	cylindrical	vertical	3	3	193	4.53	3.31	22.5	3.48
Const*	Al alloy	cylindrical	horizontal	5	5	51	6.14	4.49	60.51	4.80
Const*	Al alloy	cylindrical	vertical	5	5	47	6.22	4.47	60.29	4.83
Const*	Al alloy	cylindrical	horizontal	8	8	22	6.14	4.0	118.9	4.17
Const*	Al alloy	cylindrical	vertical	8	8	15	9.65	6.67	224.9	6.82
Pore Aspect Ratio (Section 5.2.4)										
In-house	Al pure	cylindrical	NA	4.5	4.5	81	5.77	4.02	47.33	4.36
In-house	Al pure	cylindrical	NA	4.5	13.5	54	7.34	4.40	67.25	4.93

*Table 6. Pore size of closed porosity for different foam samples. *Constellium.*

Manufacturer	Matrix Metal	Preform Shape	Machining Direction	Preform Size in mm		CT Measured Pore Size (Closed Porosity Only)				
				Diameter	Length	Total Number of Pores	Mean Max Length mm	Mean Min Length mm	Mean Pore Volume mm^3	Mean Volume Equivalent Spherical Diameter mm
Pore size and Machining Direction (Sections 5.2.2 and 5.2.3)										
Const*	Al alloy	cylindrical	NA	2	2	3277	0.301	0.188	0.006	0.180
Const*	Al alloy	cylindrical	horizontal	3	3	414	0.275	0.121	0.001	0.107
Const*	Al alloy	cylindrical	vertical	3	3	288	0.302	0.135	0.003	0.118
Const*	Al alloy	cylindrical	horizontal	5	5	1126	0.282	0.175	0.005	0.176
Const*	Al alloy	cylindrical	vertical	5	5	1264	0.284	0.176	0.004	0.175
Const*	Al alloy	cylindrical	horizontal	8	8	365	0.498	0.269	0.015	0.229
Const*	Al alloy	cylindrical	vertical	8	8	245	0.518	0.282	0.021	0.268
Pore Aspect Ratio (Section 5.2.4)										
In-house	Al pure	cylindrical	NA	4.5	4.5	0	NA	NA	NA	NA
In-house	Al pure	cylindrical	NA	4.5	13.5	1	0.227	0.103	0.001	0.113

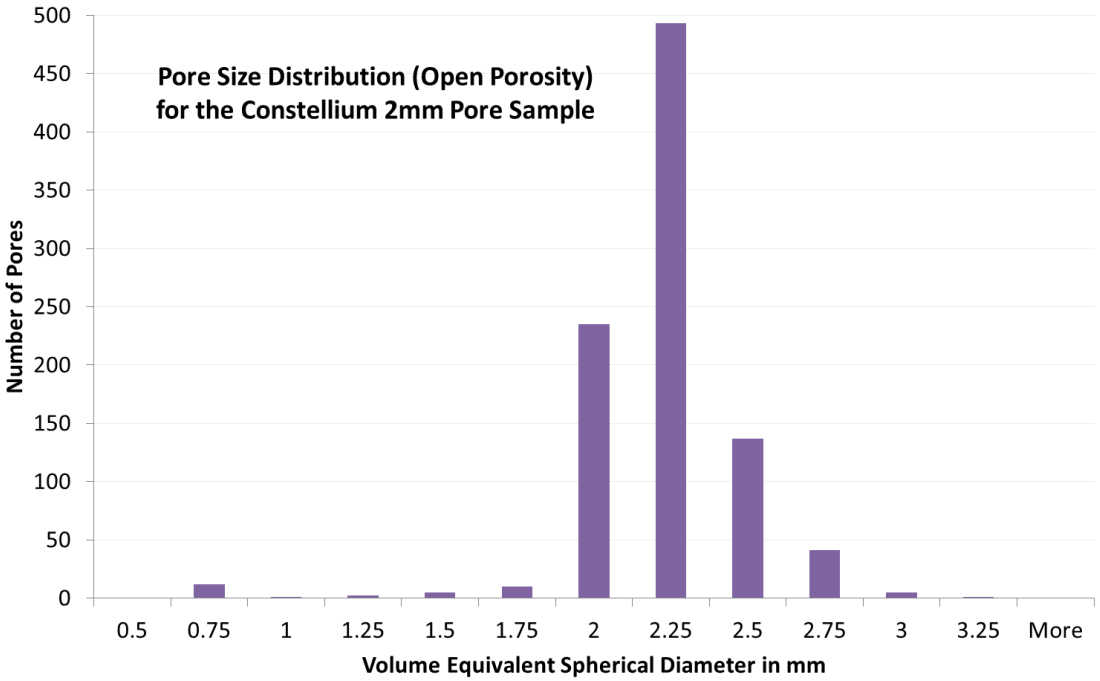

Figure 47. Histogram showing the pore size distribution of the open porosity for a Constellium-produced, 2mm pore sample.

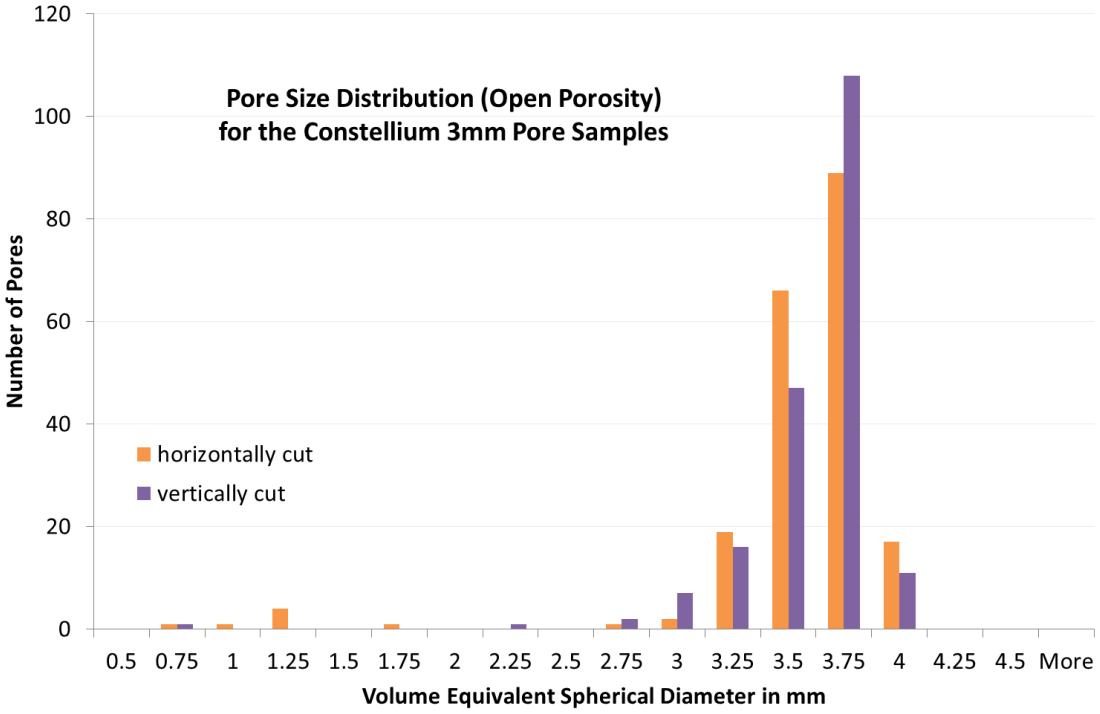

Figure 48. Histogram showing the pore size distribution of the open porosity for Constellium-produced, 3mm pore samples cut both horizontally and vertically from a block.

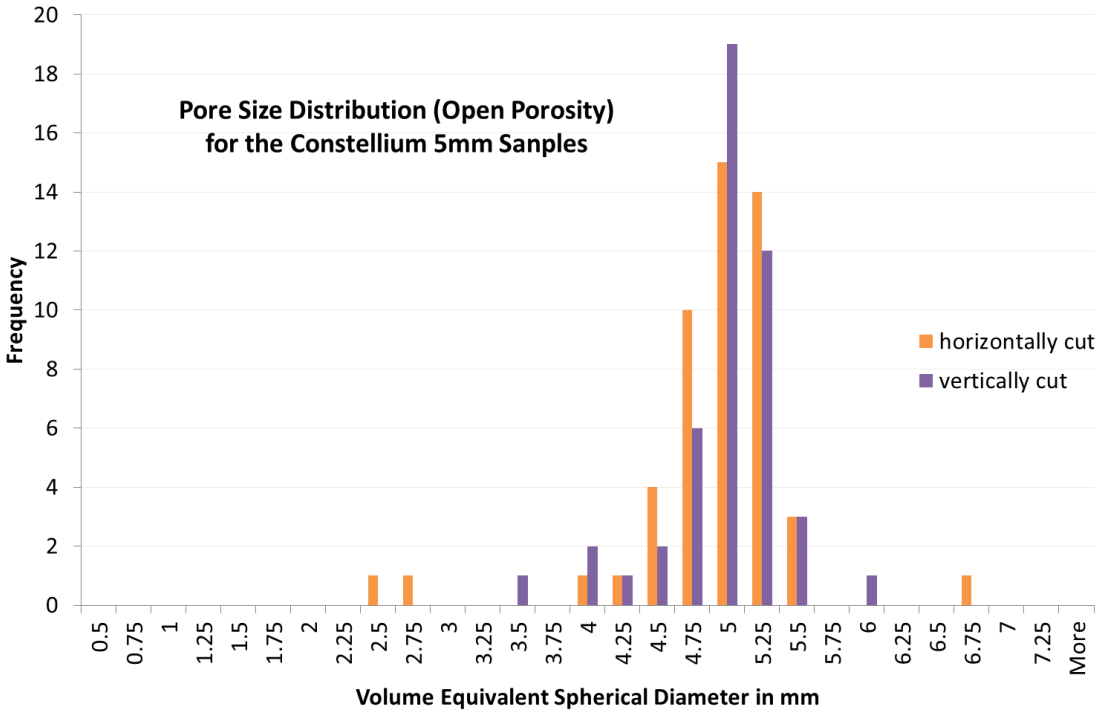

Figure 49. Histogram showing the pore size distribution of the open porosity for Constellium-produced, 5mm pore samples cut both horizontally and vertically from a block.

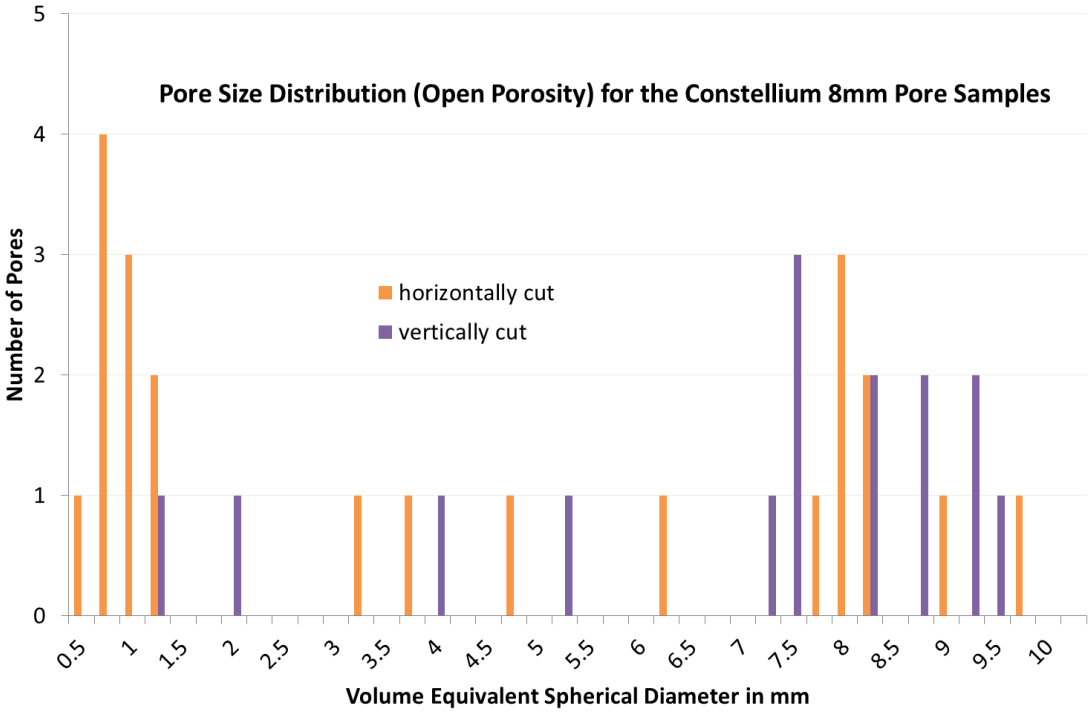

Figure 50. Histogram showing the pore size distribution of the open porosity for Constellium-produced, 8mm pore samples cut both horizontally and vertically from a block.

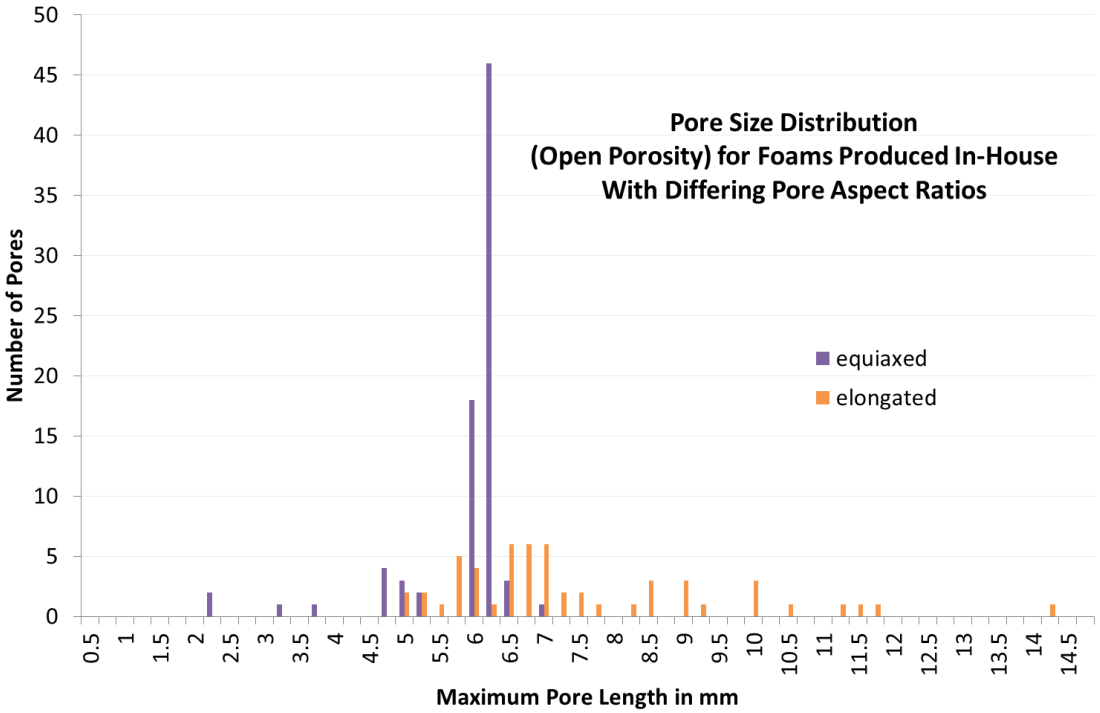

Figure 51. Histogram showing the pore size distribution of the open porosity for foams made in-house with differing pore aspect ratios, equiaxed and elongated.

All the samples contain pores much smaller than the preform/intended pore size. These are probably created by preform fragments/chips that have broken off during filling of the mould. As the sample size is fixed, it is obvious that the number of pores per sample decreases as the pore size increases. As the number of pores per sample decreases, the average pore size is affected more and more by the presence of the small, unintended pores; this is especially true for the 8mm pore size samples which contain very few pores per sample.

The graphs of pore size distribution (figures 47 to 51) are good visualisation tools that provide a better understanding of the range and modal pore size. For the Constellium-produced foams, the manufacturer suggested pore size is generally a good representation of the actual pore size with respect to the volume equivalent spherical diameter. The exception to this is the 3mm pore samples that appear to be slightly larger than expected. The majority of pores in the 3mm samples actually fall between 3.26mm and 3.75mm, implying that the preform dough was cut inaccurately.

The 8mm samples seem to have three relatively distinct groups of pore size; small (less than 2mm); medium (3.01mm and 6.25mm) and large (7.01mm and 9.75mm). The small pores are most likely a result of preform fragments/chips. The medium pores could be due to fully broken preform, i.e. one pellet that has broken into roughly two parts. The large pores most likely represent unbroken (and almost unbroken) preform pellets. These type of pores will be found in all the samples and not just the 8mm pore size however, as the number of pores in the 8mm sample are so few, the different groups are more defined and thus can be more easily distinguished from one another.

Over all pore sizes, the samples machined horizontally from the parent block tend to have a higher frequency of smaller pores compared to those machined vertically. For the in-house samples with differing pore aspect ratio, the pore size distribution graph in figure 51 shows the pore size in terms of the measured maximum pore length. As the pores are cylindrical, this length will be slightly larger than the suggested pore length (which is the cylinder length) as shown in figure 52.

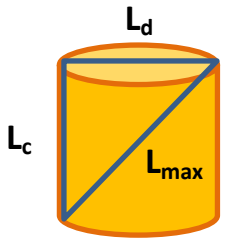

Maximum pore length L_{max} > suggested pore length L_c

$$L_{max}^2 = L_c^2 + L_d^2 \text{ (pore diameter)}$$

Figure 52. Schematic showing the maximum and suggested pore length for cylindrical pores.

For the equiaxed (4.5mm diameter x 4.5mm length) pore sample, the majority of pores have a maximum length that falls between 5.76mm and 6.25mm. Using Pythagoras' theorem and assuming the pore diameter is approximately 4.5mm (set by the extrusion die) this relates to a pore length of roughly between 3.6mm and 4.34mm, slightly shorter than the suggested pore length. Very few pores (17 out of a total of 81) fall outside of this range, implying that little breakage of the pellets

occurred and the smaller than expected pore length is due to the dough being cut inaccurately. Unfortunately for the elongated pore size, the automatic algorithm to separate objects was unable to accurately identify full pores and tended to split single pores into two or more parts as shown in figure 53. The image-based pore size measurement is therefore unreliable and the maximum pore length is much smaller than in reality. Further and more bespoke image analysis is required to rectify this.

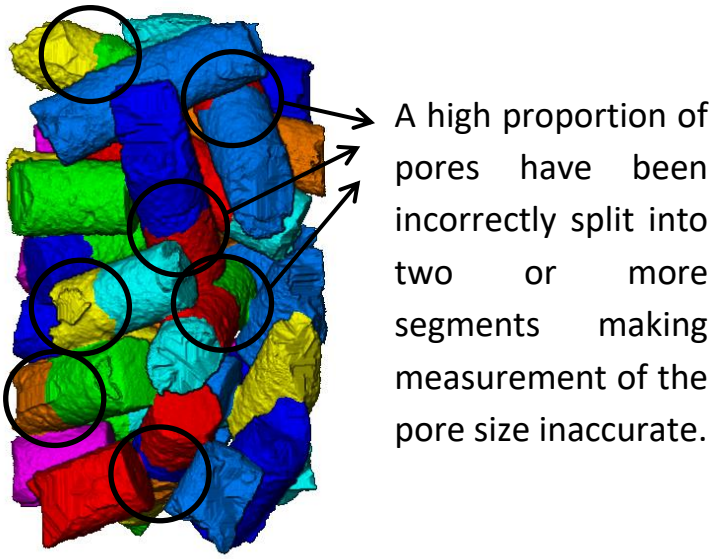

Figure 53. Segmented volume showing open porosity of foam with elongated pores but where the pores have been inaccurately separated.

There is no discernible trend between the number or size of the closed porosity in relation to the open porosity pore size. Again this suggests the closed porosity is a result of processing conditions and is unrelated to the preform/ open porosity size.

It should be noted that only a selection of samples were imaged (and thus characterised) using x-ray CT therefore, for consistency, all volume fraction/porosity values given in other sections of this work are based on density measurements and were calculated during sample manufacture as described in section 2.3.

5. HEAT TRANSFER AND PERMEABILITY

In the following sections the performance and limitations of the heat transfer rig (described in detail in section 2.4) have been explored and test parameters optimised so that the rig produced the most reliable measurements.

Once sufficient test parameters had been established, investigations could focus on exploring relationships between various aspects of pore architecture and the heat transfer behaviour of foam. Explanations of, and information gained from these studies has also been detailed in this section.

5.1 RIG VALIDATION

5.1.1 REPEATABILITY

In order to better understand the level of test repeatability, multiple heat transfer tests were carried out using a single foam sample; this was machined using wire-cut EDM (see section 2.3) from a foam block with 2mm pores provided by Constellium. The sample dimensions and weight, measured using digital callipers and scientific scales accurate to 2dp were as follows; 19mm diameter, 31.05mm length and 7.40g. For all tests the flow of coolant was kept constant at 7litre/min controlled by a 0-15litre/min flowmeter (BOC) and constant pressure of 2bar controlled by a pressure regulator (Series 8500, BOC). The flow rate was chosen as the flowmeter is most accurate in the centre 50% of its scale as stated by the manufacturer (BOC). The test set up was identical to that described in section 2.4.

A total of twelve tests were carried out and each test ran for 15 minutes. Various test conditions were used; these are given in table 7.

Table 7. Test conditions for investigating the level of repeatability of the heat transfer rig

Condition	Repeat number	Flow rate re-set from 0	Change in sample position	Additional info
1	1	NO	NO	
1	2	NO	NO	
1	3	NO	NO	
2	1	YES	NO	
2	2	YES	NO	
2	3	YES	NO	
3a	1	NO	ROTATED AXIALLY	
3a	2	NO	ROTATED AXIALLY	
3a	3	NO	ROTATED AXIALLY	
3b	1	NO	ROTATED AXIALLY	SAMPLE FLIPPED 180° LONGITUDINALLY
3b	2	NO	ROTATED AXIALLY	
3b	3	NO	ROTATED AXIALLY	

During each test the pressure difference between the two chambers was also recorded using a pressure transducer with operating range of 0-100mbar (Testo 510, Testo Ltd). Readings were taken at minutes 0, 1, 3, 5, 7, 9, 11, 13 and 15. Heat transfer coefficients were calculated by means of equation 13 (see section 2.4) using averaged data collected in the final minute of each test. For each test condition set, the standard deviation of the heat transfer coefficients and pressure drops were calculated.

5.1.2 PROLONGED TEST DURATION

In order to establish at what point acceptable steady state heat transfer behaviour is reached, and thus what length of test is required, a number of prolonged tests were carried out on foam samples provided by Constellium.

Two Al-Si-Mg alloy sponge blocks were supplied in an as cast condition with average pore sizes of 2mm and 8mm. One cylindrical sample was machined from each block using a combination of conventional band-saw cutting and wire-cut electrical discharge machining (EDM) (see section 2.3). The sample dimensions and weights, measured using digital callipers and scientific scales accurate to 2dp were as follows -

2mm pore size, 19mm diameter, 31.05mm length, 7.40g

8mm pore size, 19mm diameter, 32.55mm length, 3.86g

The testing rig was set-up as described in section 2.4. For each sample the test was repeated using flow rates of 15, 25 and 35litre/min and the flowrate was controlled using a 0-50litre/min flowmeter (BOC). The pressure remained constant at 2bar for all tests and was controlled by a pressure regulator (Series 8500, BOC). Each test started with a full cylinder of compressed air and was left to run until it had been exhausted (i.e. the content gauge reached 0) or 3 hours had elapsed. Pressure readings were taken at minute 0, 1 and then every 15 minute interval until the end of the test.

For data analysis, mean values for were calculated for every minute interval throughout the tests and in turn used to calculate heat transfer coefficients using equation 13 (see section 2.4). The calculated values were then plotted on a graph of heat transfer coefficient versus time.

5.2 FOAM STRUCTURE-HEAT TRANSFER INVESTIGATIONS

5.2.1 METAL CONDUCTIVITY

Foam manufactured at the Constellium factory is done so using an aluminium casting alloy containing silicon and magnesium as alloying additions (Al_{con}). It was unfeasible to use the same alloy for foam made in-house, which instead was made using commercially pure aluminium (Al_{pure}). As a result, the two foam types are not directly comparable and so it was imperative to investigate the relationship between the foam matrix material and heat transfer.

Foam samples were made using three different metals as the matrix material; Al_{pure} (99.85%, William Rowland LTD.), Al_{con} (Al-Si-Mg, as cast condition, Constellium) and tin (99.75-99.99%, William Rowland LTD.). In order to produce samples as uniform as possible, solid salt spheres that had been sieved to fall within the range of 2.36-2.8mm diameter were used as the preform material. In addition, alike-porosity Al_{pure} and Al_{con} samples were also made using the salt dough technique. For these samples dough was made by combining NaCl (General purpose grade, Fisher Scientific), which had been pre-powdered using a hand held blender, with flour (Shipton Mill) and distilled water using a respective ratio of 70:15:15. Dough lengths were extruded six times using an electric meat grinder (model MG510, PRO1600 Series, Kenwood) and a 4.5mm diameter extrusion die. The dough lengths were left to dry and harden before being cut into 4.5mm long pellets and heat treated in a chamber furnace (Lenton Thermal Designs LTD) using a staggered heating profile with maximum temperature of 700°C over a six hour period. The pellets were transferred to the infiltration mould as individual particles to use as the preform.

Infiltration of the preforms was achieved using an infiltration rig described in detail in section 2.2 but without use of the vacuum. The furnace was heated at a rate of 20°C/min up to a hold temperature of 740°C for the Al_{pure} and Al_{con} samples and 300°C for the tin samples. Each sample had a dwell time of 1 hour 45 minutes.

Due to differences in flow behaviour of the molten metals, a trial and error approach was needed to find infiltration pressures that would produce equivalent samples for each metal i.e. with consistent percentage porosity. Details of the infiltrations selected for heat transfer testing are shown in table 8.

Note: For tin, identical porosity samples could not be realized as this would have required infiltration pressure less than the feasible minimum of the rig. The samples chosen to be tested were those closest in percentage porosity to the Al_{con} and Al_{pure} samples already produced.

Table 8. Infiltration details for samples made to investigate the effect of the matrix metal on heat transfer behaviour of foams

Matrix metal	Type of preform used	Amount of preform used (g)	Amount of metal used (g)	Infiltration pressure (bar)	Percentage porosity of samples (%)
Al_{Con}	salt spheres	200.31	282.6	2.3	72-73
Al_{Con}	salt spheres	206.13	270.12	2.4	73-75
Al_{pure}	salt spheres	210.2	264.07	2.5	72-73
Al_{pure}	salt spheres	205.5	281.03	2.6	71-74
tin	salt spheres	221.4	892.62	0.5	65-67
Al_{Con}	dough pellets	90.08	274.02	1.5	66-67
Al_{pure}	dough pellets	79.73	278.4	1.8	67-69

For each infiltration the mould was removed from the furnace and placed on a copper block to allow for unidirectional cooling. After 45 minutes the sample was removed from the mould and the top and bottom edges removed using a mechanical hacksaw. The salt was leached by immersing the sample in water overnight.

Three cylindrical samples, approximately 32mm in length by 19mm diameter, were machined from each infiltration using EDM (see section 2.3). Density and percentage porosity values for each cylindrical sample were calculated using the

exact dimensions and weight, measured using digital callipers and scientific scales accurate to 2dp. An example of each sample type is shown in figure 54.

Figure 54. Foam samples made in-house from l-r; salt spheres Al_{pure}, salt spheres Al_{con}, salt spheres tin, dough pellets Al_{pure} and dough pellets Al_{con}.

Samples were tested for their heat transfer behaviour using the rig described in section 2.4. For each sample the test was repeated using flow rates of 15, 25 and 35litre/min and the flowrate was controlled using a 0-50litre/min flowmeter (BOC). The pressure remained constant at 2bar for all tests and was controlled by a pressure regulator (Series 8500, BOC). Each test ran for 60 minutes. At minutes 0 (room temperature), 1, 5 and then every 5 minute interval until the end of the test, the pressure difference between the two chambers was also recorded using a pressure transducer with operating range of 0-100mbar (Testo 510, Testo Ltd).
Mean values were calculated for the final minute of the tests and in turn used to calculate heat transfer coefficients using equation 13 (see section 2.4). For further comparison, thermal conductivity and density measurements for the solid (i.e. un-foamed) metals were taken using standard methods described in section 2.5.

5.2.2 Pore Size

Changing the foam's pore size is possible using various foam manufacture methods, however, such wide ranging pore sizes, easily achievable using the salt dough technique, are uncommon if not unique. These large structural differences should

relate to much varied heat transfer behaviour and so the relationship between pore size and heat transfer was investigated.

Foams with four different average pore diameters; 2mm, 3mm, 5mm and 8mm, were provided by Constellium (Al-Si-Mg alloy, as cast condition). From each of the blocks cylindrical samples, approximately 32mm in length by 19mm diameter, were machined using a combination of conventional band-saw cutting and EDM. Sample dimensions were measured using digital callipers and weighed using scientific scales accurate to 2dp; these were used to calculate sample densities. An example of each sample type is shown in figure 55 and sample details have been listed in table 9.

Figure 55. Foam samples made by Constellium with average pore sizes from l-r; 2mm, 3mm, 5mm and 8mm.

Table 9. Details of samples used to investigate the effect of pore size on heat transfer behaviour.

Matrix metal	Pore Size (mm)	Pore shape	Number of Repeat Samples	Porosity Range (%)
Aluminium alloy (Alcon)	2	Cylindrical	6	70-74
Aluminium alloy (Alcon)	3	Cylindrical	15	66-75
Aluminium alloy (Alcon)	5	Cylindrical	17	77-85
Aluminium alloy (Alcon)	8	Cylindrical	17	78-89

The heat transfer capabilities of samples were assessed using the test set up as described in section 2.4. For each sample, repeat tests were run using flow rates of 15, 25 and 35litre/min and each test ran for 60 minutes. Mean values were calculated for the final minute of the tests and in turn used to calculate heat transfer coefficients using equation 13 (see section 2.4).

5.2.3 Machining Direction

As part of the industrial process, the density of the foam is in part controlled by compressing the preform into a block prior to heat treatment and infiltration. This is largely done by uniaxial pressure and it can therefore be assumed that the preform will be deformed to a certain extent parallel to the compression direction and thus the structure of the resultant foam will differ slightly in the x- and y-axes as shown in figure 56.

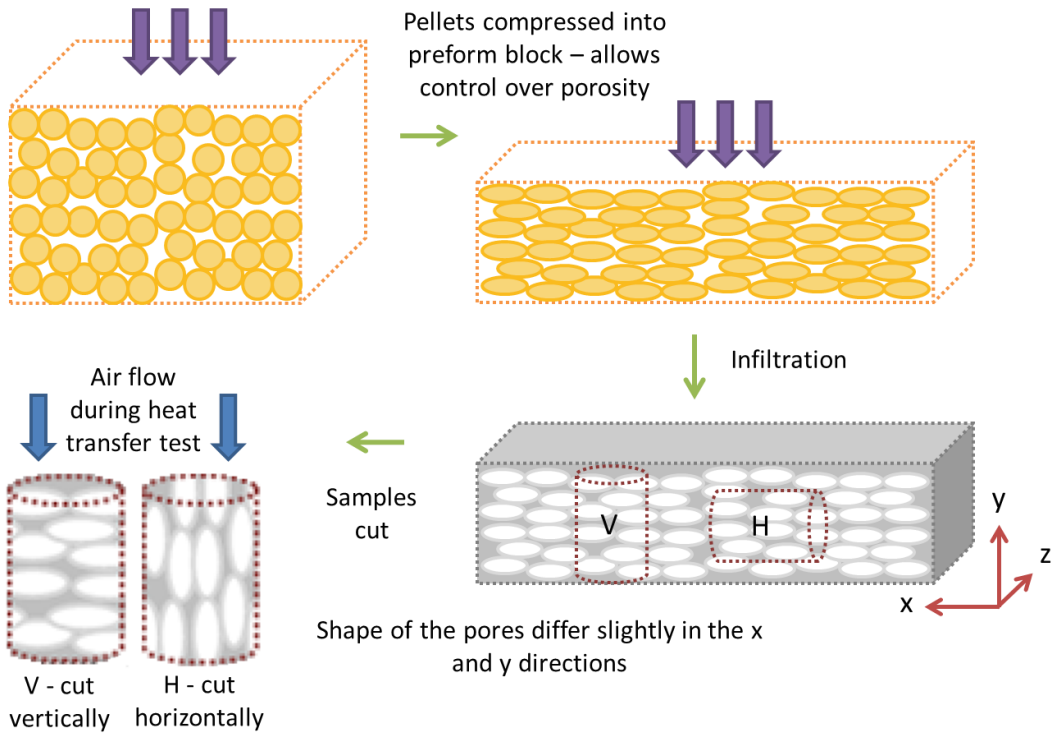

Figure 56. Schematic showing slight structural anisotropy of Constellium foam block due to preform processing

This provided an excellent opportunity to easily investigate whether small changes to the pore shape of a foam, without significantly changing the density or porosity, have an effect on the heat transfer behaviour.

Three foam blocks with average pore diameters of 3mm, 5mm and 8mm were provided by Constellium (Al-Si-Mg alloy, as cast condition). From each block a minimum total of ten cylindrical samples, approximately 32mm in length by 19mm diameter, were machined using a combination of conventional band-saw cutting and wire-cut EDM (see section 2.3). Half of the samples were machined vertically, i.e. parallel to the y-axis of the block. The remaining half were machined horizontally, i.e. perpendicular to the y-axis of the block.

Each foam sample was tested for their heat transfer performance using the method described in section 2.4. Tests ran for 60 minutes and were repeated three times per sample using flowrates of 15, 25 and 35litre/min and a constant pressure of 2bar.

The pressure difference between the two chambers was recorded throughout each test at minute 0 (room temperature), 1, 5 and then every 5 minutes interval up to 60 minutes. Mean values were calculated for the final minute of the tests and in turn used to calculate heat transfer coefficients using equation 13 (see section 2.4).

5.2.4 Pore Aspect Ratio

Using the semi-automatic method developed for in-house preform production, an easy yet effective way to radically change the shape of the foam pores was to change the aspect ratio of the dough pellets. For equiaxed pores with an aspect ratio of 1:1, the extruded dough was cut so that the pellet length is equal to its diameter (i.e. the diameter of the die used for extrusion). To create elongated pores with an aspect ratio of 1:3, the extruded dough was simply cut three times the length of its diameter. In addition, samples were also made with “pores” which ran the entire length of the sample.

Dough was made by combining NaCl (General purpose grade, Fisher Scientific), which had been pre-powdered using a hand held blender, with flour (Shipton Mill) and distilled water using a respective ratio of 70:15:15. Dough lengths were extruded six times using an electric meat grinder (model MG510, PRO1600 Series, Kenwood) and a 4.5mm diameter extrusion die. The dough lengths were left to dry and harden before being cut into 4.5mm, 13.5mm and 50mm long pellets. The pellets were heat treated in a chamber furnace (Lenton Thermal Designs LTD) using a staggered heating profile with maximum temperature of 700°C over a six hour period.

Infiltration of the preforms was achieved using an infiltration rig described in detail in section 2.2 but without use of the vacuum. The furnace was heated at a rate of 20°C/min up to a hold temperature of 740°C. Each sample had a dwell time of 1 hour 45 minutes. Eight infiltrations were carried out in total; three using the 4.5mm long, equiaxed-type preform, three using the 13.5mm long, elongated-type preform and two using the 50mm long, full-length preform. Full infiltration details are given in table 10.

Cylindrical samples, approximately 32mm in length by 19mm diameter, were machined from each infiltration using a combination of conventional band-saw cutting and wire-cut EDM (see section 2.3). An example of the full-length pore sample type, both as-cast and after machining is shown in figure 57. Examples of all the pore types; equiaxed, elongated and full-length, are shown in figure 58.

Each sample was tested for their heat transfer performance using the method described in section 2.4. Tests ran for 60 minutes and were repeated three times per sample using flowrates of 15, 25 and 35litre/min and a constant pressure of 2bar. The pressure difference between the two chambers was recorded throughout each test at minute 0 (room temperature), 1, 5 and then every 5 minutes interval up to 60 minutes. Mean values were calculated for the final minute of the tests and in turn used to calculate heat transfer coefficients using equation 13 (see section 2.4).

Table 10. Infiltration details for samples made to investigate the effect of pore aspect ratio on heat transfer behaviour of foams

Type of preform used	Amount of preform used (g)	Amount of aluminium used (g)	Infiltration pressure (bar)	No of samples produced from infiltration	Percentage porosity of samples (%)
equiaxed	91.86	281.05	1.5	3	72-73
equiaxed	79.73	278.4	1.8	3	67-69
equiaxed	96.64	277.83	2	3	63-65
elongated	104.16	290.6	0.5	3	61-62
elongated	62.43	283.46	1.4	2	60-61
elongated	92.37	275.59	1.5	4	60-61
full length	115.54	236.86	2	1	66
full length	124.2	244.2	1.8	1	73

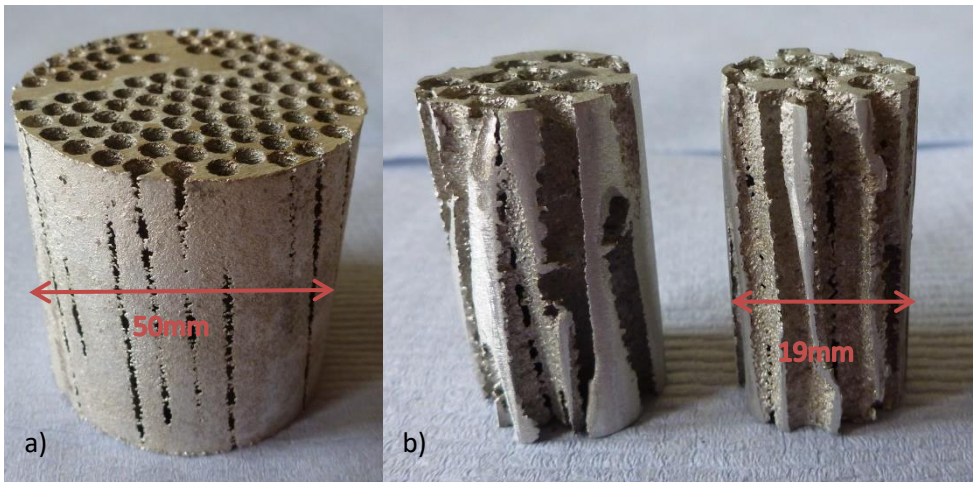

Figure 57. Full-length pore sample type, a) as-cast and b) after machining.

Figure 58. Foam samples made in-house with pores from l-r; equiaxed 4.5mm, elongated 4.5mm x 13.5mm and 4.5mm x full sample length.

5.3 Results And Discussion

In order to ensure the rig was as reliable as possible, a number of optimisation tests were performed. The results of the repeatability tests are given in table 11. Condition 1 (no change in sample position or flow rate) corresponds to the error induced by the rig and includes parameters such as the thermocouple and pressure transducer measurements. Condition 2 corresponds to human error generated as a result of manually setting the flowrate using a flowmeter. As expected, the highest degree of variation is a result of sample position and is demonstrated in conditions 3a and 3b. As the structures are random by nature, changing the sample position will have an effect on the air flow path and thus affect both the flow and thermal properties. For the heat transfer coefficient measurement, there is deviation around the mean of approximately 8.6%. The pressure drop measurement however is much more sensitive to sample position with variation from the mean being as high as 42% when the flow of air through the sample is reversed (i.e. the sample is flipped 180° longitudinally). Entrance/exit and wall effects are thought to have a

large effect on permeability measurements especially when the ratio of sample thickness to pore size is small [115][129].

Table 11. Results of the repeatability tests along with standard deviations for the different condition sets.

		Condition			
		1	2	3a	3b
		Heat transfer coefficients in W/m^2K			
Repeat	1	15.93	14.28	14.15	17.49
	2	16.27	14.32	15.12	14.95
	3	16.41	15.04	14.38	16.64
Standard deviation		**0.24**	**0.43**	**1.32**	
		1.10			
		Pressure drop at min. 15 in mbar			
Repeat	1	25.00	16.23	18.64	26.62
	2	24.93	16.15	18.38	35.98
	3	24.91	16.75	16.34	44.22
Standard deviation		**0.05**	**0.33**	**11.27**	
		8.81			

A more accurate insight into heat transfer behaviour would be gained by using a large number of repeat samples and, ideally, larger sized samples. This would reduce the likeliness that small disparities in the structure of these foams would cause disruption to the heat transfer/ flow behaviour and thus the properties could be more reliably characterised. With respect to this outcome, the number of samples tested in all subsequent investigations was maximised as far as possible given the material available (for foam provided by Constellium) and time constraints (for foam produced in-house). The size of the foam test samples remained unchanged. The overall aim of the work presented here is to advance the understanding of the relationship between the structure of foam and its heat transfer behaviour, so to ultimately improve performance in heat transfer

applications. It was decided therefore that the sample size should better represent the application rather than the bulk material. It must be noted that any reported measurements here may not be directly comparable to associated data presented by similar studies in the literature; this is especially true if vastly different sample dimensions or test set-up has been used. Nevertheless, comparison between samples tested here to discern trends should be possible.

Prolonged tests were carried out in order to find out at what point steady state heat transfer behaviour was reached. Figure 59 is a plot of heat transfer coefficient vs. time and shows that steady state (defined as when the rate of change in the measured heat transfer coefficient falls below $1W/m^2K$ over a ten minute period) is achieved, for both high and low flow rates, after approximately one hour.

To be used as an indication of permeability, the pressure drop across the samples was also measured throughout the tests and is shown in figure 60. The same trend is apparent whereby the pressure drop seems to stabilise over time, although this occurs more quickly after around 30 minutes (the instability may relate to structural changes as steady state heat flow is established).

To allow the overall heat transfer behaviour to reach steady state, including both heat transfer coefficient and pressure drop, the time length for all subsequent tests performed using the heat transfer rig was set at 1 hour.

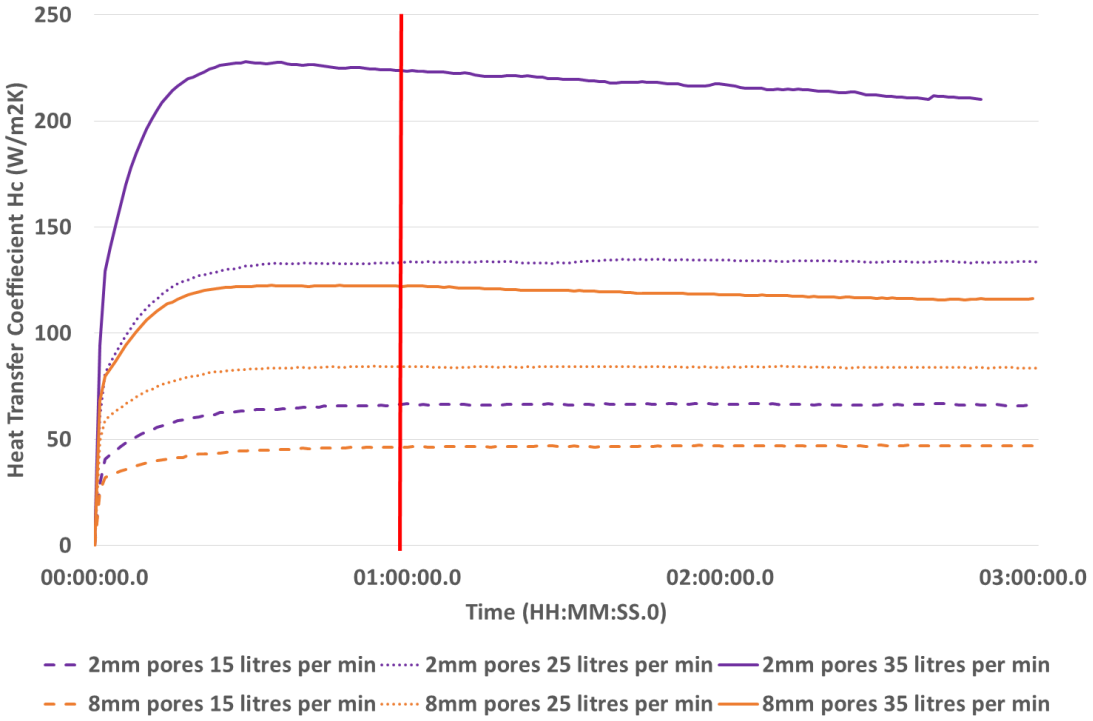

Figure 59. Plot of heat transfer coefficient vs. time for prolonged heat transfer tests

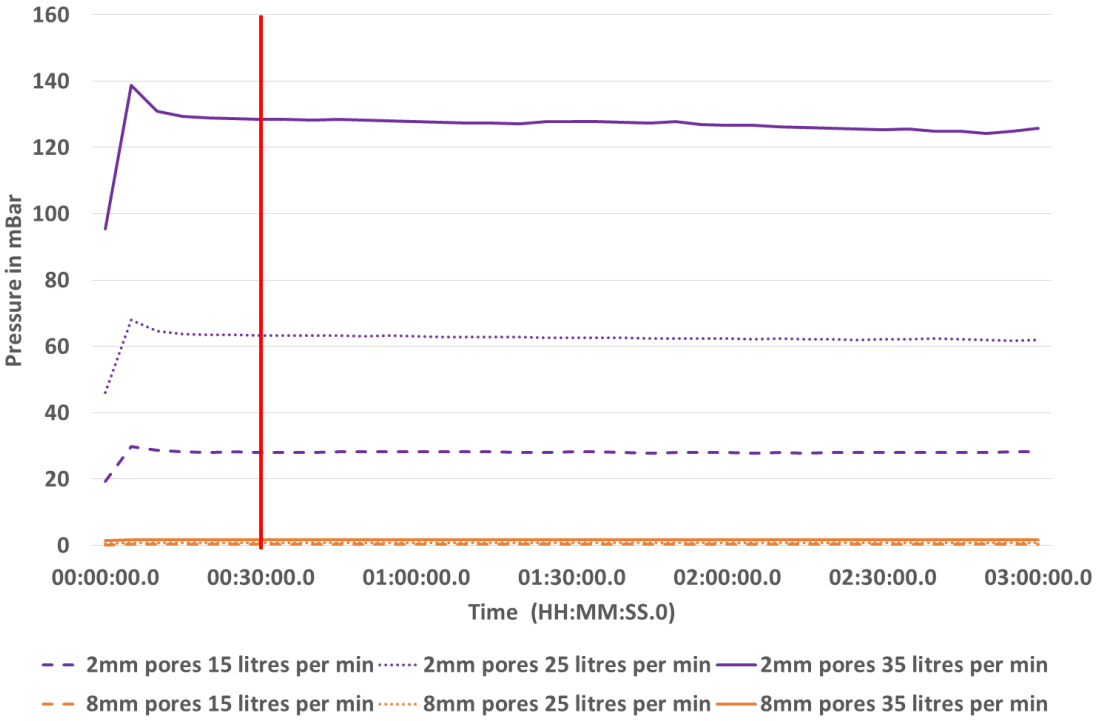

Figure 60. Plot of pressure difference vs. time for prolonged heat transfer tests

Throughout this work three different metals were used as the foam matrix material. Foams provided by Constellium, were manufactured using an aluminium casting alloy, Al_{con}, containing silicon and magnesium as alloying additions. In-house foams were made using commercially pure aluminium, Al_{pure}, Al_{con} and tin. For comparative purposes the effect of matrix material on heat transfer behaviour was investigated. The thermal conductivities of the solid metals were measured using the laser flash technique as described in section 2.5 and are represented graphically in figure 61 as well as being listed in table 12.

As expected, Al_{pure} has the highest thermal conductivity followed by Al_{con}, which is around 25% lower. The thermal conductivity of tin is roughly 70% lower than that of Al_{pure}. The measured data correlates relatively well with 300K (~room temperature) values stated in the literature; 2.37W/cm.K and 0.67W/cm.K for pure aluminium and tin respectively. The suggested thermal conductivity of Al_{con} provided by Constellium was 1.6W/cm.K, which again compares well with the measured values.

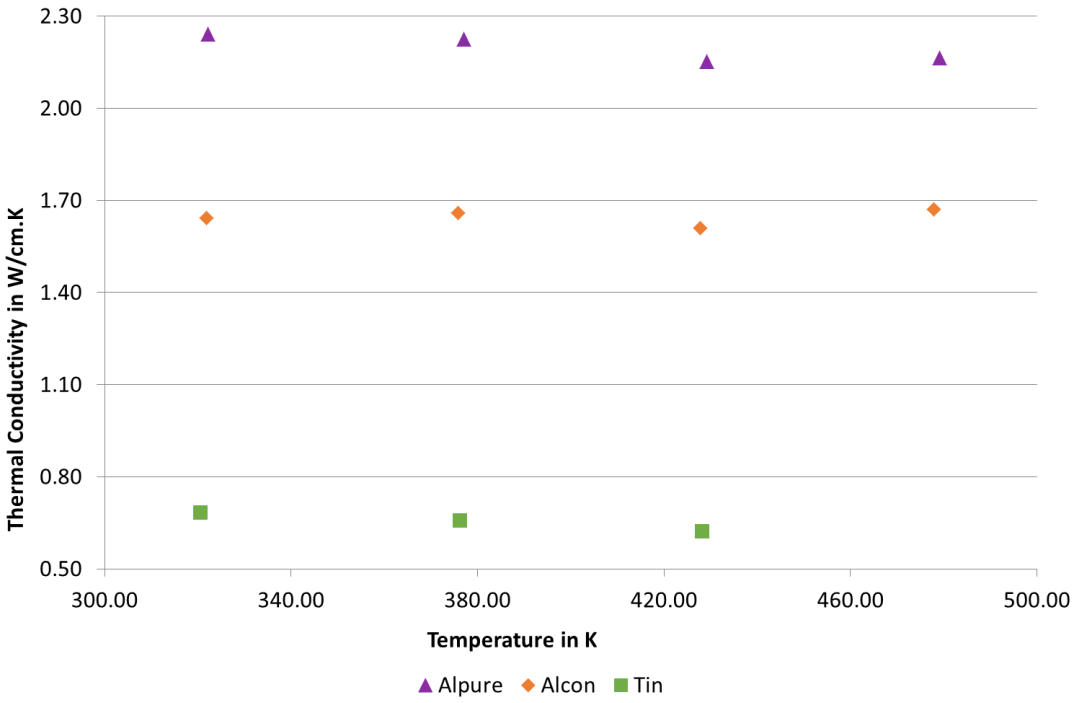

Figure 61. Plot of the solid metal thermal conductivities for Alpure, Alcon and tin, measured using the laser flash method.

Table 12. Measured thermal conductivities for Al_{pure}, Al_{con} and tin.

Temperature in °C	Temperature in K	Thermal Conductivity in W/cm.K	Thermal Conductivity in W/m.K
Al_{pure}			
49.00	322.15	2.24	224.23
104.00	377.15	2.23	222.57
156.00	429.15	2.15	215.37
206.00	479.15	2.17	216.51
Al_{con} 3 disc average			
48.67	321.82	1.64	164.29
102.67	375.82	1.66	165.92
154.67	427.82	1.61	160.95
204.67	477.82	1.67	167.02
Tin 3 disc average			
47.33	320.48	0.68	68.40
103.00	376.15	0.66	65.79
155.00	428.15	0.62	62.28

Foam samples were made in-house using each of the three metal types as the foam matrix material. Two sets were produced; one with 2.36-2.8mm, spherical pores (Al_{pure}, Al_{con} and tin) and one with 4.5mm cylindrical pores (Al_{pure} and Al_{con} only). Each set of samples were manufactured so that they were as similar as possible, given that the structure of foam is inherently random. Each sample was then tested for their heat transfer behaviour using the rig described in section 2.4.

Figures 62 and 63 show plots of average heat transfer coefficient vs flow rate for the spherical and cylindrical pore samples respectively. Across all flow rates there is a slight decrease in heat transfer coefficient for Al_{con} samples compared to those for Al_{pure}; depending on flow rate this ranges between 3.5 to 5.1% for those with spherical pores and between 2.5 to 7.5% for those with cylindrical pores. As the pore size and porosity were kept constant, this decrease can be chiefly attributed to the 25% decrease in thermal conductivity of the solid metals.

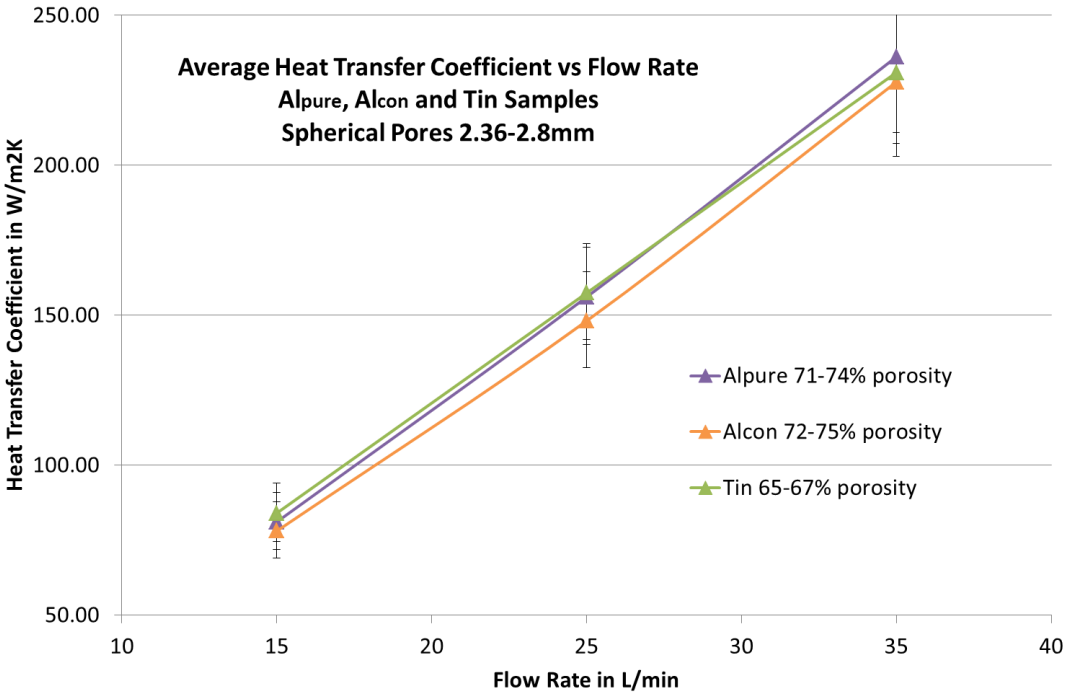

Figure 62. Plot of average heat transfer coefficient against flow rate for Al_{pure}, Al_{con} and tin samples with spherical pores, 2.36-2.8mm in diameter. Error bars show the average accumulative errors as described in section 2.4.

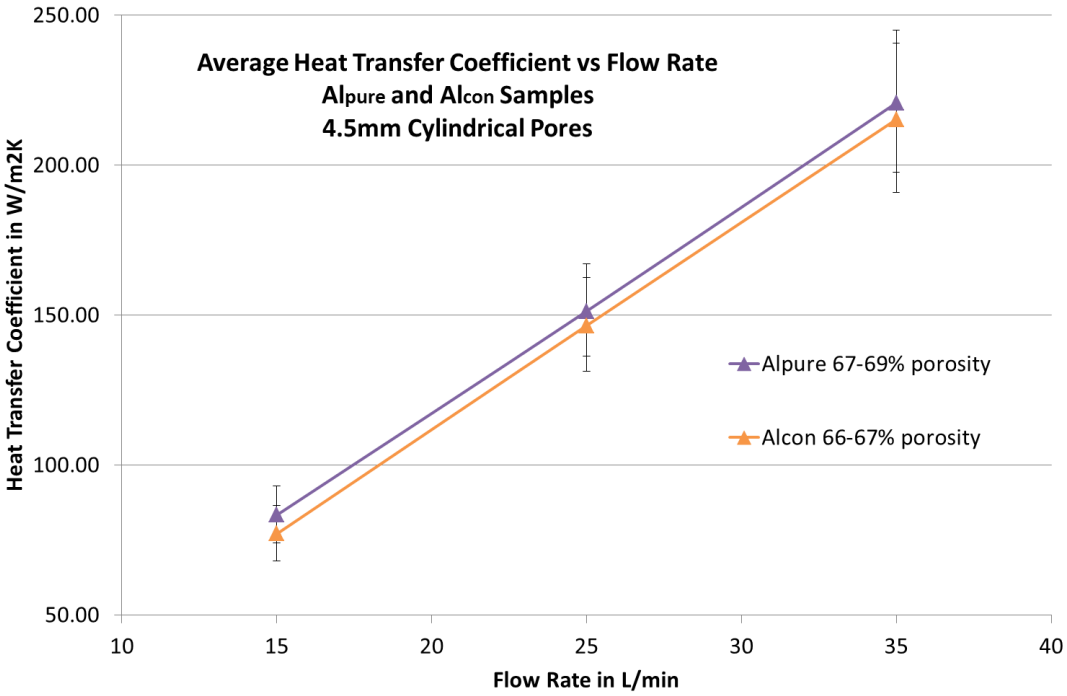

Figure 63. Plot of average heat transfer coefficient against flow rate for Al_{pure} and Al_{con} samples with 4.5mm equiaxed, cylindrical pores. Error bars show the average accumulative errors as described in section 2.4.

Unfortunately, due to limitations of the in-house manufacturing equipment, a consistent level of porosity could not be achieved using tin as the foam matrix metal and so direct comparisons to the aluminium samples cannot be made. On first impressions, figure 62 appears to show that the tin samples have very similar levels of heat transfer to those made from Al_{pure} and Al_{con}. However, this does not take into account the difference in porosity. It is generally accepted that for a uniform pore size, decreasing the porosity of the foam corresponds to an increase in heat transfer. This is especially true for metals with low thermal conductivities as increasing the relative density can significantly reduce high thermal resistance in the solid phase [29]. If this reasoning is applied to the results shown in figure 62, increasing the porosity of the tin samples to be in-line with those made from aluminium would reduce their heat transfer capability. This would mean that actually, the heat transfer of the tin samples would be inferior to those made from aluminium; a more expected outcome given the large difference in the solid metal thermal conductivities and the major contribution it is thought to have on the effective thermal conductivity of metal foam. It is possible however that in these foams, the rate determining step is the transfer of heat to the air rather than through the metal. If this was the case then the metal conductivity would be of little importance and any difference in heat transfer would be due more to variation in structure. As the tin foams have lower porosity but uniform pore size compared to the aluminium ones, it could be that more of the fine space between the salt particles were filled, increasing the surface area and thus enhancing the rate of heat transfer. A plot of heat transfer coefficient against porosity for the spherical pore samples is shown in figure 64. The range of porosity for each sample type is not wide enough for any trend to be clear.

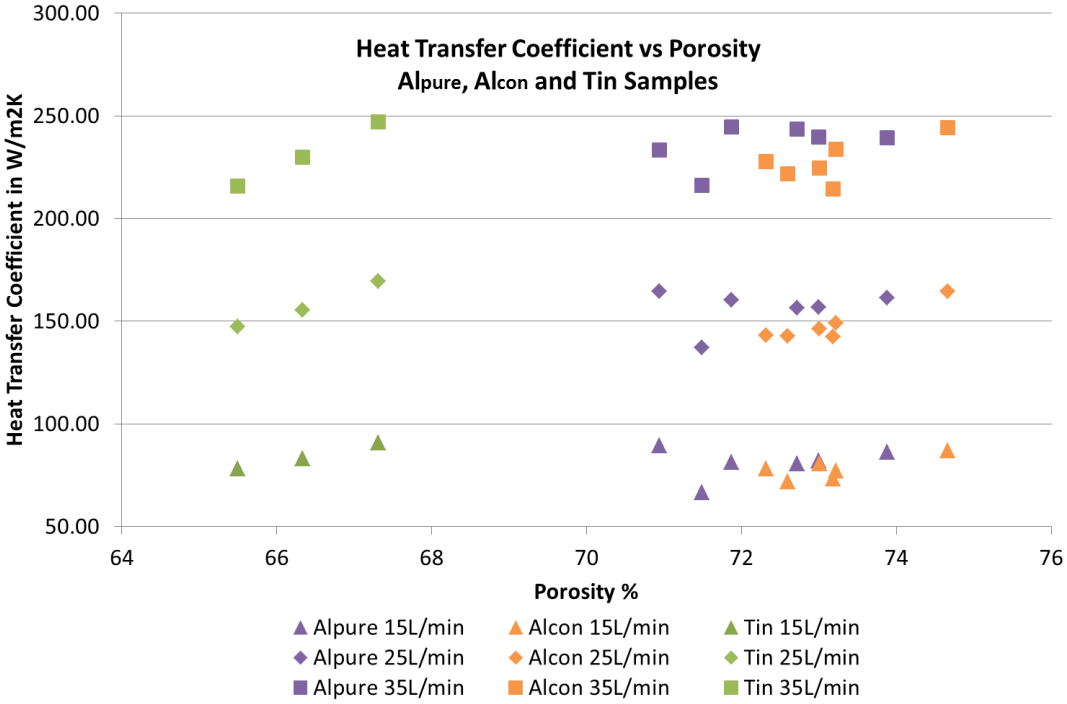

Figure 64. Plot of heat transfer coefficient against percentage porosity for Alpure, Alcon and tin samples with spherical pores 2.36-2.8mm in diameter and across flow rates of 15, 25 and 35L/min.

For each metal type, the average pressure drop at minute 60 of the heat transfer tests is plotted in figure 65 for spherical pore samples and figure 66 for cylindrical pore samples. For both pore types and over all flow rates, the average pressure drop is relatively consistent for the Al_{pure} and Al_{con} samples, only varying by a maximum of 5.8mbar (cylindrical pore samples at 35 L/min). This small variation is most likely due to minor structural variations rather than as a consequence of change in metal type. The higher amount of variation in pressure drop seen from the tin samples can again be attributed to the inconsistent density/porosity. Increasing the density of metal foam whilst keeping the pore size/shape consistent will increase the pressure drop as the additional metal will increase the resistance to fluid flow.

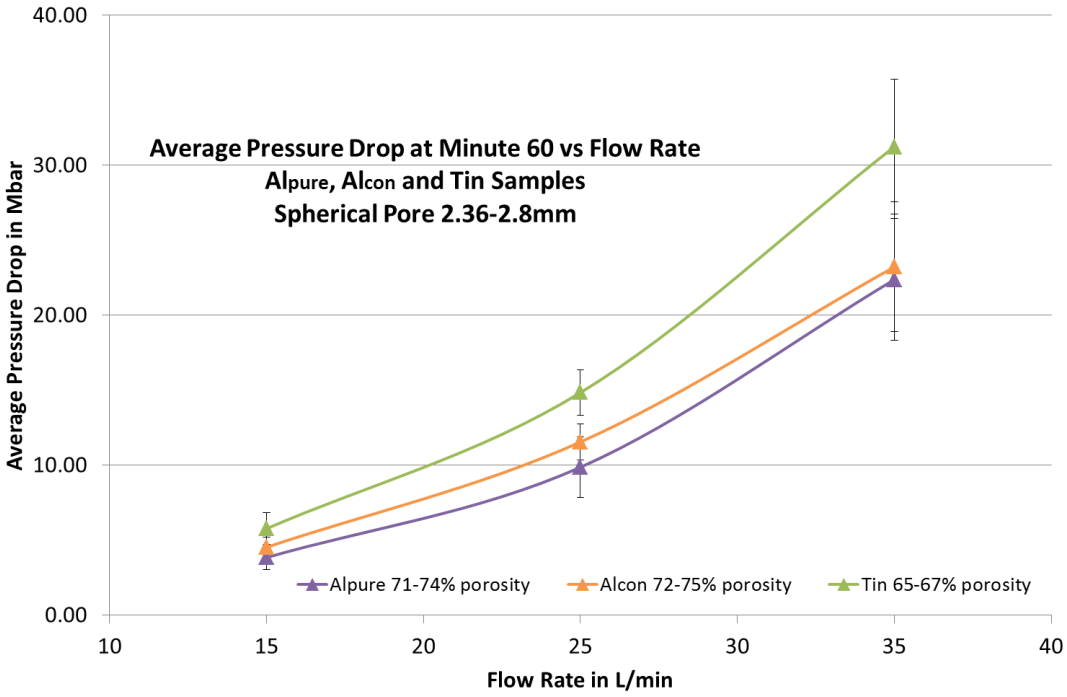

Figure 65. Plot of average pressure drop against flow rate for Al_{pure}, Al_{con} and tin samples with 2.36-2.8mm, spherical pores. Error bars show the standard deviation.

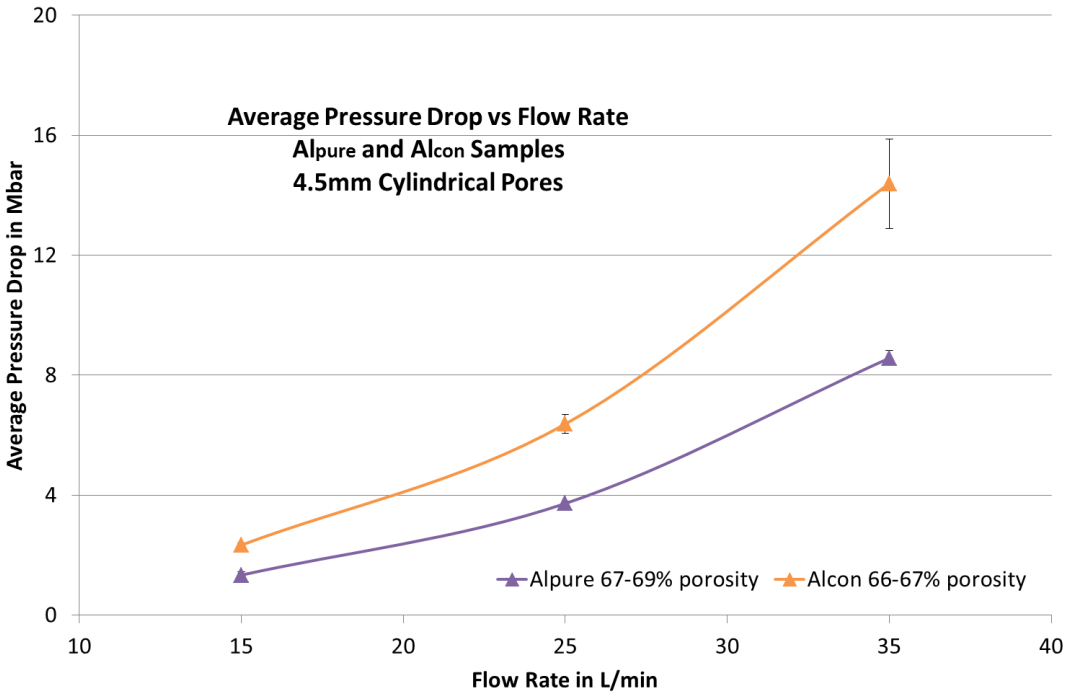

Figure 66. Plot of average pressure drop against flow rate for Al_{pure} and Al_{con} samples with 4.5mm, spherical pores. Error bars show the standard deviation.

The salt dough replication technique allows for large, controlled variation of the foam's pore size and so the relationship between pore size and heat transfer was investigated. Samples with 2, 3, 5 and 8mm pore diameters were provided by Constellium. In addition, the Al_{con}, 4.5mm pore samples made in-house for section 4.2.1 have also been included as they have consistent pore shape and foam matrix metal. All samples were tested to ascertain their heat transfer behaviour using the rig described in section 2.4. The corresponding plot of average heat transfer coefficient vs flow rate in figure 67 shows that improved heat transfer performance correlates with smaller pore diameters and this is true for all flow rates. The trend also becomes more pronounced at higher flow rates. It is possible that the smaller pore size causes increased air mixing and therefore enhanced heat extraction. It should be noted however that the range of sample porosities do not overlap for all pore sizes and so change in porosity as well as pore size will have contributed to the trend. The smaller pore size samples tend to correlate with higher density and, as discussed previously, this increase in density may improve the heat transfer behaviour simply because there is more metal to conduct the heat.

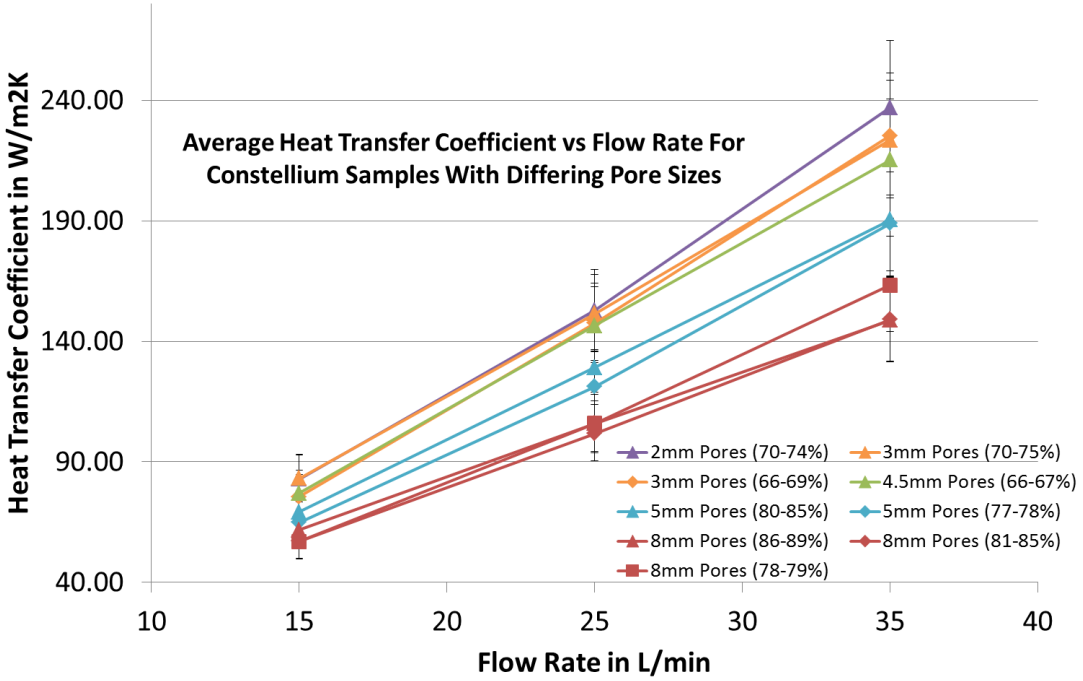

Figure 67. Plot of heat transfer coefficient against flow rate for Alcon foams with varying pore size. The percentages shown in the legend represent the porosity range of the samples. Error bars show the average accumulative errors as described in section 2.4.

To better visualise the pore size-heat transfer relationship for those samples that do have an overlap in density, figures 68 and 69 have been included and show plots of heat transfer coefficient against porosity for high (35L/min) and low (15L/min) flow rates respectively. At high flow rates 5mm pores generally show improved heat transfer over 8mm pores over the same range of sample density. Similarly, for the 2, 3 and 4.5mm pore size samples over a consistent density range, improved heat transfer is achieved with reduction of pore size. For the higher density/ smaller pore size group however, the trend is somewhat loose and may be more solidly established using more repeat samples. It may also be the case that there becomes a point at which further reducing the pore size no longer provides increased air mixing and in turn enhanced heat transfer. At low flow rates any difference in heat transfer due to change in pore size becomes much less defined.

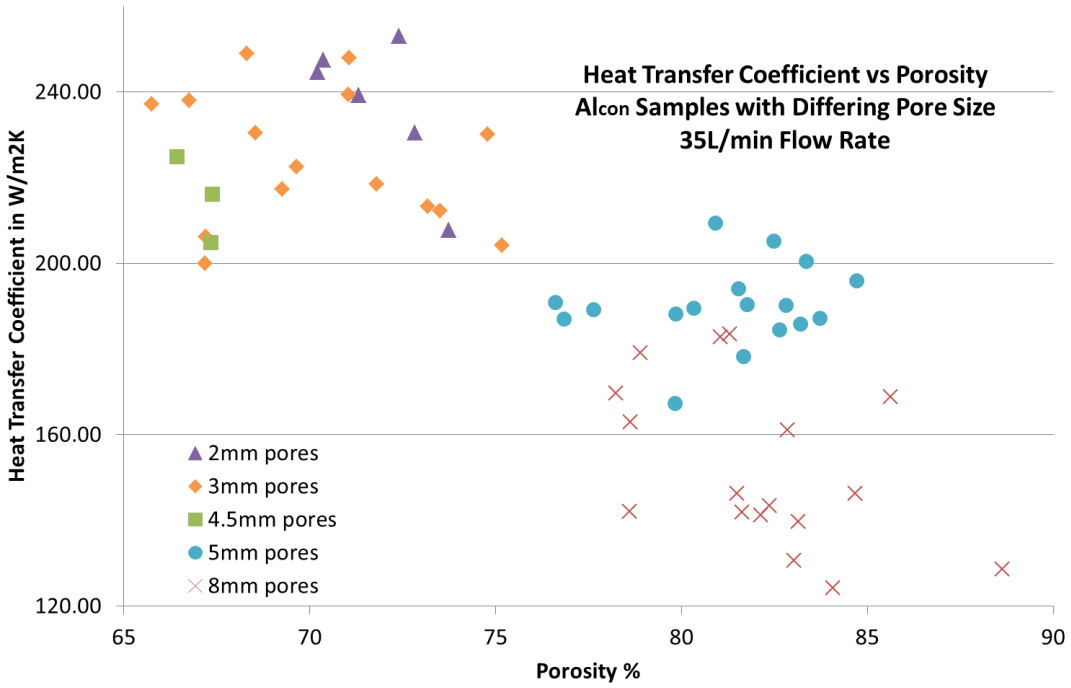

Figure 68. Plot of heat transfer coefficient against porosity for Al_{con} samples with differing pore sizes and using a flow rate of 35L/min.

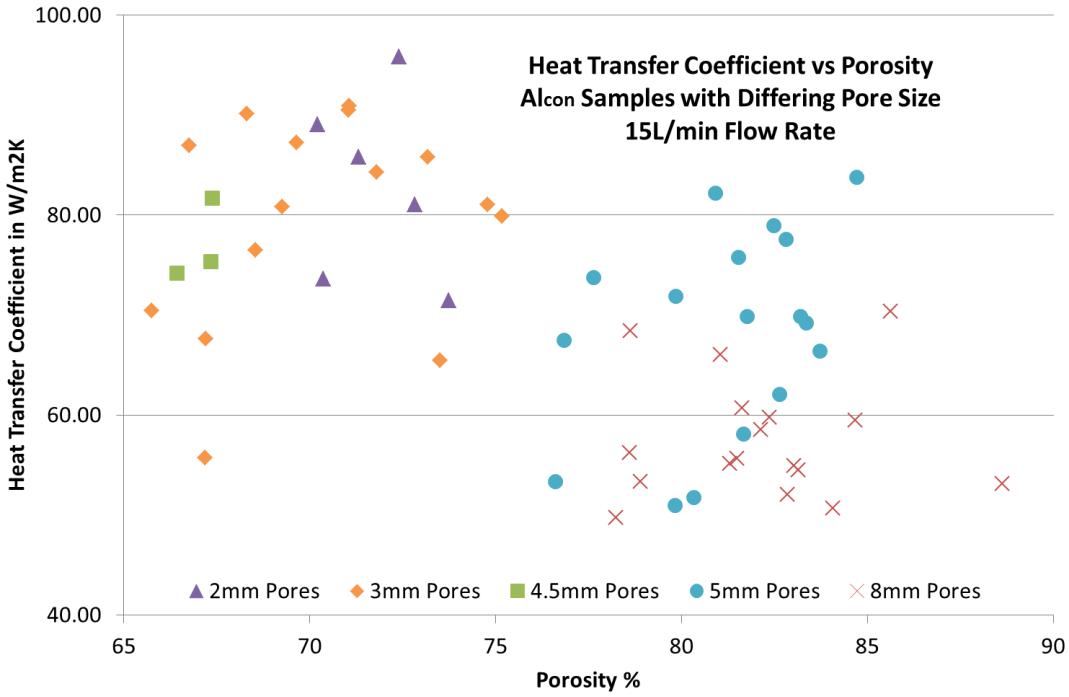

Figure 69. Plot of heat transfer coefficient against porosity for Alcon samples with differing pore sizes and using a flow rate of 35L/min.

Another important but often conflicting property to consider when looking at the overall heat transfer performance is permeability. As a measure of foam permeability the pressure drop across each sample was measured during testing. Figure 70 shows a plot of average pressure drop at test minute 60 against flow rate for samples with varying pore size. As expected a higher pressure difference and thus lower permeability corresponds to smaller pore size and vice versa. In general, the larger the pore size, the longer the free path for the air to flow; this reduces resistance and creates a less turbulent, more direct flow route.

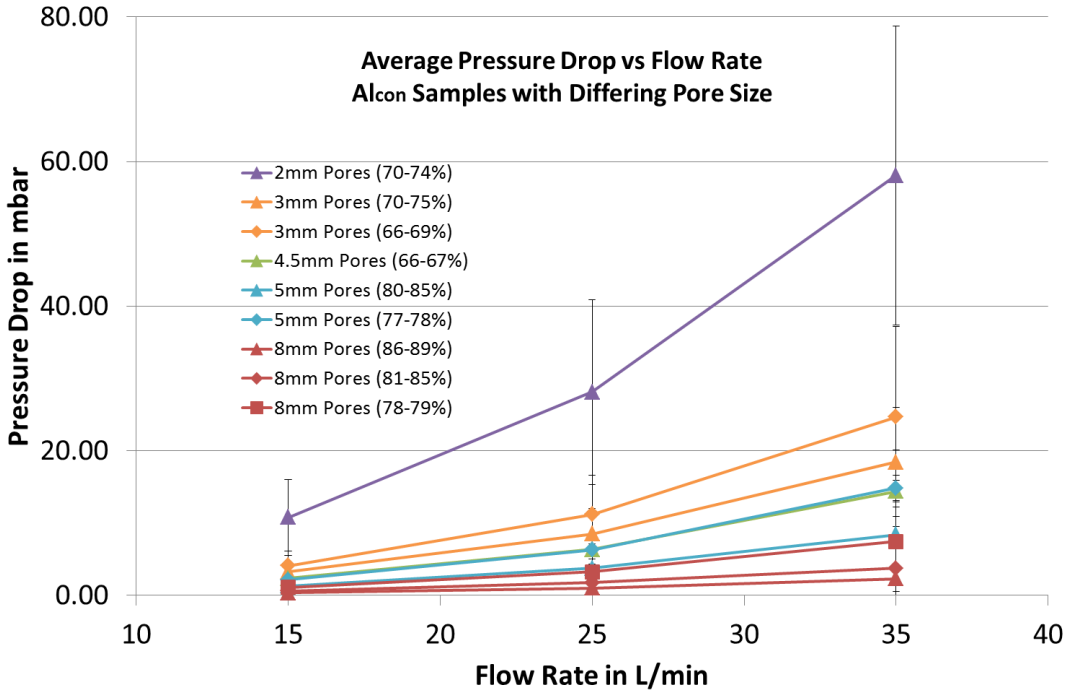

Figure 70. Plot of pressure drop against flow rate for Alcon samples with differing pore sizes. Error bars show the standard deviation.

Combining both heat transfer and permeability results it can be deduced that, as expected, enhanced heat transfer correlates with decreasing pore size but is also accompanied by an undesirable decrease in permeability. However, comparing the 2mm and 3mm pore sizes in particular, the difference in permeability would most likely outweigh any improvement in heat transfer. This is especially true for low flow rates where there is a relatively large difference in pressure drop with very little, if any, improvement in heat transfer. It would of course depend on the specific requirements of the application, but in general, metal foam heat exchangers of similar size to the samples tested here would have a beneficial compromise between heat transfer and permeability by having a pore size between 3-5mm.

A more comprehensive relationship between pore size and heat transfer behaviour may be established if a wider range of porosities could be tested over all pore sizes. However, there will be upper and lower limits to the range of porosities achievable. The upper porosity limit would be met once there is so little metal that the structure cannot support itself on removal of the preform. The lower porosity limit

would be reached when increasing the density further would result in the pore windows becoming closed and the pore structure becoming no longer interconnected. For a fixed sample size, as the pore size is increased, the lower porosity limit will also increase as more and more volume is taken up by the pores, the opposite is true for decreasing pore size.

Figure 71 shows a plot of pressure drop against porosity for the 35L/min flow rate tests and shows a number of anomalous results which contradict the general trend of increasing pressure difference with decreasing pore size.

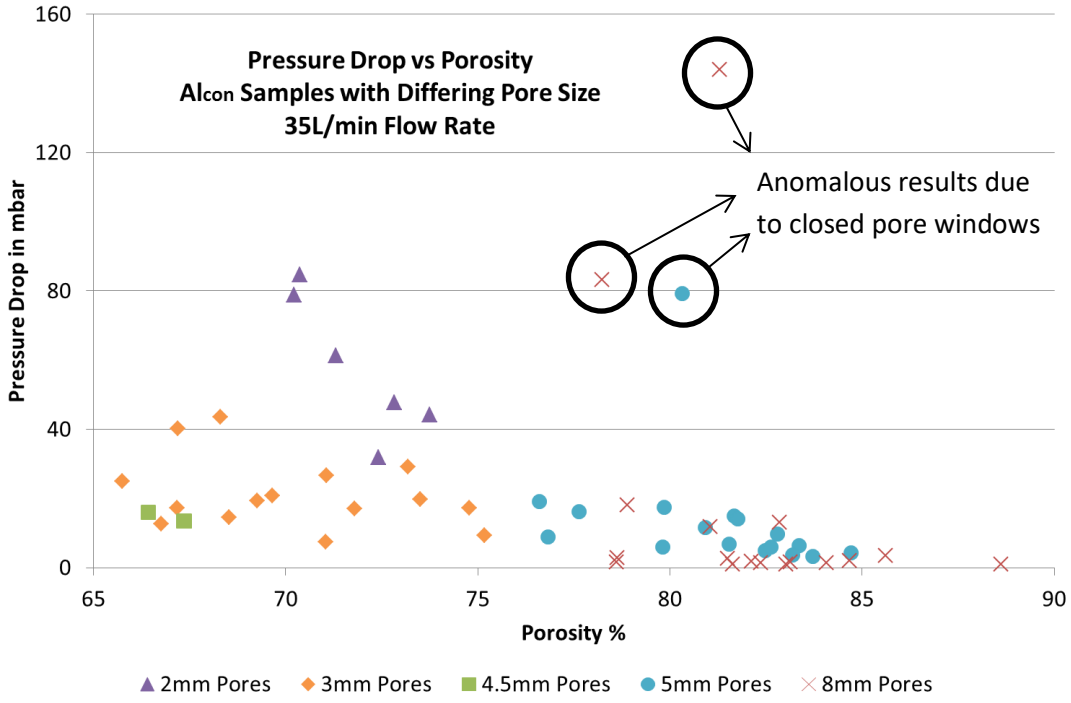

Figure 71. Plot of pressure drop against porosity for Alcon samples with differing pore size. Anomalous results have been identified.

When the samples in question were inspected, it was evident that one end of each sample was almost completely closed causing discontinuities in the interconnected structures; an example of this is shown in figure 72. It is believed that the large pressure drops can be almost entirely attributed to these defects, highlighting the need for in-depth testing but also suggesting that for the relatively small sample

size being used, at 77-78%, the lower porosity limit is possibly being approached for large pore sizes (8-5mm).

Figure 72. An 8mm pore, Alcon sample with pore window defects creating almost fully closed pores.

Due to the manufacturing technique, the structure of the foam produced by Constellium is thought to differ slightly in the x- and y-axes. The change in pore shape, with little change in density or porosity, was investigated in terms of the effect on the foam's heat transfer behaviour by testing and comparing samples machined in different directions from the same block. Figures 73, 74 and 75 show graphs of heat transfer coefficient against porosity for all (regardless of machining direction) the 8mm, 5mm and 3mm pore samples tested respectively. These graphs have been presented first to show the range of sample porosities even though the samples in each pore size set were all cut from the same block. This emphasises the randomness of the foam structure and also reinforces the fact that samples of this size cannot be used to fully describe the bulk properties of the foam.

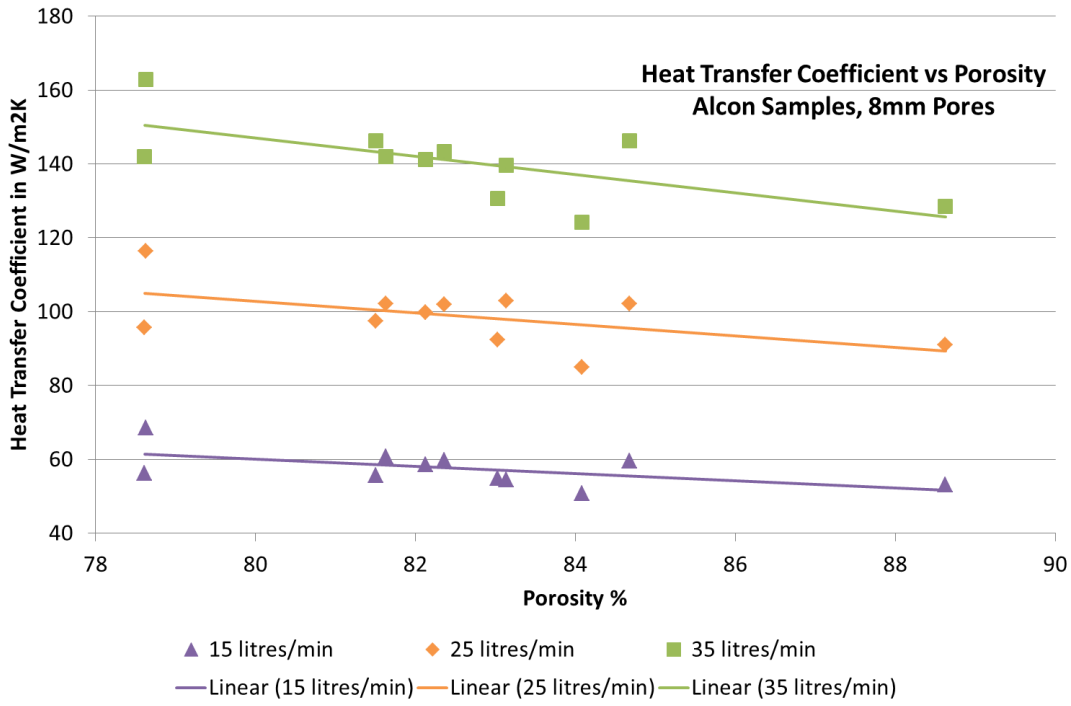

Figure 73. Plot of heat transfer coefficient against porosity for samples cut both horizontally and vertically from a foam block with 8mm pores.

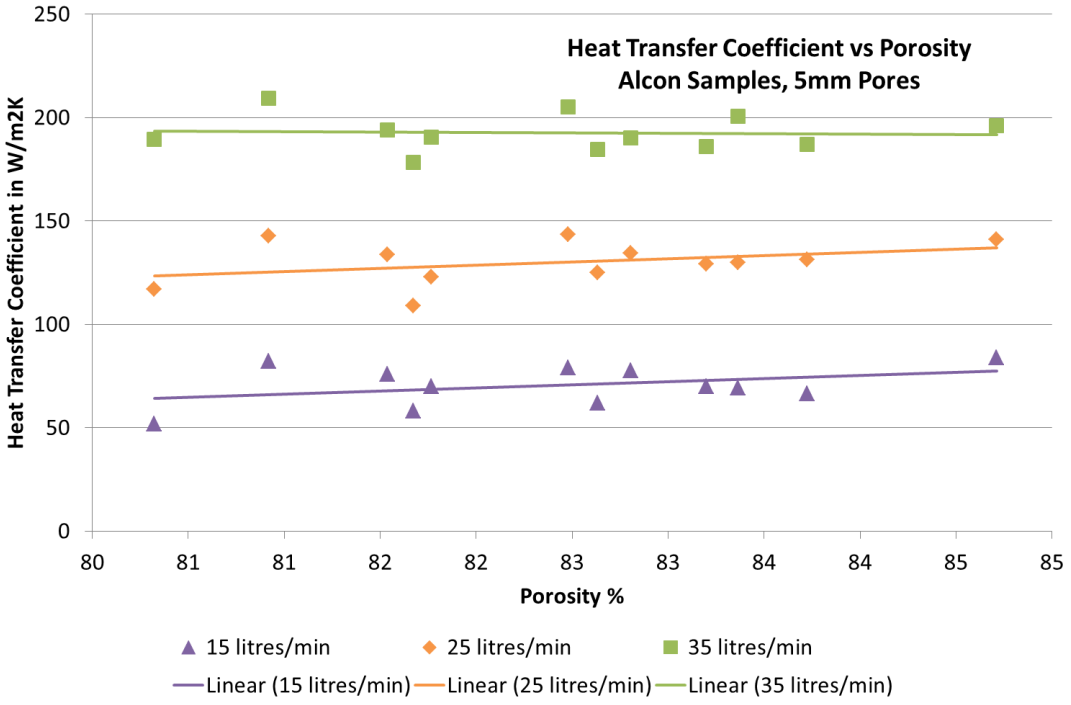

Figure 74. Plot of heat transfer coefficient against porosity for samples cut both horizontally and vertically from a foam block with 5mm pores.

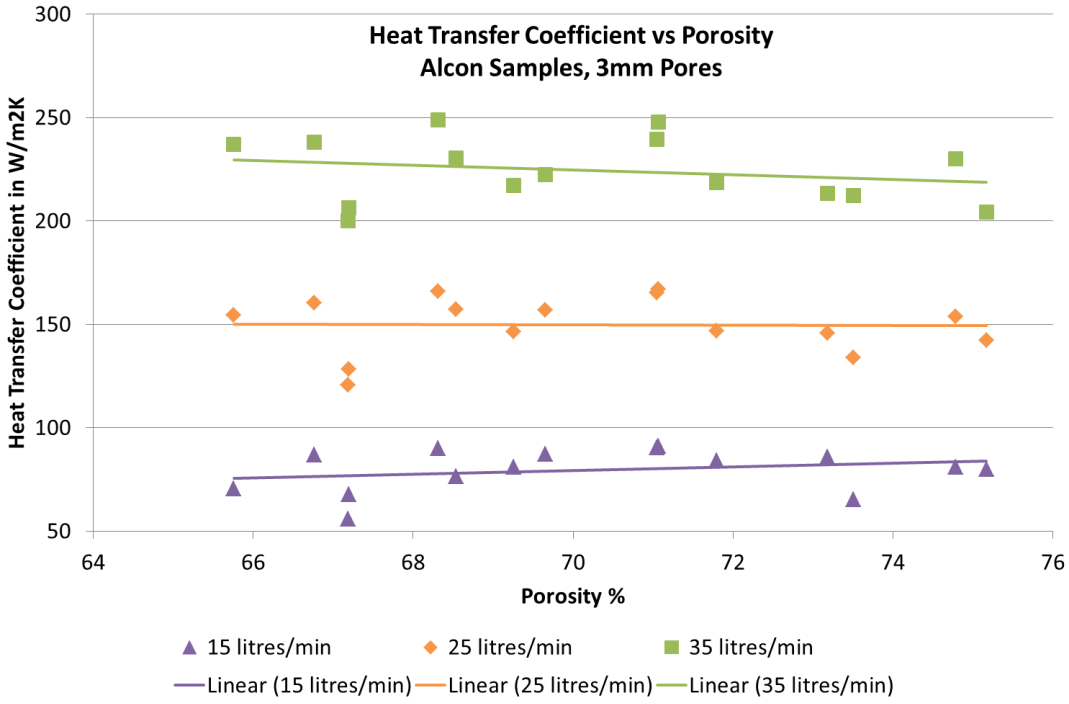

Figure 75. Plot of heat transfer coefficient against porosity for samples cut both horizontally and vertically from a foam block with 3mm pores.

The 8mm pore samples show a slight fall in heat transfer coefficient with increasing porosity whereas there is no apparent trend for both the 5 and 3mm pore samples over the porosity range tested.

Figure 76 shows a plot of average heat transfer coefficient against flow rate for the 3mm pore samples cut both horizontally and vertically from the parent block. To better show the spread of results, the individual measurements for each sample are plotted in figure 77. With respect to the samples permeability, figure 78 shows a plot of average pressure drop against flow rate.

As porosity did not correlate with heat transfer performance, all samples, regardless of porosity, were included in calculating the mean values (both heat transfer coefficients and pressure drops).

It can be seen that machining direction has no effect on heat transfer behaviour or permeability for the foam samples with 3mm pores.

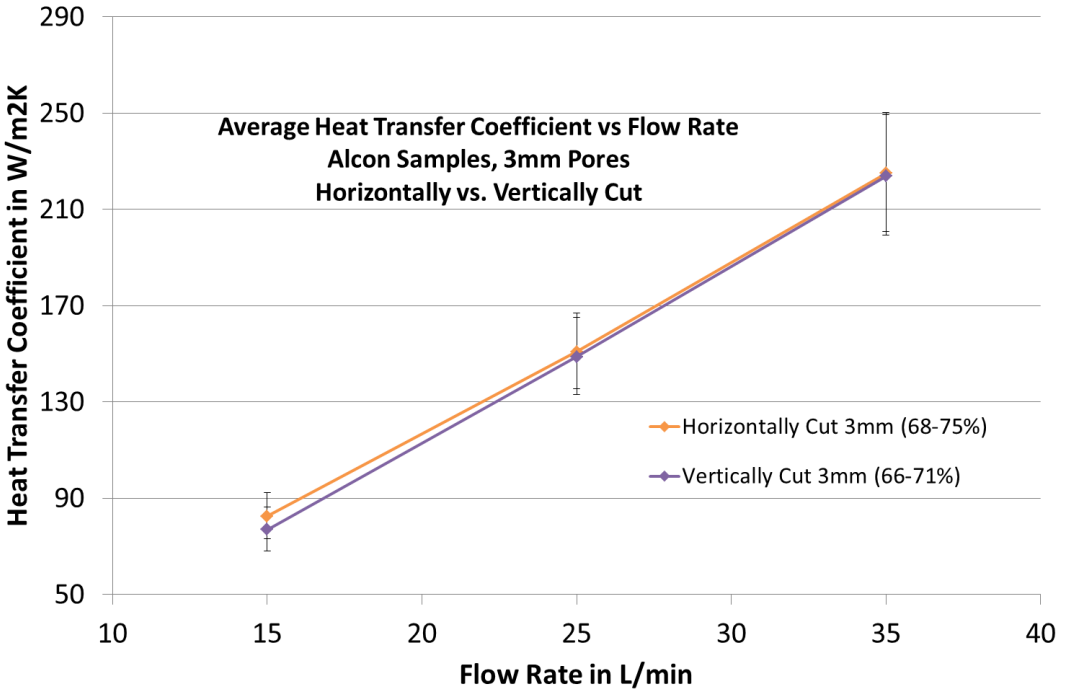

Figure 76. Plot of average heat transfer coefficient against flow rate for samples cut both horizontally and vertically from a foam block with 3mm pores. Error bars show the average accumulative errors as described in section 2.4.

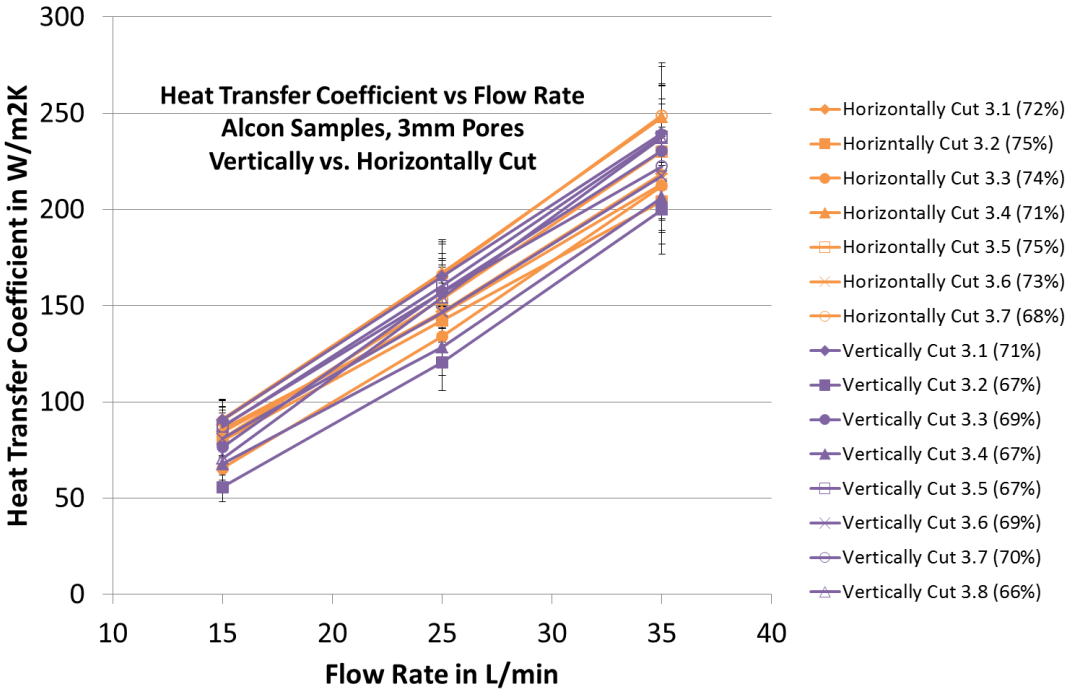

Figure 77. Plots of heat transfer coefficient against flow rate for samples cut both horizontally and vertically from a foam block with 3mm pores. Error bars show the accumulative errors as described in section 2.4.

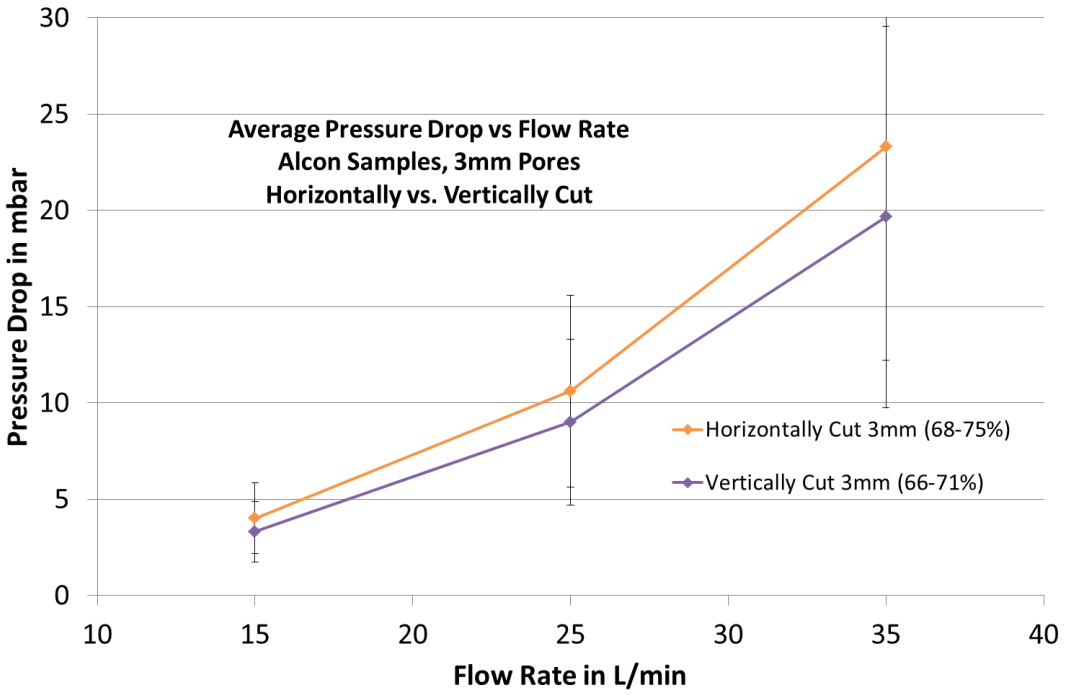

Figure 78. Plot of average pressure drop against flow rate for samples cut both horizontally and vertically from a foam block with 3mm pores. Error bars show the standard deviation.

Figures 79 and 80 respectively show averaged and individual plots of heat transfer coefficient against flow rate for samples cut both horizontally and vertically from a 5mm pore block. Figure 81 shows a plot of average pressure drop against flow rate for the 5mm pore samples. Again, as porosity did not correlate with heat transfer performance, all samples were included in calculating the mean values (both heat transfer coefficients and pressure drops). Pressure drop data for one anomalous sample was however omitted due to a pore window defect causing an extremely large pressure drop. The omitted sample has been identified in figure 82 which shows the individual plots of pressure drop against flow rate for all 5mm pore samples.

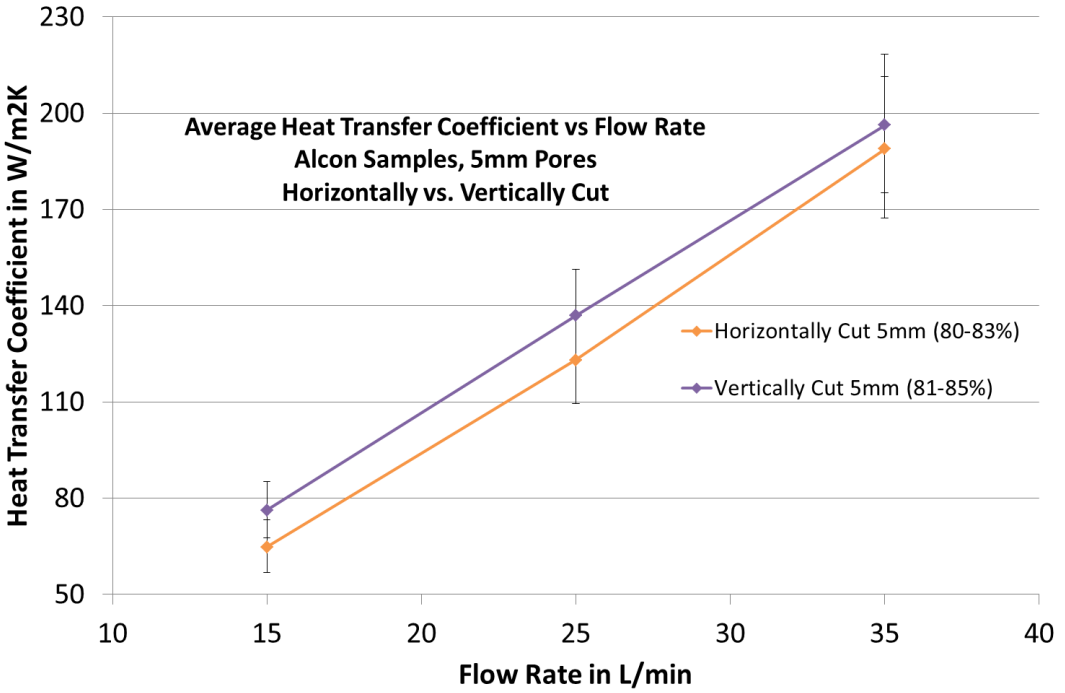

Figure 79. Plot of average heat transfer coefficient against flow rate for samples cut both horizontally and vertically from a foam block with 5mm pores. Error bars show the average accumulative errors as described in section 2.4.

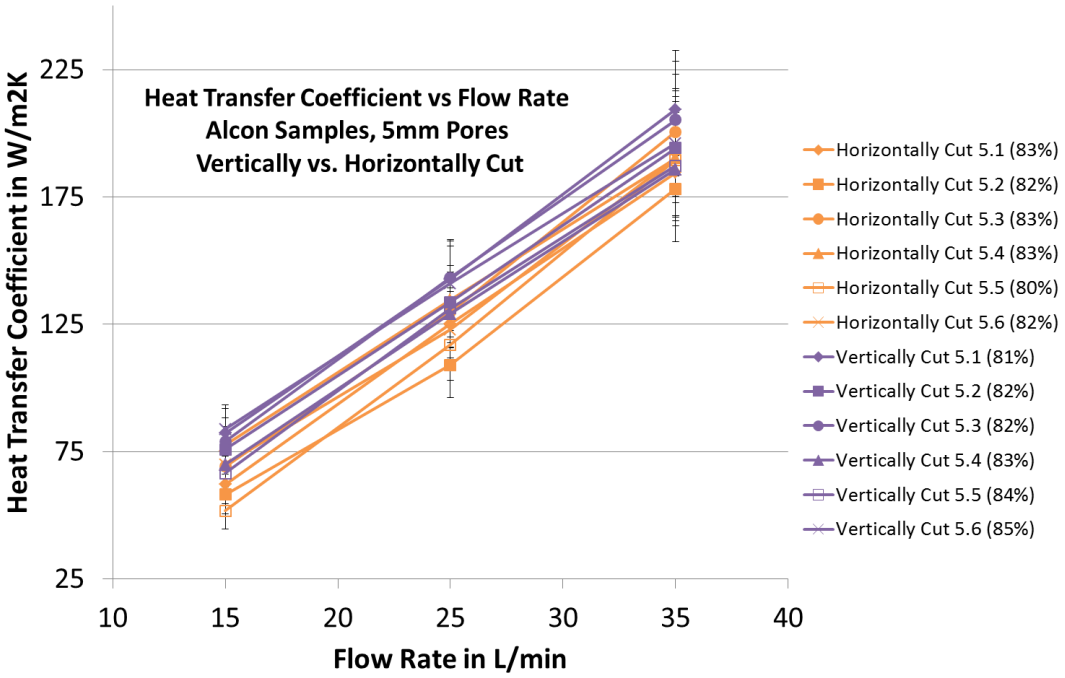

Figure 80. Plots of heat transfer coefficient against flow rate for samples cut both horizontally and vertically from a foam block with 5mm pores. Error bars show the accumulative errors as described in section 2.4.

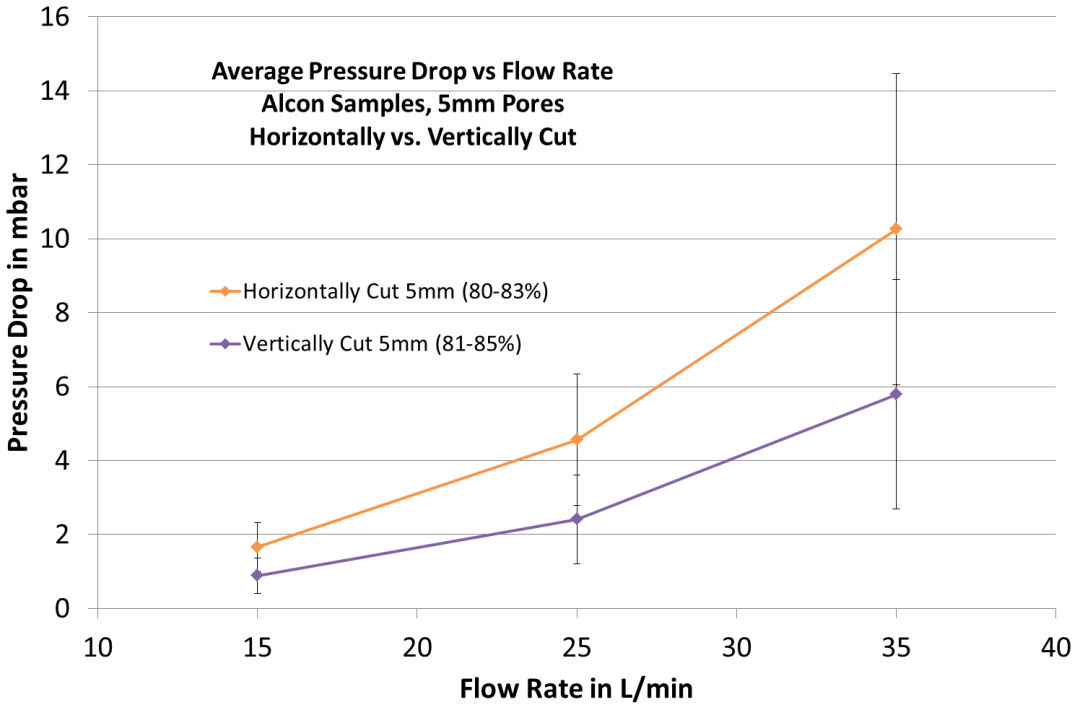

Figure 81. Plot of average pressure drop against flow rate for samples cut both horizontally and vertically from a foam block with 5mm pores. Error bars show the standard deviation.

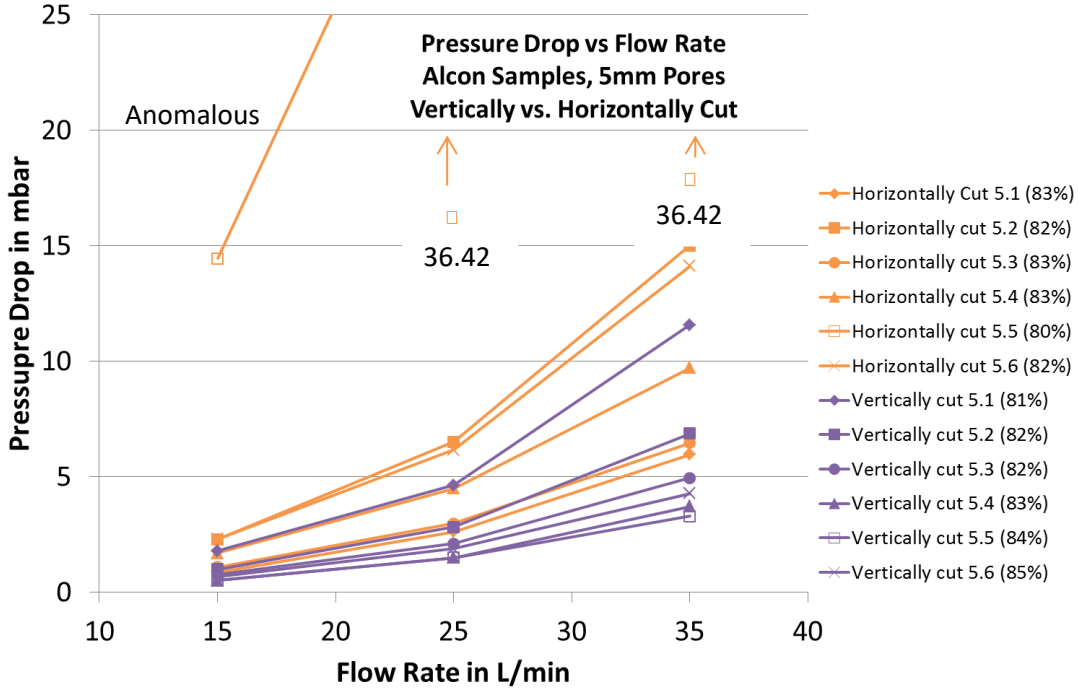

Figure 82. Plots of pressure drop against flow rate for samples cut both horizontally and vertically from a foam block with 5mm pores. An anomalous result is identified.

For the 8mm pore size, the upper (89%) and lower 2x(79%) porosity samples were excluded from mean calculations. This is so any trend would not be skewed by porosity and could be attributed to structural changes alone. Figures 83 and 84 respectively show averaged and individual plots of heat transfer coefficient against flow rate for the 8mm pore samples cut both horizontally and vertically from a block. Figure 85 shows a plot of average pressure drop against flow rate for the 8mm pore samples.

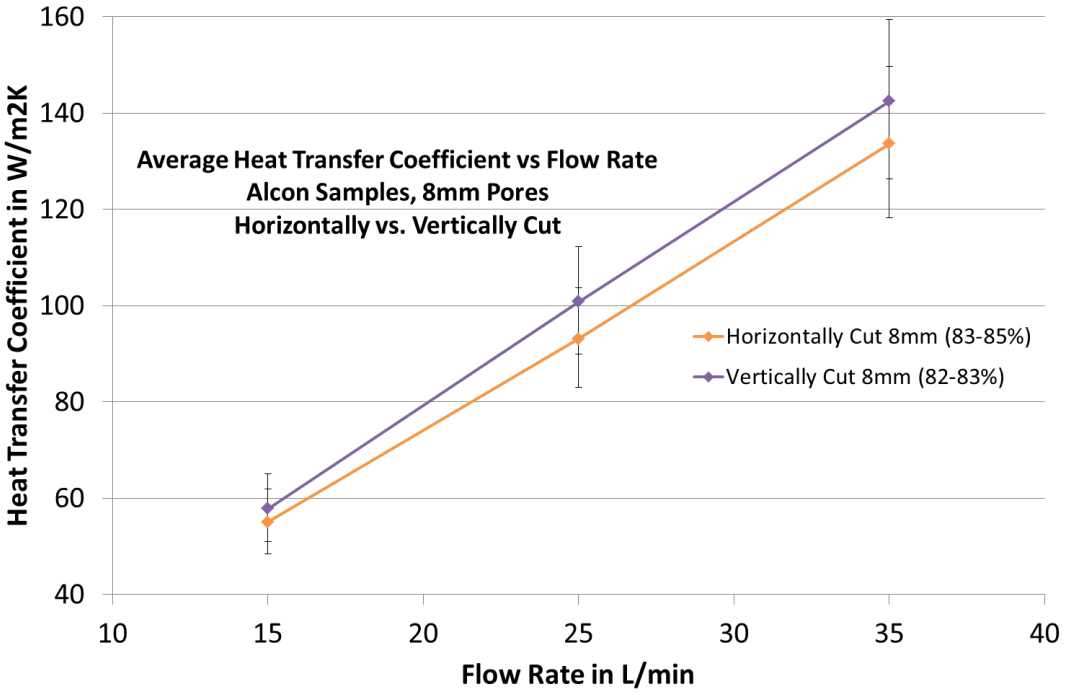

Figure 83. Plot of average heat transfer coefficient against flow rate for samples cut both horizontally and vertically from a foam block with 8mm pores. Error bars show the average accumulative errors as described in section 2.4.

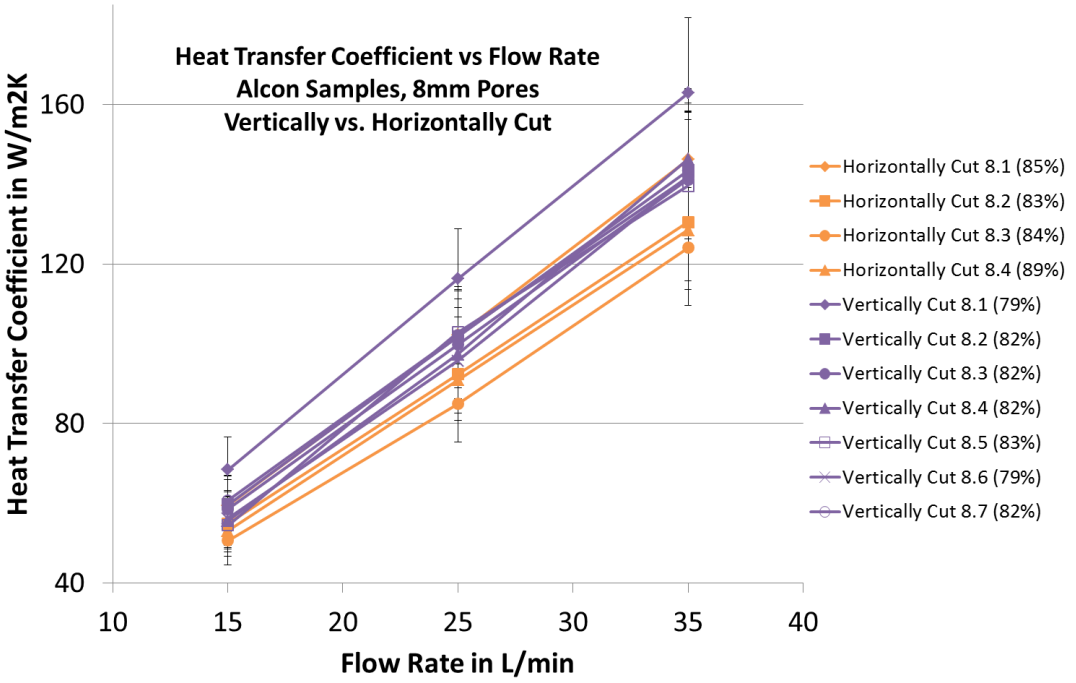

Figure 84. Plots of heat transfer coefficient against flow rate for samples cut both horizontally and vertically from a foam block with 8mm pores. Error bars show the accumulative errors as described in section 2.4. Error bars show the accumulative errors as described in section 2.4.

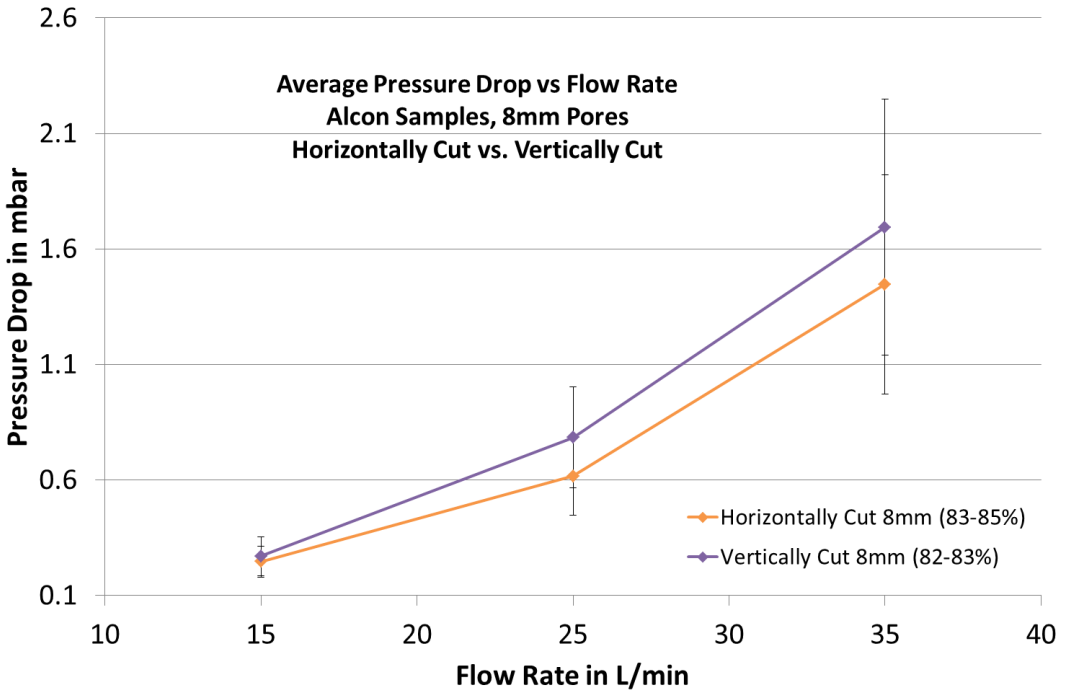

Figure 85. Plot of average pressure drop against flow rate for samples cut both horizontally and vertically from a foam block with 8mm pores. Error bars show the standard deviation.

For the larger pore sizes, 5 and 8mm, it is observed that a trend may be forming whereby samples machined horizontally (i.e. the cylinder length perpendicular to the compression direction) exhibit inferior heat transfer performance compared to those machined vertically (i.e. the cylinder length parallel to the compression direction). Although there is some overlap, and even more so when taking into account the associated errors, the magnitude of the difference is still surprising when considering the small change in pore shape expected.

Using the mid-flow rate (25litre/min) as an example, the mean heat transfer coefficients for the 5mm pore foam are 123.07W/m²K with standard deviation of 9.14 and 136.84 W/m²K with standard deviation of 6.26, for the horizontally and vertically cut samples respectively. As sample density does not correlate with the trend in heat transfer performance, it suggests that the structure of the foam is playing a significant role in the observed heat transfer behaviour and these differences are not simply due to the fact that there is more or less metal to conduct the heat in one sample than another.

Characterisation of the foam structures using x-ray tomography (see section 4.2) suggests that the horizontally cut samples contain a higher proportion of unintentional, small (<2mm) pores compared to those cut vertically. This alone could be the reason behind the difference in heat transfer behaviour. In addition, compression of the preform could also increase the pore-pore window size along this direction and may also compact the pores. When machined vertically, this may provide better paths for thermal transport laterally and thus be another reason for the enhanced heat transfer behaviour; this is shown schematically in figure 86. It is likely that larger pores will be affected more by compaction than small ones and this could explain why the same trend is not seen over all pore sizes. In the same manner, the smaller the ratio of sample size to pore size, the larger the effect of small structural changes on the flow of air and paths for thermal transport. In order to further validate the proposed relationships, it will be beneficial to test multiple sample sets machined from various different batches of foam for each pore size. Not only would this provide more repeat samples, but it would also help to rule out that the phenomenon is not just seen in isolated cases. In addition, the mesostructures of each sample type will need more in-depth characterisation via

3D x-ray tomography with the aim of gaining an understanding of exactly if and how the pore-pore interconnections (i.e. the pore windows) differ in the x- and y-axes.

The average pressure drop is very similar for samples cut both vertically and horizontally from the block. The largest difference in average pressure drop was observed for the 5mm pore samples when using a flow rate of 35L/min and this equated to a change of only 4.5mbar between horizontally and vertically cut samples. Due to the sensitivity of pressure drop when using relatively small sized samples, changes in permeability of this magnitude cannot be attributed to machining direction alone. Such a small change could be due to random structural variation rather than specifically to machining direction.

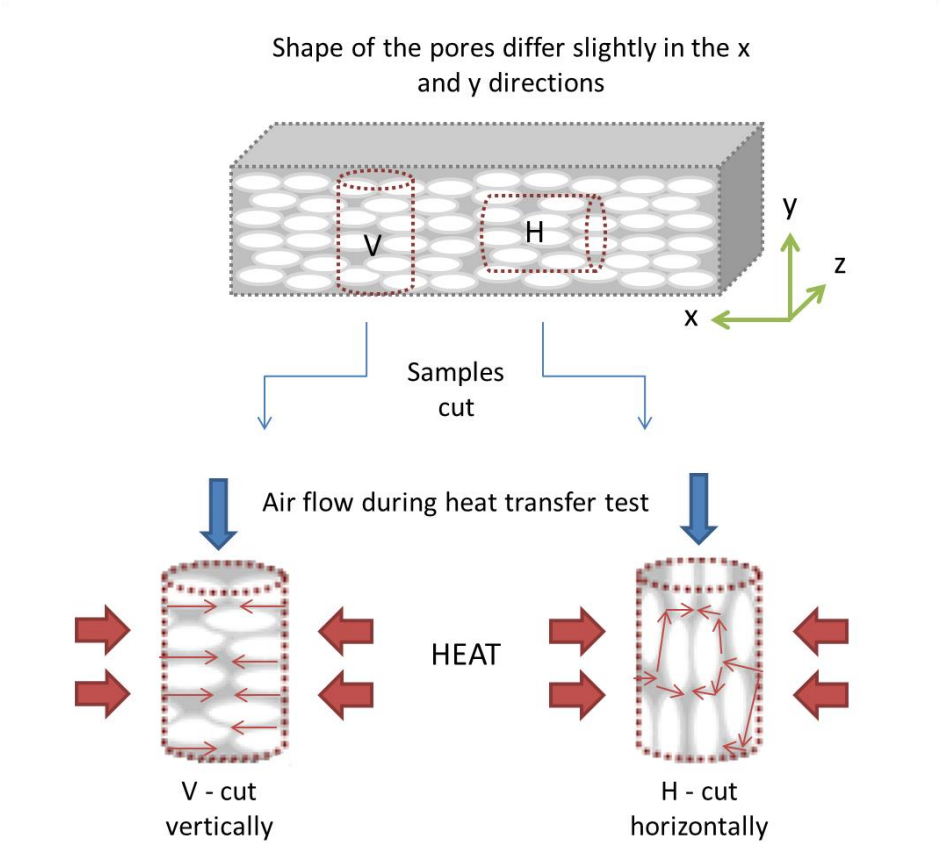

Figure 86. Schematic of possible improvement of paths for thermal transport as a result of the machining direction of samples.

This result may have good industrial implications. Although the increase in heat transfer is small, it is not achieved at the expense of permeability and there would be no change required to the manufacturing process. Improvements to heat transfer could simply be attained by relating the machining direction of parts to the direction of air flow in the intended heat transfer application.

Using the laboratory scale version of the foam production process, samples were made with pore aspect ratios of 1:1 (equiaxed) and 1:3 (elongated). Additional samples were also produced with pores spanning the entire length of the part (full-length). Heat transfer and fluid flow behaviour was measured for all samples in order to evaluate the consequence of the change in pore architecture. Figure 87 shows a plot of average heat transfer coefficient against flow rate for the samples with differing pore aspect ratio.

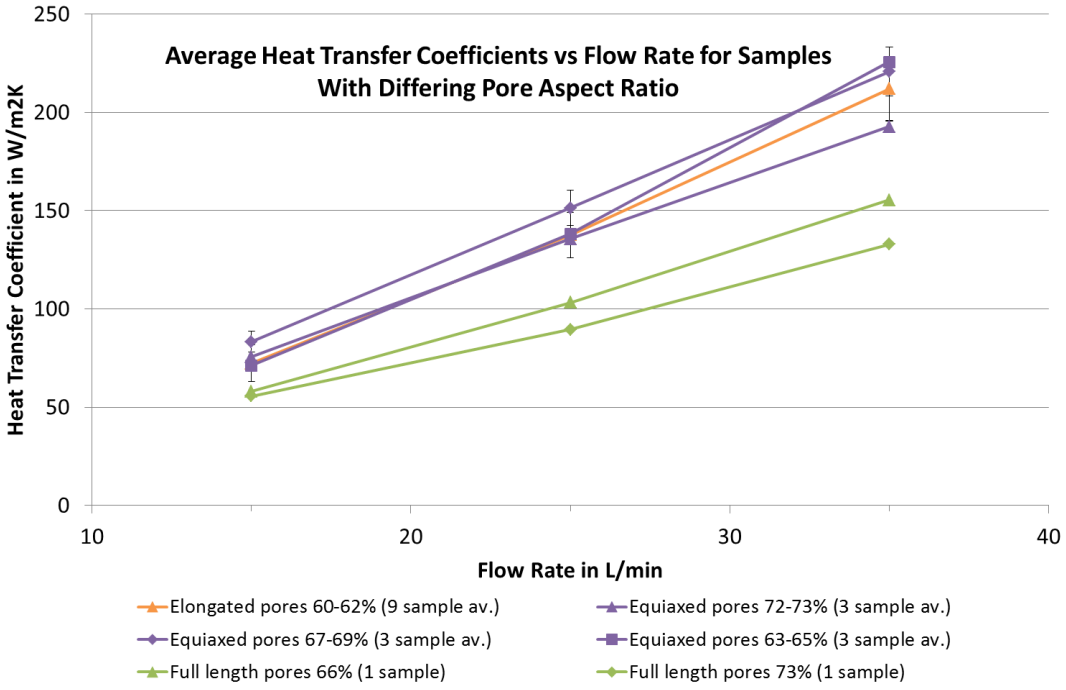

Figure 87. Plot of average heat transfer coefficient against flow rate for aluminium foam samples produced in-house with differing pore aspect ratio; equiaxed, elongated and full-length. Error bars show the standard deviation.

The graph clearly shows much inferior heat transfer for the full length pore samples over all flow rates. This emphasises the necessity for good air flow mixing and high surface area provided by the random pore arrangement of the traditional foam structure.

Due to the difference in packing behaviour between the elongated and equiaxed preform geometries, the porosities of the resultant foams did not overlap. Even when using the minimum infiltration pressure (0.5bar) it was not possible to increase the porosity above 61.7% for the elongated pore samples. Figures 88 and 89 show graphs of heat transfer coefficient against porosity for the equiaxed and elongated pore samples respectively.

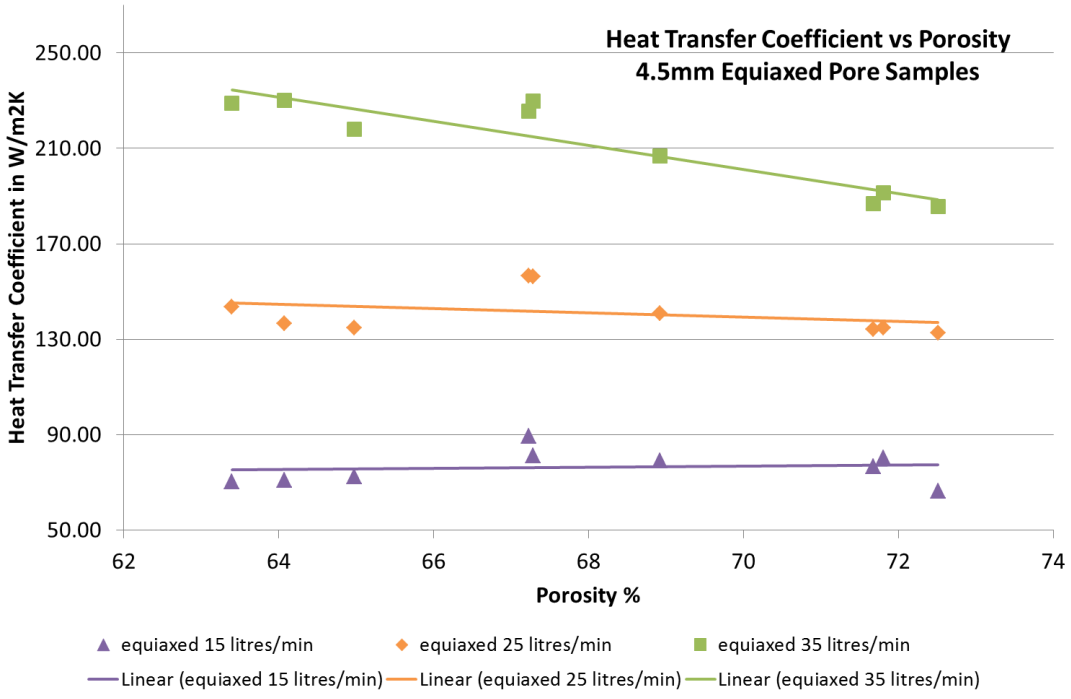

Figure 88. Plot of heat transfer coefficient against porosity for aluminium foam samples produced in-house with 4.5mm, equiaxed pores.

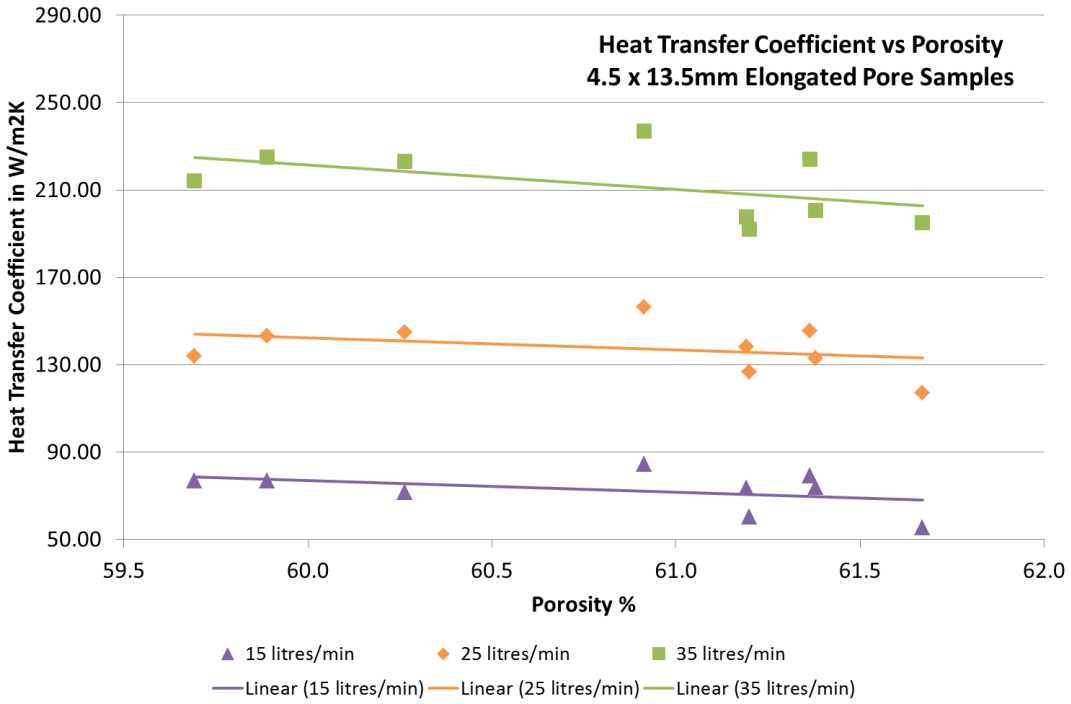

Figure 89. Plot of heat transfer coefficient against porosity for aluminium foam samples produced in-house with 4.5mm x 13.5mm, elongated pores.

Even over the small porosity range achievable for the elongated pores, heat transfer is slightly improved with decreasing porosity. The same general trend is true for equiaxed pore samples, especially at the higher 35litre/min flow rate. This relationship follows the consensus of the literature; higher density foams tend to have higher heat transfer coefficients as there is simply more metal to conduct the heat. Therefore, although the equiaxed and elongated pore samples appear to have similar heat transfer behaviour, as the porosity for the sample types are not consistent this will also be affecting the result. Taking into account the difference in porosity, it is possible that equiaxed pores actually provide improved heat transfer compared to elongated pores although the effect here has been cancelled out by the density variation.

Figure 90 shows plots of pressure drop against flow rate for samples with differing pore aspect ratio.

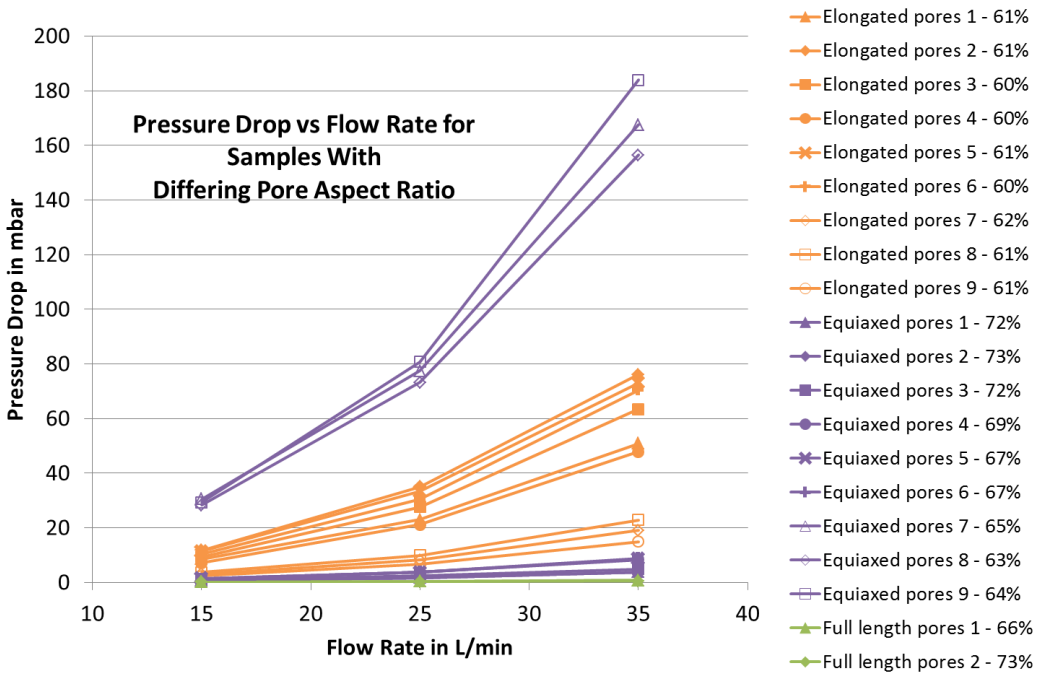

Figure 90. Plots of pressure drop against flow rate for foam samples produced in-house with differing pore aspect ratio; equiaxed, elongated and full-length.

Unsurprisingly the highest permeability samples are those with tube-like pores that span the full-length of the sample. As there are no pore walls and/or struts directly obstructing the air flow, the main disruptions to the flow path are the reduction of tube diameter as air enters the pores and friction from the walls. This is obviously beneficial to permeability but not to heat transfer behaviour.

The higher porosity, equiaxed pore samples (between 67-73%) also have very high permeability but in contrast, the lower porosity equiaxed pore samples (63-65%) have by far the lowest permeability. This difference in permeability is a direct consequence of the decrease in porosity and in turn a decrease in the pore-pore window size. Such a dramatic increase in pressure drop suggests that the porosity is approaching the lower limit, below which the windows will become fully closed. The increase in heat transfer due to increased sample density is only apparent at high flow rates and even then, compared to the change in permeability, the gain is minimal. For heat transfer applications, it is likely that a decrease in permeability to such an extent would far outweigh the small gain in heat transfer performance.

Therefore, for equiaxed pore foam produced in a similar manner to here, porosity should be maintained at or above 67% if being used as heat exchange material.

For the elongated pore samples, the range of pressure drops over the set of samples is high given the small change in porosity (59.7-61.7%). Although the pores are longer and thus provide extended free paths for the air flow, the connecting pore-pore windows can be very small. The window size depends on the points of contact between the dough pellets that make up the preform as well as the infiltration pressure. For cylindrical geometries such as those used, the points of contact can be very varied as shown in the schematic in figure 91.

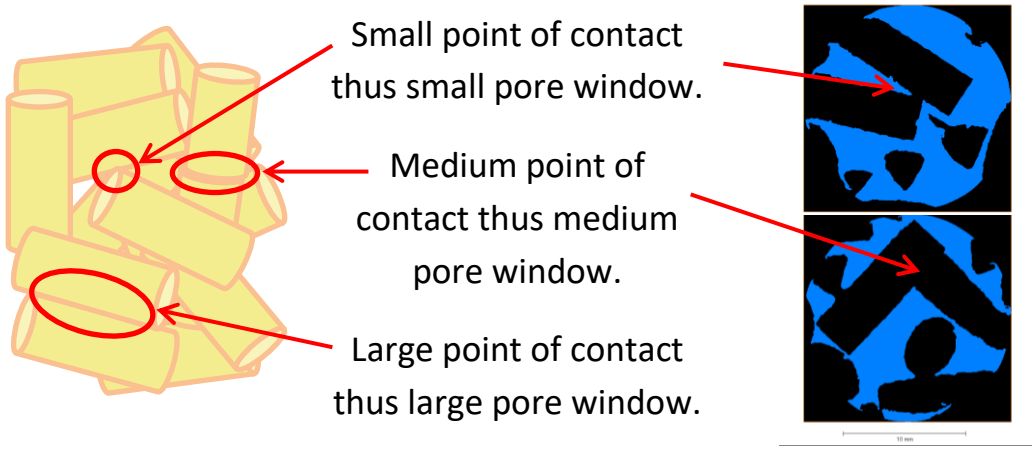

Figure 91. Schematic showing the difference in points of contact, in relation to pore window size, for cylindrical geometries. Examples of small and medium pore windows seen in 2D cross-sections of an elongated pore sample attained using x-ray tomography.

The higher permeability elongated samples are those produced using the minimum infiltration pressure (0.5bar) and so it may be that although similar amounts of metal infiltrate the preform, for the higher infiltration pressures, the metal is forced further into the fine spaces between the individual salt pellets. This will reduce the window size, which appears to be the limiting factor for permeability in foams of this type. Overall, for foams made in a similar manner to here, equiaxed pores provide better heat transfer than elongated. Equiaxed pores can also provide improved permeability if porosity is at or above 67% although an optimum balance between heat transfer performance and permeability is achieved with porosities between 67-69%.

6. Conclusions And Future Work

An in-house version of the salt-dough replication technique, based on an industrial scheme being piloted by Constellium, was developed. The technique was used to produce novel aluminium foams with different pore architectures. The thermal and fluid flow behaviour of the novel foams was investigated using a bespoke rig, previously developed by another member of the research group. Through evaluation of the results, a number of conclusions can be drawn.

The laboratory scale foam production process can reliably produce a range of foam mesostructures including extreme case samples.

- Correct dough composition is essential for the success of the salt dough replication technique. An approximate compositional range has been outlined using a ternary diagram and the composition used in this work was 70% salt, 15% flour and 15% water.
- Extrusion is an efficient and repeatable method to shape the salt dough preform and allows consistency of shape as defined by the extrusion die.
- Permitting the dough to harden before cutting allows the exact shape of the dough to be replicated in the shape of the foam pores but reduces the achievable range of foam porosity.
- To achieve a bonded preform (rather than using individual pellets), which would assist pore interconnectivity; the dough pellets should not be allowed to harden prior to being heat treated.
- Differences between the in-house and Constellium preform materials have been identified however this has no effect on the final foam product.

- The weight of the aluminium under vacuum alone is not sufficient to infiltrate molten metal into the preform thus external gas pressure is required.
- Gas-pressures between 1-2bar allow for controllable infiltration of an air filled preform (opposed to under vacuum).

Performance and limitations of the heat transfer rig, used to evaluate the heat transfer behaviour of foam samples, have been explored and parameters have been optimised to maximise reliability.

- Both heat transfer coefficient and pressure drop measurements exhibit scatter due to the inherent randomness of the foam structure.
- Pressure drop is more sensitive than the heat transfer coefficient to small structural changes and defects.
- In testing, steady state heat transfer behaviour is reached after approximately 60 minutes. Stabilization of the pressure drop occurs after around 30 minutes.

Heat transfer and permeability testing were carried out on foams with varied pore architectures. The main caveat of the work completed is the lack of overlap between porosities for the different foam structures. Because of this, firm conclusions cannot be drawn however, the formation of a number of possible relationships have been identified.

- The aluminium alloy used to produce Corevo (Constellium made) foam has a thermal conductivity approximately 25% lower than for pure aluminium, which corresponds to a reduction in heat transfer coefficient of between 2.5-7.5% depending on foam structure and flow rate.
- The type of metal used as the foam matrix material has no apparent effect on permeability.
- Improved heat transfer correlates with smaller pore diameters; this is true for all flow rates but is more pronounced at high flow rates.

- Lower permeability corresponds to smaller pore size.
- For general heat exchange applications, a pore size between 3-5mm would provide an effective balance between heat transfer and permeability.
- For pore sizes ≥5mm, uniaxial preform compaction has been identified as a possible route to higher heat transfer without affecting air flow pressure drop.
- Good air flow mixing due to the random arrangement of pores is essential for enhanced heat transfer.
- Elongation of pores (when using a rigid shape preform) does not improve heat transfer or permeability.
- For 4.5mm equiaxed pores, porosities between 67%-69% provide a useful compromise between heat transfer and permeability.

Leading on from the work presented here, the salt dough replication technique remains a highly effective method for exploring structure-heat transfer relationships. To further improve the understanding of these relationships a number of routes for future work have been suggested.

Although the shape of the preform may not translate exactly from dough to pore, a wider range of porosities can be achieved using un-hardened preform (method 3 of section 3.3). This technique allows the dough pellets to bond together before they are infiltrated and thus assists the level of interconnectivity achieved in the resultant foam. In addition, it also allows porosity to be altered using preform compaction as well as infiltration pressure. As long as pore shape is consistent throughout, this method could be used to increase the range of sample porosities when investigating the effect of metal matrix type on heat transfer behaviour. Similarly, to gain a more comprehensive overview of how important the metal conductivity is for the Corevo type foams, a variety of metals (given they are compatible with the replication technique) with a range of thermal conductivities could be used.

In the same manner, a wider overlap of sample porosity for foams with differing pore size could be investigated using the compactable salt dough preform (method 3 of section 3.3).

The investigation into machining direction showed promising results that could very easily be implemented industrially. However, as the change in pore shape is so subtle, the effect would be more solidly confirmed by increasing testing over multiple sample sets machined from various different batches of foam for each pore size. It may also be advantageous to test much larger sized samples more representative of the bulk material. This would greatly reduce any entrance/exit effects and better confirm/disprove the apparent trend.

The preform used to produce the foams with differing pore aspect ratio was left to dry before being cut. This produced hard pellets, which retained their exact shape throughout the process (method 1 of section 3.3). As a consequence, the preform filled the infiltration mould as individual pellets and preform compaction could not be used to aid porosity. In addition, due to the rigid cylindrical shape of the elongated pellets, close packing of the preform was discouraged. This further limited the range of achievable sample porosity and caused huge variation in window size resulting from the variety of different contact points between the preform. Again, by using the un-hardened preform, the porosity issue could be somewhat overcome. However, the shape of the pores, especially for the elongated pore type, would change drastically from pore-to-pore as the flexible preform would randomly deform as the pellets were packed into the infiltration mould. The foam structures produced this way would be completely different to those produced using the rigid type dough pellets and the structure could be difficult to characterise. It would however be interesting to compare the likely huge variation of structure (and thus heat transfer behaviour) that result from a relatively small variation in technique.

7. BIBLIOGRAPHY

[1] A. Bhattacharya and R. L. Mahajan, “Finned Metal Foam Heat Sinks for Electronics Cooling in Forced Convection,” *J. Electron. Packag.*, vol. 124, no. 3, p. 155, 2002.

[2] L. J. Gibson and M. F. Ashby, *Cellular Solids*, Second Edi. Cambridge University Press, 1997.

[3] G. J. Davies and S. Zhen, “Metallic foams: their production, properties and applications,” *J. Mater. Sci.*, vol. 18, no. 7, pp. 1899–1911, Jul. 1983.

[4] J. Banhart, “Manufacture, characterisation and application of cellular metals and metal foams,” *Prog. Mater. Sci.*, vol. 46, no. 6, pp. 559–632, Jan. 2001.

[5] M. F. Ashby, A. G. Evans, N. A. Fleck, L. J. Gibson, J. W. Hutchinson, and H. N. G. Wadley, *Metal Foams : A Design Guide*, Illustrate. Oxford: Butterworth-Heinemann Ltd, 2000.

[6] R. Goodall and A. Mortensen, “Porous Metals,” in *Physical Metallurgy*, 5th ed., D. Laughlin and K. Hono, Eds. Elsevier Ltd, 2013.

[7] P. Colombo and H. P. Degischer, “Highly porous metals and ceramics,” *Mater. Sci. Technol.*, vol. 26, no. 10, pp. 1145–1158, Oct. 2010.

[8] Y. Conde, J. F. Despois, R. Goodall, A. Marmottant, L. Salvo, C. San Marchi, and A. Mortensen, “Replication Processing of Highly Porous Materials,” *Adv. Eng. Mater.*, vol. 8, no. 9, pp. 795–803, Sep. 2006.

[9] R. Goodall and A. Mortensen, “Microcellular Aluminium? – Child’s Play!,” *Adv. Eng. Mater.*, vol. 9, no. 11, pp. 951–954, Nov. 2007.

[10] J. Banhart and H. Berlin, “Aluminium foams for lighter vehicles,” *Int. J. Veh. Des.*, vol. 37, pp. 114–125, 2005.

[11] J. Banhart and H. Seeliger, “Recent Trends in Aluminium Foam Sandwich

Technology," *Adv. Eng. Mater.*, vol. 14, no. 12, pp. 1082–1087, 2012.

[12] J. L. Yu, X. Wang, Z. G. Wei, and E. H. Wang, "Deformation and failure mechanism of dynamically loaded sandwich beams with aluminum-foam core," *Int. J. Impact Eng.*, vol. 28, no. 3, pp. 331–347, 2003.

[13] A. Pollien, Y. Conde, L. Pambaguian, and A. Mortensen, "Graded open-cell aluminium foam core sandwich beams," *Mater. Sci. Eng. A*, vol. 404, no. 1–2, pp. 9–18, 2005.

[14] J. Banhart and H. W. Seeliger, "Aluminium foam sandwich panels: Manufacture, metallurgy and applications," *Adv. Eng. Mater.*, vol. 10, no. 9, pp. 793–802, 2008.

[15] H. W. Seeliger, "Aluminium Foam Sandwich (AFS) Ready for Market Introduction," *Adv. Eng. Mater.*, vol. 6, no. 6, pp. 448–451, Jun. 2004.

[16] J. U. Baumeister, J. Banhart, and M. Weber, "Aluminium foams for transport industry," *Mater. Des.*, vol. 18, pp. 217–220, 1997.

[17] N. Dukhan, Ed., *Metal Foams: Fundamentals and Applications*. Lancaster, Pennsylvania: DEStech Publications Inc., 2013.

[18] F. García-Moreno, "Commercial applications of metal foams: Their properties and production," *Materials (Basel).*, vol. 9, no. 2, pp. 20–24, 2016.

[19] A. G. Hanssen, L. Olovsson, T. Børvik, and M. Langseth, "Close-range blast loading of aluminium foam panels: A numerical study," *IUTAM Bookseries*, vol. 12, pp. 169–180, 2009.

[20] Y. Xia, C. Wu, Z. X. Liu, and Y. Yuan, "Protective effect of graded density aluminium foam on RC slab under blast loading-An experimental study," *Constr. Build. Mater.*, vol. 111, pp. 209–222, 2016.

[21] B. A. Gama, T. A. Bogetti, B. K. Fink, C. J. Yu, T. Dennis Claar, H. H. Eifert, and J. W. Gillespie, "Aluminum foam integral armor: A new dimension in armor design," *Compos. Struct.*, vol. 52, no. 3–4, pp. 381–395, 2001.

[22] Cymat Technologies LTD, "SmartMetal TM." [Online]. Available: http://www.cymat.com/index.php/about-cymat/cymat-products/cymat-smartmetal. [Accessed: 13-Nov-2016].

[23] B. A. Fuganti and L. Lorenzi, "Aluminium Foam for Automotive Applications **," no. 4, pp. 200–204, 2000.

[24] A. G. Hanssen, K. Stöbener, G. Rausch, M. Langseth, and H. Keller, "Optimisation of energy absorption of an A-pillar by metal foam insert," *Int. J. Crashworthiness*, vol. 11, no. 3, pp. 231–242, 2006.

[25] S. Nesic, P. Schäffler, K. Unruh, W. Michels, and U. Krupp, "Analysis of Cellular Metals as Energy-Absorbing Elements in Car Seats," *Adv. Eng. Mater.*, vol. 13, no. 11, pp. 1056–1059, Nov. 2011.

[26] R. Destefanis, F. Schafer, M. Lambert, M. Faraud, and E. Schneider, "Enhanced Space Debris Shields for Mnned Spacecraft," *Int. J. Impact Eng.*, vol. 29, pp. 215–226, 2003.

[27] K. Thoma, M. Wicklein, and E. Schneider, "New Protection Concepts For Meteoroid/Debris Shields," in *Proceedings of the Fourth European Conference on Space Debris*, 2005.

[28] P. K. Pinnoji, P. Mahajan, N. Bourdet, C. Deck, and R. Willinger, "Impact dynamics of metal foam shells for motorcycle helmets: Experiments & numerical modeling," *Int. J. Impact Eng.*, vol. 37, no. 3, pp. 274–284, 2010.

[29] M. F. Ashby, "Metal foams: A survey," *Sci. China Ser. B*, vol. 46, no. 6, p. 521, 2003.

[30] T. J. Lu, A. Hess, and M. F. Ashby, "Sound absorption in metallic foams," *J. Appl. Phys.*, vol. 85, no. 11, pp. 7528–7539, 1999.

[31] T. J. Lu, "Ultralight Porous Metals: From Fundamentals to Applications," *Acta Mech. Sin. (English Ser.*, vol. 18, no. 5, pp. 457–479, 2002.

[32] X. Wang and T. J. Lu, "Optimised acoustic properties of cellular solids," *J. Acoust. Soc. Am.*, vol. 106, no. 2, 1999.

[33] T. J. Lu, A. Hess, and M. F. Ashby, "Sound absorption in metallic foams," *J. Appl. Phys.*, vol. 85, no. 11, pp. 7528–7539, 1999.

[34] "FoamTech Global." [Online]. Available: http://foamtechglobal.com/reference. [Accessed: 18-Jan-2017].

[35] T. Miyoshi, M. Itoh, S. Akiyama, and A. Kitahara, "ALPORAS Aluminum Foam: Production Process, Properties, and Applications," *Adv. Eng. Mater.*, vol. 2, no. 4, pp. 179–183, 2000.

[36] H. P. Degischer and B. Kriszt, *Handbook of Cellular Metals. Production, Processing, Applications*. 2002.

[37] R. Neugebauer and T. Hipke, “Machine tools with metal foams,” *Adv. Eng. Mater.*, vol. 8, no. 9, pp. 858–863, 2006.

[38] H. Nakajima, “Fabrication, properties and application of porous metals with directional pores,” *Prog. Mater. Sci.*, vol. 52, no. 7, pp. 1091–1173, 2007.

[39] B. Levine, “A new era in porous metals: Applications in orthopaedics,” *Adv. Eng. Mater.*, vol. 10, no. 9, pp. 788–792, 2008.

[40] L. P. Lefebvre and E. Baril, “Properties of titanium foams for biomedical applications,” *Adv. Eng. Mater.*, vol. 15, no. 3, pp. 159–165, 2013.

[41] C. Wen, Ed., *Metallic Foam Bone: Processing, Modification and Characterization and Properties*, First Edit. Woodhead Publishing, 2016.

[42] A. Bansiddhi, T. D. Sargeant, S. I. Stupp, and D. C. Dunand, “Porous NiTi for bone implants: a review.,” *Acta Biomater.*, vol. 4, no. 4, pp. 773–82, Jul. 2008.

[43] C. Mapelli, V. Mapelli, L. Olsson, D. Mombelli, A. Gruttadauria, and S. Barella, “Viability study of the use of cast iron open cell foam as microbial fuel cell electrodes,” *Adv. Eng. Mater.*, vol. 15, no. 3, pp. 112–117, 2013.

[44] F. Bidault, D. J. L. Brett, P. H. Middleton, N. Abson, and N. P. Brandon, “A new application for nickel foam in alkaline fuel cells,” *Int. J. Hydrogen Energy*, vol. 34, no. 16, pp. 6799–6808, Aug. 2009.

[45] X. Yu, Z. Wen, Y. Lin, S. T. Tu, Z. Wang, and J. Yan, “Intensification of biodiesel synthesis using metal foam reactors,” *Fuel*, vol. 89, no. 11, pp. 3450–3456, 2010.

[46] Cymat Technologies LTD, “Alusion Stabilized Aluminium Foam.” [Online]. Available: www.alusion.com. [Accessed: 21-Sep-2016].

[47] K. Boomsma, D. Poulikakos, and F. Zwick, “Metal foams as compact high performance heat exchangers,” *Mech. Mater.*, vol. 35, no. 12, pp. 1161–1176, Dec. 2003.

[48] C. T’Joen, P. De Jaeger, H. Huisseune, S. Van Herzeele, N. Vorst, and M. De Paepe, “Thermo-hydraulic study of a single row heat exchanger consisting of metal foam covered round tubes,” *Int. J. Heat Mass Transf.*, vol. 53, no. 15–16, pp. 3262–3274, 2010.

[49] K. Hooman and M. R. Malayeri, “Metal foams as gas coolers for exhaust gas

recirculation systems subjected to particulate fouling," *Energy Convers. Manag.*, vol. 117, pp. 475–481, 2016.

[50] A. Chumpia and K. Hooman, "Performance evaluation of single tubular aluminium foam heat exchangers," *Appl. Therm. Eng.*, vol. 66, no. 1–2, pp. 266–273, 2014.

[51] M. Odabaee and K. Hooman, "Metal foam heat exchangers for heat transfer augmentation from a tube bank," *Appl. Therm. Eng.*, vol. 36, no. 1, pp. 456–463, 2012.

[52] S. De Schampheleire, P. De Jaeger, H. Huisseune, B. Ameel, C. T'Joen, K. De Kerpel, and M. De Paepe, "Thermal hydraulic performance of 10 PPI aluminium foam as alternative for louvered fins in an HVAC heat exchanger," *Appl. Therm. Eng.*, vol. 51, no. 1–2, pp. 371–382, 2013.

[53] R. K. Shah and D. P. Selulic, *Fundamentals of Heat Exchange Design*. Wiley, 2003.

[54] "ERG Aerospace Corporation." [Online]. Available: http://www.ergaerospace.com/products/heat-exchangers.htm. [Accessed: 25-Jan-2017].

[55] "Alveotec Innovation Fonderie." [Online]. Available: http://www.alveotec.fr/en/our-achievements/heatsink-for-loupi-lighting_10.html. [Accessed: 25-Jan-2017].

[56] A. G. Evans, J. W. Hutchinson, and M. F. Ashby, "Multifunctionality of cellular metal systems," *Prog. Mater. Sci.*, vol. 43, pp. 171–221, 1999.

[57] S. Mahjoob and K. Vafai, "A synthesis of fluid and thermal transport models for metal foam heat exchangers," *Int. J. Heat Mass Transf.*, vol. 51, no. 15–16, pp. 3701–3711, Jul. 2008.

[58] Y. Yamada, K. Shimojima, Y. Sakaguchi, M. Mabuchi, M. Nakamura, T. Asahina, T. Mukai, H. Kanahashi, and K. Higashi, "Compressive properties of open-cellular SG91A Al and AZ91 Mg," *Mater. Sci. Eng. A*, vol. 272, no. 2, pp. 455–458, Nov. 1999.

[59] B. C. Körner and R. F. Singer, "Processing of Metal Foams - Challenges and Opportunities," *Cell*, no. 4, pp. 159–165, 2000.

[60] X. Badiche, S. Forest, T. Guibert, Y. Bienvenu, J. D. Bartout, P. Ienny, M.

Croset, and H. Bernet, “Mechanical properties and non-homogeneous deformation of open-cell nickel foams: Application of the mechanics of cellular solids and of porous materials,” *Mater. Sci. Eng. A*, vol. 289, no. 1, pp. 276–288, 2000.

[61] V. Poserin, S. Marcuson, J. Shu, and D. S. Wilkinson, “CVD technique for Inco nickel foam production,” *Adv. Eng. Mater.*, vol. 6, no. 6, pp. 454–459, 2004.

[62] D. T. Queheillalt, D. D. Hass, D. J. Sypeck, and H. N. G. Wadley, “Synthesis of open-cell metal foams by templated directed vapor deposition,” no. Cvd, 2001.

[63] P. Quadbeck, K. Kümmel, R. Hauser, G. Standke, J. Adler, and G. Stephani, “Open Cell Metal Foams – Application-oriented Structure and Ma- terial Selection,” 1966.

[64] P. Quadbeck, K. Kümmel, R. Hauser, G. Standke, J. Adler, G. Stephani, and B. Kieback, “Structural and material design of open-cell powder metallurgical foams,” *Adv. Eng. Mater.*, vol. 13, no. 11, pp. 1024–1030, 2011.

[65] N. J. Mills, *Polymer foams handbook: engineering and biomechanics applications and design guide*, First Edit., no. April. Butterworth-Heinemann, 2007.

[66] A. H. Brothers and D. C. Dunand, “Density-Graded Cellular Aluminum,” *Adv. Eng. Mater.*, vol. 8, no. 9, pp. 805–809, Sep. 2006.

[67] A. Kennedy, “Porous Metals and Metal Foams Made from Powders,” in *Powder Metallurgy*, K. Kondoh, Ed. InTech, 2012.

[68] Y. Y. Zhao, T. Fung, L. P. Zhang, and F. L. Zhang, “Lost carbonate sintering process for manufacturing metal foams,” *Scr. Mater.*, vol. 52, no. 4, pp. 295–298, Feb. 2005.

[69] Y. Y. Zhao and D. X. Sun, “A novel sintering-dissolution process for manufacturing Al foams,” *Scr. Mater.*, vol. 44, no. 1, pp. 105–110, Jan. 2001.

[70] R. Surace, L. A. C. De Filippis, A. D. Ludovico, and G. Boghetich, “Influence of processing parameters on aluminium foam produced by space holder technique,” *Mater. Des.*, vol. 30, no. 6, pp. 1878–1885, Jun. 2009.

[71] B. Jiang, N. Q. Zhao, C. S. Shi, X. W. Du, J. . Li, and H. . Man, “A novel method for making open cell aluminum foams by powder sintering process,” *Mater.*

Lett., vol. 59, no. 26, pp. 3333–3336, Nov. 2005.

[72] A. Mansourighasri, N. Muhamad, and a. B. Sulong, "Processing titanium foams using tapioca starch as a space holder," *J. Mater. Process. Technol.*, vol. 212, no. 1, pp. 83–89, Jan. 2012.

[73] S. Xie and J. R. G. Evans, "High porosity copper foam," *J. Mater. Sci.*, vol. 39, no. 18, pp. 5877–5880, 2004.

[74] Z. X. Guo, C. S. Y. Jee, N. Özgüven, and J. R. G. Evans, "Novel polymer–metal based method for open cell metal foams production," *Mater. Sci. Technol.*, vol. 16, no. 7–8, pp. 776–780, 2000.

[75] Q. Tan, P. Liu, C. Du, L. Wu, and G. He, "Mechanical behaviors of quasi-ordered entangled aluminum alloy wire material," *Mater. Sci. Eng. A*, vol. 527, no. 1–2, pp. 38–44, 2009.

[76] P. Liu, Q. Tan, L. Wu, and G. He, "Compressive and pseudo-elastic hysteresis behavior of entangled titanium wire materials," *Mater. Sci. Eng. A*, vol. 527, no. 15, pp. 3301–3309, 2010.

[77] P. Liu, G. He, and L. H. Wu, "Impact behavior of entangled steel wire material," *Mater. Charact.*, vol. 60, no. 8, pp. 900–906, 2009.

[78] B. K. Lee and K. J. Kang, "High strength-per-weight cellular metals fabricated of wires," *Adv. Eng. Mater.*, vol. 10, no. 9, pp. 835–839, 2008.

[79] A. E. Markaki, V. Gergely, A. Cockburn, and T. W. Clyne, "Production of a highly porous material by liquid phase sintering of short ferritic stainless steel fibres and a preliminary study of its mechanical behaviour," *Compos. Sci. Technol.*, vol. 63, no. 16, pp. 2345–2351, 2003.

[80] W. E. Frazier, "Metal additive manufacturing: A review," *J. Mater. Eng. Perform.*, vol. 23, no. 6, pp. 1917–1928, 2014.

[81] L. E. Murr, S. M. Gaytan, F. Medina, E. Martinez, J. L. Martinez, D. H. Hernandez, B. I. Machado, D. A. Ramirez, and R. B. Wicker, "Characterization of Ti-6Al-4V open cellular foams fabricated by additive manufacturing using electron beam melting," *Mater. Sci. Eng. A*, vol. 527, no. 7–8, pp. 1861–1868, 2010.

[82] R. Goodall, A. Marmottant, L. Salvo, and A. Mortensen, "Spherical pore replicated microcellular aluminium: Processing and influence on properties,"

Mater. Sci. Eng. A, vol. 465, no. 1–2, pp. 124–135, Sep. 2007.

[83] K.-S. Chou, "A novel method for making open-cell aluminum foams with soft ceramic balls," *Scr. Mater.*, vol. 44, no. 5, pp. 105–382, Mar. 2002.

[84] E. M. Castrodeza and C. Mapelli, "Processing of brass open-cell foam by silica-gel beads replication," *J. Mater. Process. Technol.*, vol. 209, no. 11, pp. 4958–4962, Jun. 2009.

[85] Y. Boonyongmaneerat and D. C. Dunand, "Ni-Mo-Cr Foams Processed by Casting Replication of Sodium Aluminate Preforms," *Adv. Eng. Mater.*, vol. 10, no. 4, pp. 379–383, Apr. 2008.

[86] J. F. Despois, A. Marmottant, Y. Conde, R. Goodall, L. Salvo, C. San Marchi, and A. Mortensen, "Microstructural Tailoring of Open-Pore Microcellular Aluminium by Replication Processing," *Mater. Sci. Forum*, vol. 512, pp. 281–288, 2006.

[87] R. Goodall, J. Despois, A. Marmottant, L. Salvo, and A. Mortensen, "The effect of preform processing on replicated aluminium foam structure and mechanical properties," *Scr. Mater.*, vol. 54, no. 12, pp. 2069–2073, Jun. 2006.

[88] C. Gaillard, J. Despois, and A. Mortensen, "Processing of NaCl powders of controlled size and shape for the microstructural tailoring of aluminium foams," *Mater. Sci. Eng. A*, vol. 374, no. 1–2, pp. 250–262, Jun. 2004.

[89] L. J. Gibson, "Mechanical Behaviour of Metallic Foams," *Annu. Rev. Mater. Sci. Mater. Sci.*, vol. 30, pp. 191–227, 2000.

[90] A. H. Benouali, L. Froyen, J. F. Delerue, and M. Wevers, "Mechanical analysis and microstructural characterisation of metal foams," *Mater. Sci. Technol.*, vol. 18, no. 5, pp. 489–494, 2002.

[91] E. Maire, A. Fazekas, L. Salvo, R. Dendievel, S. Youssef, P. Cloetens, and J. M. Letang, "X-ray tomography applied to the characterization of cellular materials. Related finite element modeling problems," *Compos. Sci. Technol.*, vol. 63, no. 16, pp. 2431–2443, 2003.

[92] A. Elmoutaouakkil, L. Salvo, E. Maire, and G. Peix, "2D and 3D Characterization of Metal Foams Using X-ray Tomography," *Adv. Eng. Mater.*, vol. 4, no. 10, pp. 803–807, 2002.

[93] E. Maire, P. Colombo, J. Adrien, L. Babout, and L. Biasetto, “Characterization of the morphology of cellular ceramics by 3D image processing of X-ray tomography,” *J. Eur. Ceram. Soc.*, vol. 27, no. 4, pp. 1973–1981, 2007.

[94] M. Saadatfar, F. Garcia-Moreno, S. Hutzler, A. P. Sheppard, M. A. Knackstedt, J. Banhart, and D. Weaire, “Imaging of metallic foams using X-ray micro-CT,” *Colloids Surfaces A Physicochem. Eng. Asp.*, vol. 344, no. 1–3, pp. 107–112, Jul. 2009.

[95] O. B. Olurin, M. Arnold, C. Korner, and R. F. Singer, “The investigation of morphometric parameters of aluminium foams using micro-computed tomography,” *Mater. Sci. Eng. A*, vol. 328, no. 1, pp. 334–343, 2002.

[96] C. Y. Zhao, S. A. Tassou, and T. J. Lu, “Analytical considerations of thermal radiation in cellular metal foams with open cells,” *Int. J. Heat Mass Transf.*, vol. 51, no. 3–4, pp. 929–940, 2008.

[97] P. Ranut, “On the effective thermal conductivity of aluminium metal foams: Review and improvement of the available empirical and analytical models,” *Appl. Therm. Eng.*, vol. 101, pp. 496–524, 2016.

[98] R. Goodall, L. Weber, and A. Mortensen, “The electrical conductivity of microcellular metals,” *J. Appl. Phys.*, vol. 100, no. 4, 2006.

[99] K. Boomsma and D. Poulikakos, “The Effects of Compression and Pore Size Variations on the Liquid Flow Characteristics in Metal Foams,” *J. Fluids Eng.*, vol. 124, no. 1, p. 263, 2002.

[100] M. Medraj, E. Baril, V. Loya, and L.-P. Lefebvre, “The effect of microstructure on the permeability of metallic foams,” *J. Mater. Sci.*, vol. 42, no. 12, pp. 4372–4383, Mar. 2007.

[101] J. W. Paek, B. H. Kang, S. Y. Kim, and J. M. Hyun, “Effective Thermal Conductivity and Permeability of,” vol. 21, no. 2, pp. 453–464, 2000.

[102] J. Sauerhering, S. Angel, T. Fend, S. Brendelberger, E. Smirnova, and R. Pitz-Paal, “ICNMM2008-62311, Characterisation of Flow and Heat Transfer in Sintered Metal Foams,” in *ASME 6th International Conference on Nanochannels, Microchannels, and Minichannels*, 2008, pp. 121–127.

[103] S. Mancin, C. Zilio, A. Diani, and L. Rossetto, “Experimental air heat transfer and pressure drop through copper foams,” *Exp. Therm. Fluid Sci.*, vol. 36, pp.

224–232, Jan. 2012.

[104] A. Mortensen, “Permeability of open-pore microcellular materials,” *Transport*, vol. 53, pp. 1381–1388, 2005.

[105] M. D. M. Innocentini, L. P. Lefebvre, R. V. Meloni, and E. Baril, “Influence of sample thickness and measurement set-up on the experimental evaluation of permeability of metallic foams,” *J. Porous Mater.*, vol. 17, no. 4, pp. 491–499, Aug. 2009.

[106] Y. A. Cengel, *Heat And Mass Transfer: A Practical Approach*, Third. McGraw-Hill, 2006.

[107] W. H. Hsieh, J. Y. Wu, W. H. Shih, and W. C. Chiu, “Experimental investigation of heat-transfer characteristics of aluminum-foam heat sinks,” *Int. J. Heat Mass Transf.*, vol. 47, no. 23, pp. 5149–5157, Nov. 2004.

[108] D. Angirasa, “Experimental investigation of forced convection heat transfer augmentation with metallic ® brous materials,” vol. 45, pp. 919–922, 2002.

[109] C. Y. Zhao, W. Lu, and S. A. Tassou, “Thermal analysis on metal-foam filled heat exchangers. Part II: Tube heat exchangers,” *Int. J. Heat Mass Transf.*, vol. 49, no. 15–16, pp. 2762–2770, 2006.

[110] A. Bhattacharya and R. L. Mahajan, “Metal Foam and Finned Metal Foam Heat Sinks for Electronics Cooling in Buoyancy-Induced Convection,” *J. Electron. Packag.*, vol. 128, no. 3, p. 259, 2006.

[111] C. Y. Zhao, T. J. Lu, and H. P. Hodson, “Natural convection in metal foams with open cells,” *Int. J. Heat Mass Transf.*, vol. 48, no. 12, pp. 2452–2463, Jun. 2005.

[112] M. S. Phanikumar and R. L. Mahajan, “Non-Darcy natural convection in high porosity metal foams,” *Int. J. Heat Mass Transf.*, vol. 45, no. 18, pp. 3781–3793, Aug. 2002.

[113] P. M. Kamath, C. Balaji, and S. P. Venkateshan, “Convection heat transfer from aluminium and copper foams in a vertical channel – An experimental study,” *Int. J. Therm. Sci.*, vol. 64, pp. 1–10, Feb. 2013.

[114] S. Mancin, C. Zilio, A. Cavallini, and L. Rossetto, “Heat transfer during air flow in aluminum foams,” *Int. J. Heat Mass Transf.*, vol. 53, no. 21–22, pp. 4976–4984, Oct. 2010.

[115] E. Baril, a. Mostafid, L.-P. Lefebvre, and M. Medraj, “Experimental Demonstration of Entrance/Exit Effects on the Permeability Measurements of Porous Materials,” *Adv. Eng. Mater.*, vol. 10, no. 9, pp. 889–894, Sep. 2008.

[116] N. Dukhan and K. Patel, “Effect of sample’s length on flow properties of open-cell metal foam and pressure-drop correlations,” *J. Porous Mater.*, vol. 18, no. 6, pp. 655–665, Oct. 2010.

[117] N. Dukhan and M. Ali, “Effect of Confining Wall on Properties of Gas Flow Through Metal Foam: An Experimental Study,” *Transp. Porous Media*, vol. 91, no. 1, pp. 225–237, Sep. 2011.

[118] D. R. Poirier and G. H. Geiger, *Transport Phenomena in Materials Processing*. Warrendale: PA: TMS, 1994.

[119] L.-P. Lefebvre, J. Banhart, and D. C. Dunand, “Porous Metals and Metallic Foams: Current Status and Recent Developments,” *Adv. Eng. Mater.*, vol. 10, no. 9, pp. 775–787, Sep. 2008.

[120] O. Reutter, E. Smirnova, J. Sauerhering, S. Angel, T. Fend, and R. Pitz-Paal, “Experimental Investigation of Heat Transfer and Pressure Drop in Porous Metal Foam,” in *ASME 4th International Conference on Nanochannels, Microchannels, and Minichannels (ICNMM2006)*, 2006, pp. 461–466.

[121] G. Zaragoza, “Aluminium Foams For Heat Transfer Applications, PHD Thesis,” University of Sheffield, 2013.

[122] T. Abdulla, “The Effect of Pulsed Bipolar Plasma Electrolytic Oxidation Coatings on the Mechanical Properties of Open Cell Aluminium Foams,” University of Sheffield, 2013.

[123] V. Boljanovic, *Metal Shaping Processes*. Industrial Press, Inc, 2009.

[124] G. Zaragoza and R. Goodall, “Development of a device for the measurement of thermal and fluid flow properties of heat exchanger materials,” *Measurement*, vol. 56, pp. 37–49, 2014.

[125] W. M. Haynes, D. R. Lide, and T. J. Bruno, Eds., *CRC Handbook of Chemistry and Physics*, 93rd ed. Boca Raton: CRC Press, 2012.

[126] W. J. Parker, R. J. Jenkins, C. P. Butler, and G. L. Abbott, “Flash method of determining thermal diffusivity, heat capacity, and thermal conductivity,” *J.*

Appl. Phys., vol. 32, no. 9, pp. 1679–1684, 1961.

[127] P. Gaal, M. A. Thermitus, and D. Stroe, “Thermal conductivity measurements using the flash method,” *J. Therm. Anal. Calorim.*, vol. 78, no. 1, pp. 185–189, 2004.

[128] D. R. Lide, Ed., *CRC Handbook of Chemistry and Physics*, 86th ed. CRC Press, 2005.

[129] N. Dukhan and M. Ali, “Strong wall and transverse size effects on pressure drop of flow through open-cell metal foam,” *Int. J. Therm. Sci.*, vol. 57, pp. 85–91, Jul. 2012.

[130] “engineeringclicks.com.” [Online]. Available: https://www.engineeringclicks.com/electro-discharge-wire-cutting-edwc/. [Accessed: 27-Mar-2017].